FLUORESCENCE IMAGING BASED ANALYSIS OF ACTIN TURNOVER: LONGITUDINAL PROFILING OF STEM CELL PHENOTYPES DURING DIFFERENTIATION

BY

PRAKHAR MISHRA

A Dissertation submitted to the

School of Graduate Studies

Rutgers, The State University of New Jersey

in partial fulfillment of the requirements

for the degree of

Doctor of Philosophy

Graduate program in Cell and Developmental Biology

Written under the direction of

Dr. Prabhas V. Moghe

And approved by

_____

_____

_____

_____

_____

New Brunswick, New Jersey

October 2020

ABSTRACT OF THE DISSERTATION

FLUORESCENCE IMAGING BASED ANALYSIS OF ACTIN TURNOVER: LONGITUDINAL PROFILING OF STEM CELL PHENOTYPES DURING DIFFERENTIATION

By PRAKHAR MISHRA

Dissertation Director:

Dr. Prabhas V. Moghe

Stem cells derived from adults have become the focal point of cell-based regenerative therapies. The most commonly used stem cells, mesenchymal stem cells (abbreviated MSCs), have several traits such as the ability to migrate to injury site, immunomodulation, *in vitro* expansion and differentiation into a variety of cells. However, the widespread usage of MSCs is hampered by poor characterization, tissue culture induced senescence and innate heterogeneity that makes it challenging to predict their clinical efficacy. The traditional methods for evaluation of stem cells are primarily terminal assays that rely on discrete time-point data sets that offer limited, discontinuous information and often overlook the intrinsic phenotypic diversity of these cells. In this thesis, we address some of these issues by developing a novel platform for live cell imaging which can be used to monitor evolving MSCs by generating continuous data sets over the course of several hours or several days while sparing the cells for multiplexing with other traditional assays. Our imaging-based approach relies on a cell permeable fluorogenic probe, SiR-actin (SA), that

becomes fluorescent only when it labels endogenous actin filaments (F-actin). The idea of harnessing actin as a sentinel stem cell reporter is supported from past research conducted by Moghe lab and numerous other research groups, as the cytoskeleton can modulate and display the phenotypic changes associated with lineage commitment. Unlike previous research that focused primarily on morphology of actin cytoskeleton, we focused on utilizing the shifting actin turnover rates in response to extracellular cues as the key reporter metric. After SA labelling, actin reorganization leads to removal of the SA probe from F-actin binding sites and subsequent decline in SA fluorescence. When cells are cultured in differentiation media, the rate of fluorescence loss of SA provided insights about the kinetics of lineage specific change in actin reorganization. We report that initiation of differentiation involves decline in actin turnover during adipogenesis and chondrogenesis within few hours. By combining SA with another F-actin probe, phalloidin, we were able to parse heterogenous single cells across the standard tri-lineages (adipogenic, osteogenic and chondrogenic) within 1 hour of stimulation. In addition, our approach enabled assessment of *in vitro* aging by demonstrating a slowdown in actin turnover within 1 hour of analysis. Next, to establish the link between actin turnover and stem cell differentiation, we employed immunolabeling to demonstrate co-occurrence of altered actin turnover with differentiation markers in MSCs as well induced pluripotent stem cells (iPSCs). We also propose that inherent actin turnover status of individual cells could be a determinant of their differentiation potential. To this end, we isolated cells based on differential SA expression and found that the actin turnover plays a role in determining the ability to differentiate towards osteogenic or adipogenic fate. In summary, we propose actin turnover as a novel dynamic marker as it provides immediate readouts of changing cell states that could be utilized to forecast stem cell behavior towards regenerative therapies.

ACKNOWLEDGEMENTS

Humans are simple creatures with complex traits that are honed over time. I suppose it is the perpetual process of "growing-up" that brings out our personal inclinations and qualities. In my case, one trait stood out among every other feature, curiosity. My 'curiosity' inspired me to venture on an exciting journey to pursue a Ph.D. It mostly felt that I had to be a one-man army to get here, but I stand on the shoulders of several people who have helped me, I want to thank everyone sincerely.

Foremost, Dr. Prabhas Moghe, my thesis adviser, an astute researcher, and a charismatic leader, has been a versatile mentor throughout my journey. When I struggled with the streak of unfruitful projects, I had his unwavering support. When I felt stuck with unexpected roadblocks, he listened to me patiently and shared his intellect to help me move forward. At times when I was complacent (this rarely happens during Ph.D.), he asked the blunt yet necessary questions. Here, I list my three favorite ones and I hope to continue asking these questions as a researcher and a person before making a decision about doing anything: 1. So what? 2. Why would one care about this? 3. What's the big picture? During my journey under your wing, Dr. Moghe, I have grown to become a more confident and resourceful scientist, many thanks.

I express my gratitude to Dr. Joachim Kohn, my first mentor at Rutgers University. I had the opportunity to be associated with his group briefly and interacted with excellent researchers: Drs. Sanjeeva Murthy, Yong Mao, Joseph Steele, Alexandra Pastino, Antonio Merolli, Zheng Zhang, Murat Guvendiren and Hilton Kaplan. Years of association with Kohn lab resulted in some wonderful collaborations and papers. I will dearly remember your wise counsel as you guided me to get where I stand today.

I want to thank my two other committee members, Drs. Rick Cohen and Martha Soto. Dr. Rick Cohen is a sharp researcher with near unlimited patience. Over the years, he was there to discuss and nurture my ideas to reach fruition. His expertise in stem cells and molecular biology helped me hone my skills and intellect immensely. Dr. Cohen, I am glad to have you as a co-author in my final paper as a Ph.D. candidate. Dr. Soto, has been my go-to adviser regarding actin biology. Her pragmatic inputs helped me to focus on the important questions in my project.

I had the pleasure to work with several knowledgeable researchers in the Moghe lab. Dr. Vidya Ganapathy remained a critical yet kind mentor. Although our projects did not overlap, I greatly admire her general keenness towards science and helping the “kids”. Thank you for looking out for me, VG. Dr. Nicola Francis remained a friendly and insightful presence during my journey. I thank her for the brain-storming sessions even when you were running around briskly. Harini, one of the most efficient and down to earth Ph.D. friends in the lab. Thank you, Harini, for being there and bringing cheer in challenging situations. Nanxia, you are a diligent researcher and a caring friend. I foresee a bright future for you as a strong leader. Amber, it is rare to see an ever-smiling face at a formal research lab while pulling off 10+ hours of bench work in a day. Thank you for your kind presence. Daniel Martin, thank you for “picking my brains”, our conversations helped me find new directions for this research work. Sebastian Vega and Varun Arvind, thank you for letting me be a part of your research paper, I consider myself fortunate to collaborate with you. Anandika, thank you for offering me your guidance during my early days at Moghe lab. Jay, I wish you luck to keep up the good work.

It is amazing how much of an impact we have on each other without even realizing it. At different stages during my Ph.D., I came across stellar individuals who helped me, at times with words or then through their actions. Dr. Richard Padgett, thank you for

inspiring me to seek opportunities in the face of adversity. Dr. Bonnie Firestein, thank you for sharing your own Ph.D. story to inspire me. Carolyn Ambrose, thank you for your constant support during all these years, keep up the fitness routine. Dr. Janet Alder, thank you for offering your kind help to me and all other students. Arthur Roberts, thank you for your ideas and assistance with flow cytometry. BME administrative staff: Larry, Stratos, Robin and Linda, many thanks.

I also want to thank my mentors from before I joined Moghe lab. First, Himanshu Joshi sir, who taught me the value of having a 'logical approach' towards problem solving and the importance of the ability to tell a story especially in science. Dr. Alok Dube (RRCAT-Indore, India), thanks for taking me on during my undergrad and allowing me to get my first hands on experience with research. Dr. Nigel Fraser, a renowned virologist at UPenn, many thanks for taking me on for a long-term research project which resulted in my first first-author paper, and my first DSLR camera. Dr. Susanna Lewis (UPenn), my first employer, thank you for your kindness and support during my stint at Roth lab. At Rutgers, I had brief but impactful interaction during my rotation with Dr. Mike Kiledjian and Dr. Ki-Bum Lee, thank you.

I want to thank my friends who offered their advice or sometimes just the means to distract myself from the work. Vibhor Gupta, thanks for being my first good friend in USA and providing constant support for many years. Amber Verma, my friend since the first time I went to school. Cheers to years of friendship and joyous times. Nick Ruskoski, thanks for helping me with the basics of biological bench work. Members of RSVP group not mentioned yet: Rahul, Rachit, Shreyas, Subbu and Swati, thanks for making USA feel like home. At Rutgers, I want to thank Lin-Ing, Ryan, Ilija, Mark, Perry and Ambroise for the good times.

I want to dedicate all my accomplishments to date to my parents, Aparna Mishra and Pavan Mishra. I hope to make you proud someday. My constant mentor, sister and friend, Pankhuri Mishra, an undercover sage disguised as a silly girl, thanks for being there for me ALWAYS, and bringing two more joyful people into my life, Mukund and Nyesha. Rupali, thanks for your unconditional love, which I hope keeps growing.

Lastly, I want to share a simple theory for success that I developed during my Ph.D.: Success requires n+1 attempts, where n is the necessary number of failures.

PRIOR PUBLICATIONS

The following chapters in this dissertation were previously published as listed below:

- Chapter 3 has been published in its entirety:

  Mishra P, Martin DC, Androulakis IP, Moghe PV. Fluorescence Imaging of Actin Turnover Parses Early Stem Cell Lineage Divergence and Senescence. Sci Rep. 2019 Jul 17;9(1):10377. doi: 10.1038/s41598-019-46682-y. PMID: 31316098

- Chapter 4 has been published in its entirety:

  Mishra P, Cohen RI, Zhao N, Moghe PV. Fluorescence-based actin turnover dynamics of stem cells as a profiling method for stem cell functional evolution, heterogeneity and phenotypic lineage parsing. Methods. 2020 May 28:S1046-2023(20)30026-8. doi: 10.1016/j.ymeth.2020.05.020. Online ahead of print. PMID: 32473293

TABLE OF CONTENTS

LIST OF FIGURES & SUPPLEMENTARY DATA

Chapter 1: Introduction

1.1 Stem cells

The concept of stem cells emerged at the end of 19th century to describe the ability of certain tissues (blood, skin, etc.) to self-renew despite being composed of short-lived cells [2]. Broadly, two main types of stem cells exist, embryonic and non-embryonic [7]. Embryonic stem cells (ESCs) are collected from inner cell mass of human blastocysts [8]. ESCs possess the ability to produce cells across all three germ layers, and virtually provide unlimited cells for tissue repair and drug screening [11]. ESCs are cultured on adherent but growth-arrested layer of cells known as feeder cells to provide appropriately conditioning substratum {Llames, 2015 #487}. ESCs can be differentiated after removal from the feeder layer and maintenance in suspension, which results in aggregation of cells to form embryoid bodies. [12]. *In vitro* differentiation is a key feature that supports usage of ESCs in disease models and for other therapeutic applications, however teratoma formation and ethical issues have hindered their widespread usage in clinic [13]. Non-embryonic stem cells, mostly adult stem cells, can be easily isolated and expanded from diverse tissues but have limited differentiation potential. These adult multipotent cells are discussed in detail in the following section. Another type of stem cells, induced pluripotent stem cells (iPSCs), show extensive self-renewal and differentiation potential similar to ESCs. iPSCs are reprogrammed differentiated (somatic) cells that are induced to attain embryonic-like state via forced expression of defined transcription factors (Yamanaka factors: Oct3/4, Sox2, c-Myc and Klf-4) [14]. As such, iPSCs offer the ability to derive and expand cells from patients for disease modeling and cell-based therapies [15]. Still there are major challenges associated with iPSCs, such as non-standardized tissue culture practice, retention of somatic mutations after reprogramming, genomic instability, and the risk of tumorigenicity [16, 17]. Due to the ethical dilemma presented by ESCs and the

outstanding problem of clinical translatability with iPSCs, adult stem cells, such as mesenchymal stem cells (MSCs), could be an exciting alternative for cell based regenerative therapies [18]. In addition to their regenerative potential, MSCs can play an important function in tissue homeostasis and repair by secreting factors to modulate immune cells [19]. The usage of MSCs has few barriers, senescence related loss of functionality and inherent heterogeneity that makes their standardization challenging. In the following section, we will explore the MSCs in depth to understand the popularity of these cells among the clinical researchers across the world. A quick example that shows the key interest in MSCs is that researchers have developed protocols to generate MSCs from iPSCs or ESCs to avoid the risk of uncontrolled growth and rapid proliferation, however the production methods, culture conditions and safety need to be streamlined further [20, 21].

1.1.1 Mesenchymal Stem Cells (MSCs)

Developing a better understanding of various functional attributes of MSCs is the principal focus of this thesis. The term MSCs was described first by Caplan as a representative term for small progenitor cells that demonstrate the ability for bone and cartilage formation in embryos and adults [22]. Unlike most of the hematopoietic cells, MSCs display substrate adhesion and fibroblastic phenotype. In their seminal work of 1999 (~currently 25,000 citations), Pittenger et al. isolated MSCs from bone marrow aspirates of adults and showed several qualities of these cells including: stable phenotype, adhesion, tri-lineage (bone, adipose, cartilage tissues) differentiation potential and tissue culture expansion [23]. An elusive question remains relevant even today: What defines MSCs? There is a lack of consensus for annotating MSCs from various sources, but the minimum criteria to define MSCs as described by Dominici *et al.* include: i) plastic adherence during standard culture conditions; ii) the expression of CD105, CD73 and CD90, and lack of expression of CD45,

CD34, CD14 or CD11b, CD79alpha or CD19 and HLA-DR surface molecules; and iii) the ability to differentiate to osteoblasts, adipocytes and chondroblasts in [24]. The above criteria seems to be non-exhaustive as new features are constantly being added or the existing parameters are debated. For instance, Riekstina et al. described expression of embryonic stem cell markers Oct4, Nanog, alkaline phosphatase and SSEA-4 in bone marrow derived MSCs [25]. By definition, MSCs are expected to possess clonogenicity and tri-lineage potency, but only a fraction exhibits multipotency, indicating that MSCs are comprised of a heterogeneous population [26]. In an *in vitro* study, after 6d of culture, 50% of progeny cells were found to have originated from 9% of the initial population [27]. One of the earliest descriptions of population heterogeneity was provided by Mets and Verdonk who showed existence of two MSC subtypes: type I and II, where type I cells were smaller and "fibroblastic" morphologically while the type II cells were more "epithelial" and larger. They also reported that the type I cells divide rapidly and their proportion declines with sub-culturing in conjunction with increased type II cells [28]. Another standard property of MSCs is the ability to form colonies when seeded at low density. The enumeration of colony forming unit fibroblasts (CFU-F) is frequently used to determine their clonal expansion and plastic adherence [29]. The most common and longest utilized adult source tissue for human MSCs is the bone marrow [23, 30]. This thesis is primarily centered around MSCs, so the following section is dedicated to provide a broader overview regarding their diverse properties and functions.

1.1.2 Properties and Significance of MSCs

Despite years of extensive research focused on MSCs, the MSCs pose challenges to ready classification and functional definition. This multi-faceted problem exists partly due to a complex characterization based on combination of physical, phenotypical and functional properties. The problem of poor characterization is also attributed to inherent

heterogeneity at multiple levels between: donors, tissues of origin, clones derived from single colonies (interclonal heterogeneity) and intra-population (within cultured cells) [31]. Furthermore, MSCs can vary significantly based on isolation protocol, cryopreservation method, and culture condition across different laboratories [32]. For instance, comparison of MSC-like cells from testis biopsies, ovary, hair follicle and umbilical cord Wharton's jelly for the expression of surface markers to verify stemness revealed heterogeneity in the expression of different standard markers: CD105, CD90 associated with differential osteogenic potential and proliferation [33]. The problem of heterogeneity of MSC populations makes it challenging to develop standard MSC preparations and raises concerns about safety/efficacy for clinical usage.

When described initially, MSCs were thought to differentiate to make bone and cartilage tissues only, but gradually the number of cell types kept growing [22]. In addition to tri-lineage potency, MSCs have also been shown to differentiate to other lineages such as myocytes, cardiomyocytes, hepatocytes and neurons [34]. Of these, only the typical tri-lineage fates have been explored in this thesis. Theoretically, osteogenesis and adipogenesis are usually considered to have a reciprocal relationship in terms of differentiation pathways and functionality [35]. The cell fate decision involves numerous overlapping signaling pathways that regulate the primary transcription factors, Runt-related transcription factor 2 (Runx2) and peroxisome proliferator-activated receptor-γ (PPARγ) during adipogenesis and osteogenesis, respectively [36]. *In vitro* differentiation on typical cell culture dishes can be stimulated with induction media for both lineages, with appropriate plating density of the cells. In addition, appropriate biomechanical stimulation could further help cells to differentiate [37]. For instance, adipocytes are favored by soft substrates, unlike bone formation favored by stiff substrates [38]. For

chondrogenesis, cells are cultured in 3D pellets to allow proper organizational stratification required for cartilage formation [39].

In addition to providing restorative support, MSCs also have cytokines and growth factors in their therapeutic repertoire. MSCs hinder the proliferation of activated T cells and the formation of cytotoxic T cells [40]. MSCs modulate immune response from major cell types involved in alloantigen recognition and elimination, including antigen presenting cells, T cells and natural killer cells and also reduce inflammatory response [41]. MSCs also enjoy the immune privileged status that favors their allogenic application. MSCs influence the immune system by secreting a variety of factors including transforming growth factor beta, prostaglandin E2, tumor necrosis factor stimulated gene-6 protein, indoleamine 2,3-dioxygenase, and nitric oxide [42]. MSCs have the ability to home to the site of injury and release anti-inflammatory cytokines [43]. Recent findings indicate that apart from the cytokine-mediated effects, apoptotic, metabolically inactivated, or even fragmented MSCs possess an immunomodulatory potential showing cytokine independent mechanisms [44]. Previously it was thought that discrete signaling pathways are involved in differentiation, cell morphological change and immunomodulation. It is possible that these pathways might be mutually exclusive. For instance, treatment of equine adipose tissue-derived stem cells (ADSCs) with interleukin-1β and/or TNF undermined their tenogenic properties partly by reducing expression of the tenogenic transcription factor, Scleraxis [45]. Paracrine factors from MSCs might be important even without providing cells for restoration, e.g. paracrine signaling from injected MSCs resulted in improvement of cardiac function after infarction [46]. Further studies are required to design culture conditions to achieve a desired cellular response or a particular clinical indication.

MSCs possess the ability to attach to the tissue culture dish and keep replenishing the pluripotent cells, however prolonged in-vitro maintenance may lead to spontaneous differentiation resulting in constant diminishing pool of proliferating multipotent cell population [47]. Furthermore, increase in passage results in decline in tri-lineage differentiation potential which could be exacerbated by donor age [48]. The impact of aging in MSCs was demonstrated by Rombouts et al. in a time-course in-vivo study after engraftment. They reported better homing efficiency in freshly isolated MSCs (55-65%) compared to cultured cells with 10% after 24 hours, and close to 0% homing efficiency after 48 hours of cell culture [49]. Proteomic profiling of *in vitro* aged cells revealed decline in Fas ligand, CD98, CD205, and CD106 along with increase in expression of CD49c, CD63, and class 1 and 2 major histocompatibility complex molecules, along with the expression of early senescence marker CDKN2A p16 [50]. Phenotypic changes arising from donor age or in-vitro culture have been reported along with concurrent decline in clonogenicity and differentiation potential, therefore, it is important to focus on phenotypic markers as an early predictor of aging [51]. Synthetically designed biomaterial based interventions and modified tissue culture systems have shown some promise in prolonging the functionality of MSCs *in vitro* [47, 52]. There is a need to establish quality control standards to ensure adequate MSC functionality prior to therapeutic usage.

1.1.3 Clinical Applications of MSCs

MSCs have gained widespread usage in the field of regenerative medicine. Keyword search on pubmed yields ~64,000 results and over 1,100 registered clinical trials using the phrase “mesenchymal stem cells”. MSCs exhibit multipotency, pro-angiogenic activity, paracrine signaling and immunomodulation making them a suitable candidate for regenerative medicine. MSCs have shown some promising results in clinical studies for a few diseases including: graft versus host disease, Crohn’s disease, osteogenesis imperfecta, diabetes,

neurological disease, bone injury, cartilage damage, myocardial infarction, hematological disease, graft-versus-host disease and inflammatory diseases, and autoimmune diseases [53]. The new paradigm of MSC based therapeutics relies on paracrine and immunomodulatory activity of MSCs in addition to providing reparative function.

Improvement in tissue culture technique could further improve therapeutic functions of MSCs. For instance, Rosova et al. demonstrated that hypoxic pre-conditioning (cell culture in the presence of 1-3% O_2 instead of the normoxic 21%) resulted in increased motility along with increased expression of increased growth factor expression and revascularization *in vivo* [54]. The notion of preconditioning MSCs based on the intended application is getting support from diverse research labs of late. Interested readers are directed to a recent review paper that describes improved efficacy of MSC based therapies following priming with hypoxia, pharmacological drugs, biomaterials cytokines, growth factors, and culture conditions [55]. Some of the main challenges to MSC based therapeutics include, tumorigenicity, heterogeneity, poor characterization, and *in vitro* senescence [56]. Usually a target dose of 100-150 million cells can be generated from 25 mL of bone marrow after 3 week long cell culture [57, 58]. As mentioned previously, 3 weeks of cell culture might be too long, because cells start losing their functional attributes as soon as the cell culture begins. Newer biomaterials (composite hybrid scaffolds, biomimetic 3D scaffolds etc.) are being tested to prolong the proliferation and differentiation potential of these cells [59].

Alternative approaches to the usage of MSCs have been explored to avoid issues including poor characterization, immunogenicity, and tumorigenicity. One way to prevent cell-cell interaction induced reaction in the host is to encapsulate MSCs and rely on their paracrine secretion of cytokines to upregulate anti-inflammatory factors and suppress pro-inflammatory cytokines in activated macrophages[60]. Another approach involves

harnessing MSCs mediated paracrine effect to some extent via extracellular vesicles carrying a cargo of miRNA, mRNA, bioactive lipids and proteins [61]. Due to their superior safety profile compared to whole cells and relatively safe prolonged storage compared to whole cells, the extracellular vesicles might offer novel therapeutic edge [61]. For instance, when cultured in MSC-conditioned medium, cardiomyocytes were protected from mitochondria-mediated apoptosis through reduced cytochrome C release and caspase-3 activation [62]. Exosomes, a type of extracellular vesicle, have the size in the range of 40-150nm nanoparticle range and are currently examined as new therapeutic paradigm for diseases of liver, kidney, heart and brain [63]. The emerging field of exosome based cell therapy needs to address a few concerns such as: variability in cargo based on MSC tissue origin, culture condition, and intercellular interaction making it necessary to establish quality control standards for consistent production [64].

Lastly, MSCs need to be better characterized and utilized based on the intended therapeutic application. For instance, Boregowda et al. reported CLIP scale where high TWIST1 expression was predicted to be beneficial in diseases where angiogenesis is required, such as stroke or limb ischemia and low TWIST1 expressing populations were predicted to be better suited for treating inflammatory and immune-related disorders, such as acute tissue or organ injury and graft-versus-host disease (GVHD) [65]. Thus, prior to employing MSCs for GVHD treatment, it should be important to validate anti-inflammatory capacity of the MSCs and the immune-compatibility should be matched with appropriate donor.

1.2. Methods to evaluate MSC functionality

1.2.1 Traditional terminal assays

Typically, the assessment of MSC functionality involves analysis of proliferation, differentiation, immunomodulation, and paracrine activity using assays for protein expression, gene expression and labeled or unlabeled cell analysis (for example, cell or tissue imaging). Given the large heterogeneity among MSCs, there is a need to identify more precise yet general cellular markers to standardize the MSC cultures prior to clinical applications. The classical methods for phenotypic evaluation of MSC differentiation include: alkaline phosphatase (ALP) and alizarin red S staining for osteoblasts, oil red O staining for adipocytes, and alcian blue staining for chondrogenesis [66]. The protein expression level of differentiation related genes could be assayed by immunostaining [67, 68]. Transcriptome (cDNA microarray) and proteome expression (MALDI-TOF-MS) profiles of MSC preparations have been described to define MSC preparations, and could illustrate the differences in cells functional attributes due to culture conditions [34, 69]. Cell proliferation can be assessed by expression of proliferation markers (e.g. Ki67) or CFU-F (clonogenic capacity) assay [70]. The immunomodulatory effect of MSCs can be assayed based on transwell co-cultures with immune cells such as human peripheral blood mononuclear cells (PBMC) under T cell stimulatory condition (or other cell types such as macrophage, natural killer cells etc.), followed by quantitative analysis of T cell proliferation. The aforementioned methods require 1-4 weeks of cell culture and associated supplementation of growth factors for validating differentiation; making them expensive, tedious and time-consuming. These assays yield average results from cell population overlooking heterogeneity. However, the tested MSCs cannot be recovered for further testing, as these are terminal assays that require cell fixation or lysis.

Several researchers have realized the importance of addressing heterogeneity among stem cells to develop their predictive methods. Marklein et al. conducted functionally relevant morphological profiling (FRMP) using machine learning to identify morphological subpopulations, based on nuclei and whole cell morphology descriptors, to predict immunosuppressive quality of MSCs during regulation of activated $CD4^+$ and $CD8^+$ T cells [71]. During osteogenesis, the early gene expression and ALP activity was found to be highly variable and poorly correlated with long term maturation and osteogenesis of MSCs as shown by mineralization. Therefore, a multivariate approach has been suggested to complement the traditional methods [72]. Yao et al. elucidated paracrine activity of MSCs by single cell gene profiling (high through-put qPCR) after injecting MSCs and showed elevated secreted factors in infarcted murine heart [46]. Metabolic changes during adipogenic differentiation were studied *in vitro* using nuclear magnetic resonance spectroscopy [73].

Although traditional methods have been modified to perform analysis at the level of a single cell such as western blot, qPCR, and mass spec methods [31], these methods do not lend themselves to preparative workflow for the use of cells for regenerative or clinical applications. By the time the assessment of MSC functionality in a small batch of cells is performed, the majority of cells undergo senescence, further exacerbating the levels of heterogeneity, thus leading to a disconnect between the phenotypic quality of the test and the applied batch of cells. In addition, fixed-cell assays result in loss of information regarding long term or short-term instantaneous responses. Therefore, it is important to develop a real-time cell tracking method to probe MSC characteristics.

1.2.2 Live cell assays

Real time monitoring of evolving morphological changes is needed for MSCs to indicate cellular response to extracellular cues instead of fixed-cell assays because of non-linear

phenotypic divergence. For instance, upon treatment with growth factors in a heterogeneous population, each cell follows a different timeline to reach the intended functionality, and even if two identical clones were exposed to an extracellular cue, the spatiotemporal interaction remains stochastic. In this example, the analytics precision will further benefit from single cell profiling instead of bulk methods that largely overlook the outlier cells that deserve special attention to develop the understanding of stem cell biology further. Some of the known live gene expression analysis could be performed by quantifying mRNA abundance measurement using molecular beacons, spherical nucleic acids and fluorescent reporters. For live cell protein analysis, fluorescent reporters can be used via fluorescence readers or imaging [31].

For industrial applications, high throughput automated platforms need to be used to promote both quality of results and cost-effectiveness. Label-free imaging platforms are able to forecast osteogenic potential in MSCs [74]. The label free approach excludes the staining step which itself might create unwanted morphological changes in the cells [75]. A few multi-parametric approaches have been attempted to automate analysis, for instance, high dimensional flow cytometry coupled with machine learning methods have been evaluated to assist with gating and avoid manual analysis. Combining multiple tools for flow cytometry makes it a promising bioinformatics strategy for high-dimensional single cell analysis [76]. Their method distinguished initial sub-populations, revealed cell subsets, and characterized subset features. In another hybrid approach cytonuclear whole cell high content machine learning based analysis suggested that cytoskeletal rearrangement could predict immunosuppressive capacity [71].

Recently, live cell microarrays were generated by patterning cells to characterize cell-cell interactions, reaction to stimuli and cell interactions with microenvironment. Such a method can visualize the results either label-free by electrochemical detection

methods [e.g. magnetic resonance imaging (MRI)] or by fluorescent/bioluminescent probes for specific biological targets [77]. Live cell imaging approach enables constant monitoring of cell sub-populations multiple times, thereby it can help to determine cell functionality and forecast their behavior by matching with the traditional methods. In chapter 3 and 4 of this thesis, we will introduce a novel live cell imaging method to probe MSC functions.

1.2.3 Predictive markers to MSC functionality

Immunophenotypic markers on MSC have been characterized extensively to predict differentiation potential. In section 1.1, we described the defining surface markers for MSC sub-populations, and newer candidate markers including Stro-1, SSEA-4, CD271 and CD146 have been added to the list, but the expression of these markers varies largely depending on the tissue of origin [78]. Maleki et al. compared expression of CD105 across MSC surface marker positive cells from 4 different tissues (testis, ovary, hair follicle and Wharton's jelly) and found it was associated with osteogenic potential in 3 out of 4 sources, while high expression of CD90 was associated with higher growth and differentiation potential only in 2 out of 4 sources [33]. MSCs from bone marrow, adipose tissue and skin demonstrate differences in surface markers and differentiation potential [79, 80]. The large panel of surface markers makes it impossible to come up with a straightforward and high throughput method to reliably predict MSC functionality.

Live cell imaging-based approaches can allow spatiotemporal monitoring of MSCs in response to extracellular cues. Li et al. developed fluorescent RNA-based probes to assess transcriptional regulation of Runx2 and Sox9 mRNA during MSC differentiation [81]. Yang et al. described a fluorescence transgene expression system to probe kinetics of chondrogenesis in rabbit MSCs [82]. Some newer approaches involve non-invasive and label free analysis of live cells, for instance, Quinn et al. used quantitative metabolic

imaging using endogenous fluorescence of live cells [83]. Markelein et al. proposed another composite nucleo-cytoskeleton based profiling method that was able to correlate 3rd day morphology to mineralization of MSCs after 35 days in culture, but this method was performed with fixed cells. Matsuoka et al. described a label free phase-contrast imaging approach where they were able to predict bone differentiation (ALP activity and calcium deposition) after 3 weeks of cell culture within 3 days of initiation of cell culture [74]. Our lab previously described a high-content imaging-based approach using actin morphometric features to forecast MSC differentiation within 24 hours of stimulation [84]. However, at the time this work was conducted with fixed cells. In addition, most of the aforementioned predictive imaging-based tools showed change in cell shape during MSC differentiation. Therefore, we hypothesized that live imaging of actin might be able to provide a richer dataset and the ability to discern subtle phenotypic variations in MSCs for predicting their behavior and understanding the kinetics of differentiation.

The next section is focused on a review of the significance of actin cytoskeleton in MSC biology and the role of cytoskeletal dynamics in providing valuable insights to probe MSC diverse functions.

1.3. Biology of the Actin Cytoskeleton

Actin is one of the most abundant and highly conserved proteins found in all eukaryotic organisms. By virtue of its ability to form versatile architectures in a dynamic fashion, actin provides mechanical support and generates force, which could be used in a variety of essential cellular activities, such as motility, maintenance of cell shape, cytokinesis, endocytosis, intracellular transport, mechanotransduction, transcription regulation, cell-

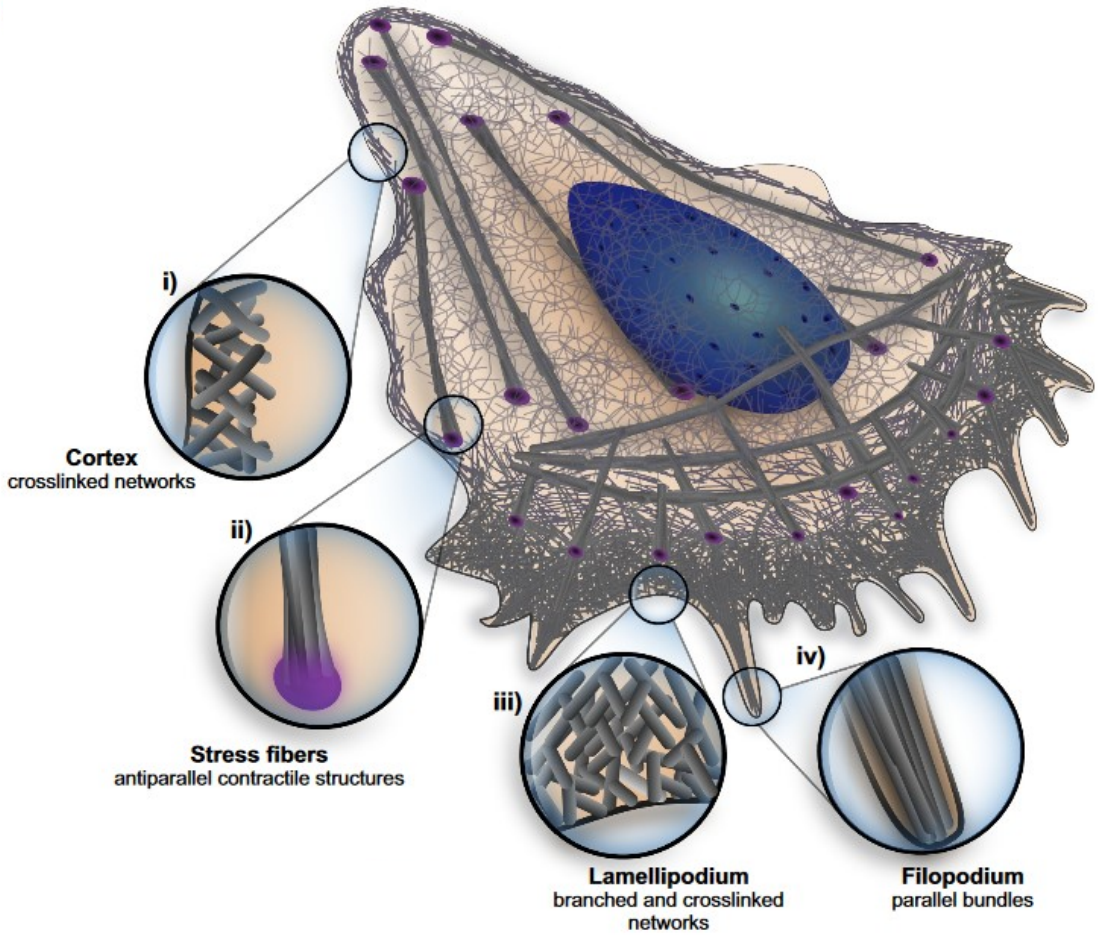

Fig. 1.1. Actin architecture in a motile in a motile cell: schematic showing major actin structures in a moving cell: i) the cell cortex; ii) stress fiber; iii) the lamellipodium; and filopodia. Figure adapted from Blanchoin et al. [1] (License number: 4883180904610)

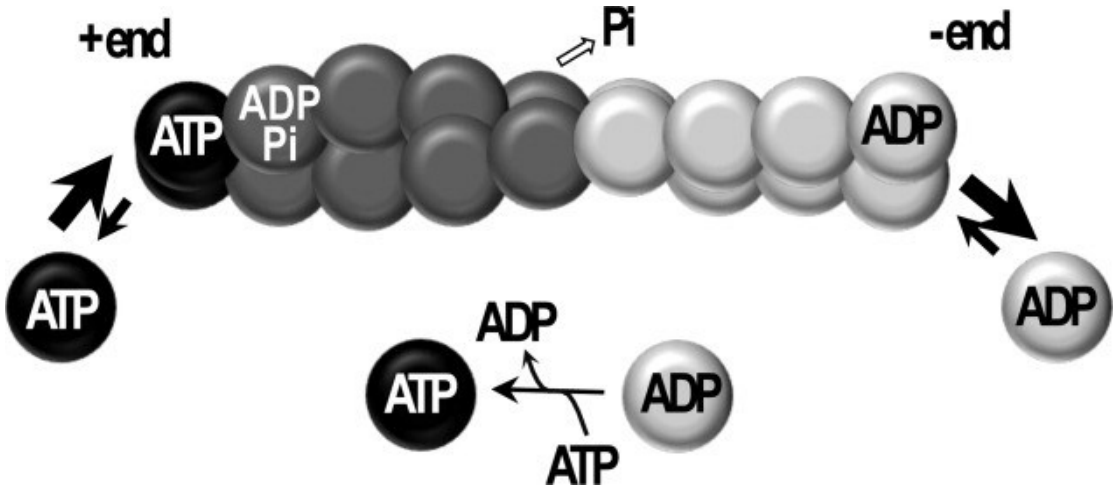

Fig. 1.2. Actin treadmilling: schematic of active actin filament dynamics, showing the steady state conditions in the presence of ATP where ADP dissociates mainly from the -end of the actin filament, the monomer exchanges the nucleotide from ADP to ATP, and then ATP-G-actin attaches primarily at the +end. ATP hydrolysis and addition of G-actin units, the inorganic phosphate (Pi) is retained, creating an intermediate ADP-Pi state before its release to the ADP-bound form [5]. The

cell communication, differentiation and biochemical signaling. Actin cytoskeleton mediates the formation of cellular structures such as lamellipodia, filopodia, stress fibers and focal adhesions in a dynamic manner during these processes [85]. Lamellipodium at the leading edge of the cells is formed by branched and crosslinked networks drive the cell migration by generating force by polymerizing against the cell membrane [86]. Parallel bundles of actin constitute finger-like filopodium that plays an important role in cell-cell signaling, responding to chemoattractants, and adhesion to extracellular matrix (ECM) [87]. Cell shape is primarily driven by a thin actomyosin layer, cortex, that lies underneath the plasma membrane [88]. The actomyosin is formed by interaction of bipolar myosin II filaments with anti-parallel actin filaments that convert chemical energy of (ATP) into mechanical energy to generate contractile forces [89]. Another category of contractile structures is formed by anti-parallel bundles of actomyosin arrays called stress fibers [90].

Cells usually consists of 3D network of the aforementioned structures interspersed with contractile bundles that assist the cell cytoskeleton interaction with ECM via focal adhesion sites [Fig. 1.1, for detailed review, refer to [1]].

A cell has a pool of monomeric actin (G-actin) that can polymerize to make polar double helical filaments (F-actin). The initial formation of F-actin involves assembly of stable multimer of actin monomers, defined as nucleation, is a rate limiting step due to energetically unfavored actin dimer intermediates and activity of other actin binding proteins (ABPs, discussed later). Actin polymerization takes place by reversible noncovalent assembly of G-actin units involving hydrolysis of adenosine 5'-triphosphate (ATP)[2]. After ATP hydrolysis, the release of inorganic phosphate(Pi) takes place at a slower rate that creates 3 nucleotide bound states: ATP state, intermediate ADP-Pi state and the final ADP state [91].

The final F-ADP state and concurrent Pi release destabilize the actin-actin interaction. The resulting actin filaments are polar as addition or removal of G-actin takes place more readily at the pointed (also known as "-end"). ATP-G-actin addition is favored at the fast-growing barbed end (also known as "+end"). At steady state, removal of monomers from the –end is balanced by elongation of +end, this dynamic process, known as actin treadmilling, results in ongoing turnover of actin, even in resting cells [Fig. 1.2, [10]]. At the whole cell level, equilibrium state of polymerizable actin monomers is established by the composite dynamics of all networks, to define the size and turnover kinetics of coexisting actin networks [9]. However, in addition to treadmilling, there are other protein-mediated processes that not only play a role in actin turnover but dictate the actin assembly right from the initial nucleation step.

1.3.1 Role of actin binding proteins in regulation of cytoskeletal microfilaments

Actin cytoskeleton structures are highly dynamic and require multiple proteins to regulate every step right from initiation of polymerization to depolymerization for maintaining the G-actin pool. The actin monomer consists of 2 major domains with two large clefts, the upper cleft binds the nucleotide (ATP/ADP), while the lower cleft undergoes nucleotide associated conformational change to facilitate interaction with actin binding proteins (ABPs) [92]. Within a cell, spontaneous and uncontrolled actin polymerization is inhibited by G-actin binding proteins such as profilin and β-thymosin actin [93]. Actin monomers can exist in 3 forms: free G-actins, profilin-actin and β-thymosin actin; of these only the first two represent the polymerizable pool of monomers while b-thymosin-actin is sequestered and hence remains unavailable. β-thymosin prevents monomeric actin from joining actin filaments but participates in exchanging actin with profilin to facilitate regulated actin polymerization [94]. Profilin is considered as a general actin housekeeping factor as it binds G-actin to prevent spontaneous actin nucleation and elongation of filaments at +end [95]. Nucleation or de novo actin filament formation requires assembly of a G-actin trimer, an energetically unfavored step, but *in vivo* it is crucial to execute this step rapidly [96]. Subsequent addition of monomers is more stable, likely due to complementary intermolecular interactive forces [3]. Arp2/3 complex, the first actin nucleator to be discovered, by itself is an inefficient nucleator, but when coupled with nucleation promoting factor (NPF) catalyzes new filament formation from the side of an existing filament to generate a branched structure. Some of the well characterized NPFs include Wiskott-Aldrich Syndrome protein (WASP) and WASP Verprolin homologs (WAVEs). These NPFs utilize allosteric modulation to activate Arp2/3 complex to promote efficiency of actin nucleation [97]. Another group of nucleating proteins, formins, are

multidomain, homodimeric proteins featuring a formin homology2 (FH2) domain that interacts with the barbed end of an actin filament and serves dual purpose as actin nucleators and elongation factors [98]. Formin FH1 domains bind profilin-actin complexes and transport them quickly to the +end associated with the FH2 domain [99]. Formins aid in formation of linear actin filaments and play a key role in structuring stress fibers, actin rings and actin cables [100]. In addition to formins, some other family of nucleating proteins such as, Cobl, TARP, Lmod, JMY, act by stabilizing dimer or trimer [3]. These nucleating proteins regulate the spatiotemporal origin and structural organization of actin networks. After overcoming the rate limiting nucleation step, filament elongation takes place processively by formin activity at the barbed end, and also by a dedicated family of proteins such as Ena/VASP [93]. Ena/VASP antagonize capping proteins and act as processive actin polymerase [101]. Therefore, Ena/VASP promote Arp2/3 complex generated branches at lamellipodia and in filopodia or focal adhesions, promote formation of unbranched F-actin bundles [102]. The filaments can grow freely at the barbed ends until monomer pools are exhausted or capping proteins interfere with elongation. *In vivo*, capping proteins have a higher association rate constant, therefore filaments will be shorter unless provided support from actin elongation factors that shield capping proteins while moving along with the growing +end [100]. The actin filaments can also be combined together to produce higher order structures such as meshworks or actin

bundles by the activity of actin crosslinking proteins such as α-actinin, filamin, fascin, fimbrin,scruin and some formins [103].

In contrast to elongation factors, capping proteins obstruct filament growth by direct binding at the +end [104]. The activity of capping proteins is regulated by competition with Formins and ena/VASP to bind the positive end, and also by direct binding with other proteins such as V-1 or WASH(WASP and SCAR homologue) complex, CARMIL (capping protein, Arp2/3 and myosin linker), and CD2AP (CD2-associated protein) via allosteric hindrance [105]. Lastly, along with the slow disassembly during

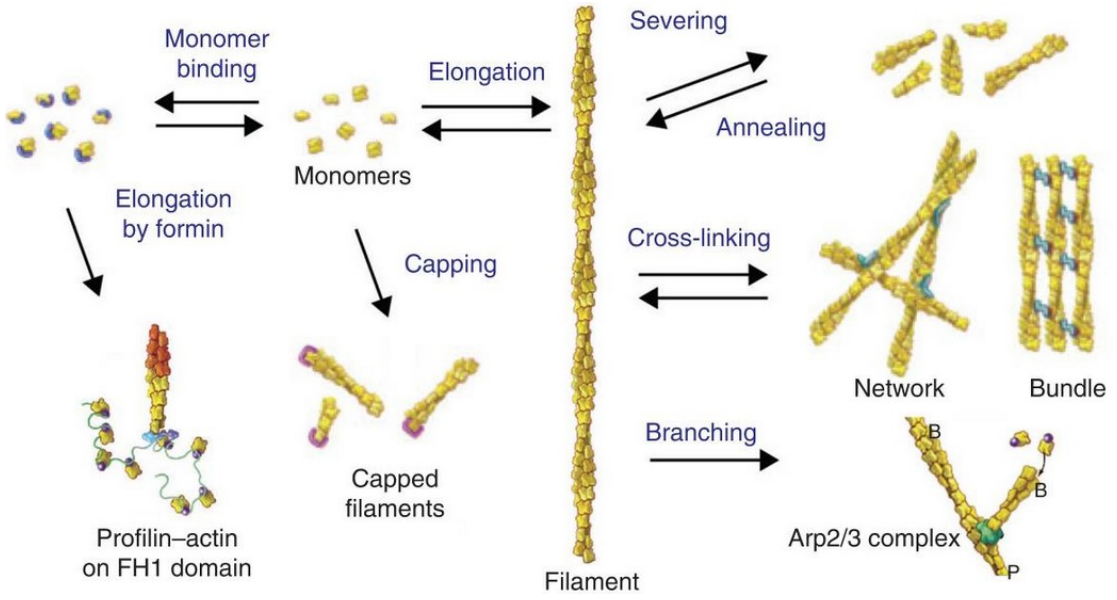

Fig. 1.3. Actin binding proteins and their activity: schematic showing family of actin binding proteins. Figure excludes tropomyosin which binds sides of filaments. Figure adapted from [3] with permission from Dr. Thomas Pollard.

actin treadmilling described previously, there are additional ABPs that lead to actin filament depolymerization. Actin depolymerizing factor (ADF)/cofilin family of proteins can accelerate actin disassembly by promoting filament turnover to restore the G-actin pool. ADF/cofilin preferentially binds ADP-F-actin sub-units instead of newly formed ATP-F-actin at the +end and induce structural change causing destabilization which leads

to filament severing [9]. Following the filament severance by ADF/cofilin activity, the monomers can be recycled back by synergistic activity of cyclase-associated protein (CAP) [106]. In order to generate force and cell membrane movement, actin assembling proteins (such as Arp2/3 complex) collaborate with other proteins such as capping protein, cofilin and profilin to assemble and disassemble motile actin networks [107]. The actin architecture, dynamics and activity of ABPs is largely driven by Rho family of GTPases, described in the next section.

1.3.2 Rho GTPases and signaling networks shape the Actin cytoskeleton

The regulation of actin cytoskeleton at different locations is highly controlled for precise actin reorganization based on the cellular activity (for instance locomotion, changing cell shape, etc.). It is now well established that the family of Rho GTPases act as molecular switches to merge signaling inputs from cell surface receptors via chemical messengers such as cytokines, growth factors are transduced to generate a coordinated output for effector proteins to regulate spatial actin polymerization [85, 108]. The extracellular signal is received by the cell surface receptors (ligand binding to tyrosine kinase receptors, GPCRs), adhesive interactions (ECM and cell-cell adhesion, integrin signaling), or mechanical stress [109]. These stimuli induce Rho-GTPases cycle between two conformations: GTP-bound active state and GDP-bound inactive state. GTPases recognize target proteins when “on” and generate a response by GTP hydrolysis to return to the “off” state [110]. RhoA, Rac1 and cdc42 are considered primary regulators of actin dynamics [111]. RhoA promotes stress fiber formation mediated by effector proteins, mDia1 (mammalian Dia1) and Rho-associated protein kinase (ROCK), where the former facilitates bundling of parallel filaments to make dorsal stress fibers, while the latter activates LIM domain kinase 1 (LIMK1) to hinder ADF/cofilin mediated actin depolymerization [112]. Besides, ROCK mediated phosphorylation inactivates myosin

light chain phosphatase to engage myosin II for the assembly of contractile actomyosin filaments [113]. In lamellipodia, Rac GTPase stimulates WAVE [WASP (Wiskott–Aldrich syndrome protein) verprolin homologous] protein to produce branched protrusions by activating Arp2/3 complex [114]. Cdc42 GTPase also activates Arp2/3 complex through a separate activator, N-WASP (neuronal WASP). Cdc42 promotes filopodia formation after Arp2/3 complex facilitates initiation and mDia mediates elongation [115]. Rho GTPases play a key role in multiple signaling pathways, where they can work synergistically or interfere with the activity of other GTPases. Following is an example of Rho GTPase crosstalk in the context of modulation of actin dynamics. As mentioned previously, RhoA can regulate LIMK via ROCK-dependent phosphorylation to inhibit cofilin mediated actin filament disassembly, in addition, Rac and cdc42 also regulate LIMK activity via a separate effector (PAK1) to phosphorylate cofilin [116]. Furthermore, Rho-actin cytoskeleton interaction also plays an important role in mechanosensing ability of the cell. Dupont et al. reported that Rho and actin cytoskeleton are required to maintain nuclear localization of transcription factors YAP (Yes-associated protein)/TAZ(transcriptional coactivator with PDZ-binding motif) in MSCs, and inhibition of either Rho or actin cytoskeleton sequestered YAP/TAZ in cytoplasm thereby blocking their transcriptional activity [117]. When active, YAP/TAZ can interact with genes such as RUNX2, TBX5 and p73 to regulate gene expression [118]. Therefore, Rho-GTPases work together in modulating actin

cytoskeleton network to fine tune cellular activities such as adhesion, migration and differentiation [116].

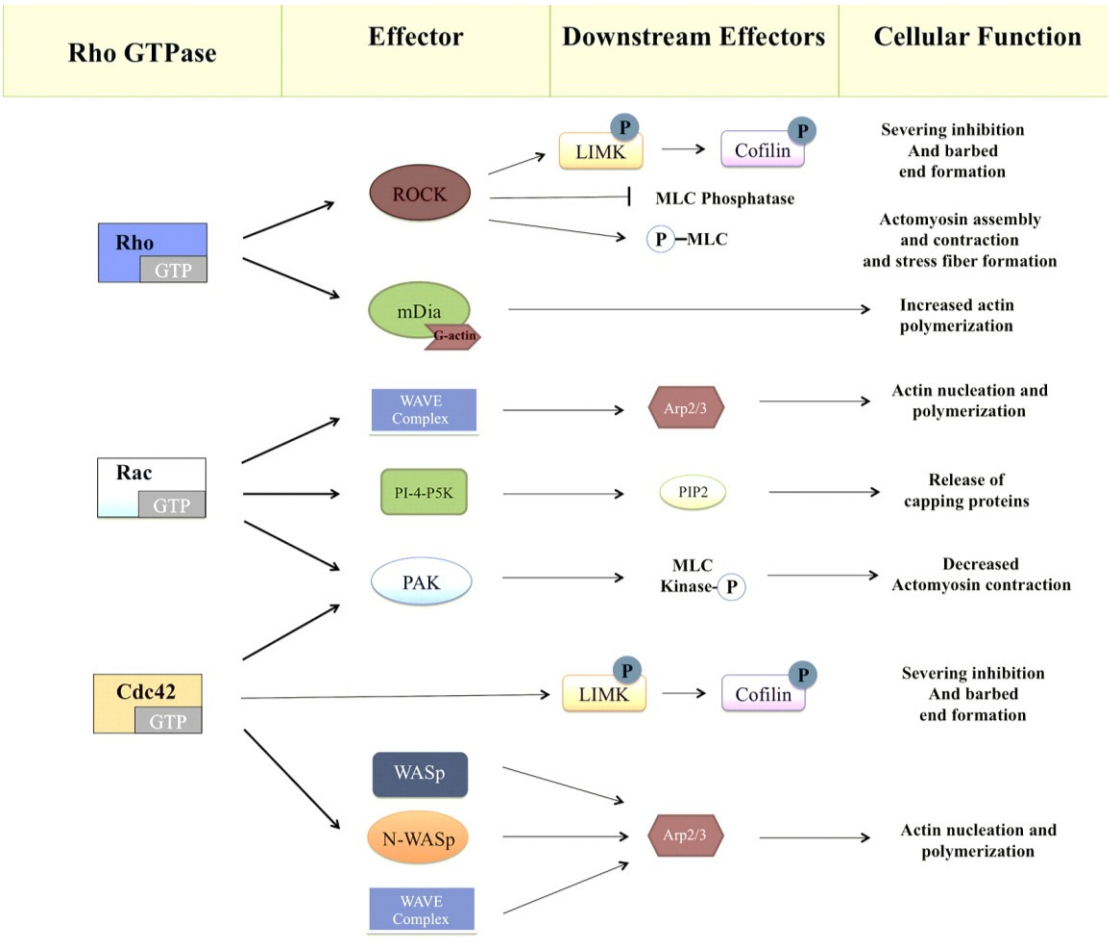

Fig. 1.4. Rho GTPases and downstream effectors: schematic showing three major Rho GTPases, RhoA, Rac and Cdc42 and the function of their effector proteins to regulate actin organizational dynamics. Figure adapted from Hanna et al. [4] (License number: 4874340640701)

1.4. Role of actin cytoskeleton in guiding cellular activities beyond motility

1.4.1 Actin during stem cell differentiation

Cytoskeletal contractile forces play an important role in guiding differentiation. Kilian et al. demonstrated that the cell shape, independent of soluble factors, influences MSC differentiation by involving focal adhesion and myosin-generated contractility [119]. MSCs on soft substrate have less spreading, fewer stress fibers and favor adipogenesis or chondrogenesis; in contrast on stiff substrates, Rho-induced stress fiber formation and actin assembly favors myogenic or osteogenic differentiation [120, 121]. How biophysical cues influence transcription is an important question to understand stem cell response to the microenvironment. Connelly et al. employed micropatterned surfaces to guide epidermal stem cell differentiation but found that differentiation was not affected by ECM composition, but rather the actin cytoskeleton shape regulated the activity of a transcription factor serum response factor (SRF). SRF activity in nucleus induced genes FOS and JUNB correlated with the differentiation to keratinocytes [122]. Cytoskeletal changes are translated to nucleus by shuttling of ABPs. For instance, mDia1 shuttles to nucleus when cytoskeleton is disrupted, to join intranuclear mDia2 and promote filament formation and also induces branching by Arp2/3 complex recruitment to modulate adipogenesis and osteogenesis [123]. Inhibiting gene expression of another ABP, cofilin/ADF or hindering its activation through LIMK1 inhibition in MSCs enhanced cell viability and osteoblastic differentiation, while cytoD mediated inhibition of actin polymerization had the opposite outcome [124]. At molecular level, actin depolymerization reduced FAK, p38 and JNK activation that play an important role in osteogenic differentiation [124].

Even in ESCs, several researchers have reported modulation of cell fates by actin cytoskeleton. In murine embryonic stem cells, cytoskeletal disruption by cytochalasin D resulted in upregulated expression of chondrogenesis markers: type II collagen, Sox9, aggrecan while downregulating stemness markers [125]. Cytoskeletal rearrangement following ROCK inhibitor, Y-27632, promoted neuronal differentiation in embryonic stem cells by extracellular signal-regulated kinase (ERK) maybe activated via Ras/Raf/MEK, the PI3K/PKC or the Cdc42/Rac signaling pathways [126]. Poor survival of human ES cells was considered an obstacle to research due to no option for subcloning, but application of ROCK inhibitor (Y-27632) modulates cytoskeleton which resulted in diminished dissociation-induced apoptosis, promoted survival, increase cloning efficiency, and permitted differentiation to telencephalic progenitors [127, 128]. shRNA-mediated knockdown of serine/threonine kinases or LIMK2 increased mesenchymal to epithelial transition, reduced cofilin phosphorylation and disrupted actin filaments during reprogramming of mouse embryonic fibroblasts, suggesting that kinase networks regulate pluripotency and have a role in cytoskeletal remodeling during somatic cell reprograming [129]. In human ESCs, ROCK inhibition decreases myosin light chain, to promote cloning efficiency of ESCs after dissociation [130]. Y27632 treatment of fibroblast feeder cells induced epithelial reprogramming of cells so they could multiply indefinitely [131].

Similar to ESCs, ROCK inhibition mediated cytoskeletal regulation in iPSCs also promoted plating efficiency with anti-apoptotic effect and also promoted ECM-cells interaction [132]. Cytoskeletal rearrangements were reported to drive the morphogenesis of neuronal precursors and migrating/mature neurons in iPSCs [133]. As another example, Toyoda et al. showed Rho-associated kinases and non-muscle myosin II activity inhibited differentiation of human IPSCs to pancreatic endoderm [134]. Besides *in vitro* studies, iPSCs pretreatment with ROCK inhibitor resulted in increased transplantation

efficiency of induced cardiomyocytes [135]. Therefore, cytoskeletal remodeling plays a key function during iPSC reprogramming, initiation of differentiation and modulation of cell fates.

In general, cells display actin morphological changes during differentiation. In a study that compared mouse embryonic stem cells (ESCs), reprogrammed iPSCs, and embryonic fibroblasts, stem cells showed less developed cytoskeleton in stem cells compared to fibroblasts. Thus, expression levels for SMA, vimentin, lamin A, and nestin were distinctly lesser for ESCs than MEFs. When analyzed, iPSC samples were found to be heterogeneous, with most cells displaying similar patterns of cytoskeletal proteins to ESCs and a small subpopulation alike MEFs. Therefore, dedifferentiation results in return to a less developed state of cytoskeletal remodeling [136]. Besides the aforementioned cells, several studies have shown participation of actin cytoskeleton in guiding differentiation; for example, the expression of actin bundling protein, Fascin in human dendritic cells was found to correlate with dendritic morphology and cell differentiation [137]. Human pluripotent stem cells derived MSCs showed rapid differentiation to neural-like cells when treated with ROCK inhibitor showing characteristic post-mitotic neurons, extensive dendritic growth and neuron-specific marker expression i.e. differentiation was enhanced by cytoskeletal rearrangement [138]. Neuronal differentiation proceeds via substantial reorganization of cytoskeleton and the reorganization is time-dependent [139].

Given the heterogeneity of expression of cytoskeletal markers and actin regulated differentiation in MSCs and iPSCs, a systematic investigation of cytoskeletal dynamics and evolution may provide a rich set of insights into the active differentiation and lineage restriction processes. In chapter 3 and chapter 4, we have explored the potential of actin dynamics as a live-cell profiling marker during MSC differentiation.

1.4.2 Actin mechanotransduction

Mechanical cues direct complex cell behaviors by influencing cellular processes including but not limited to cell spreading, migration, differentiation, and cell division. In-vivo, cells are surrounded by an ECM composed of proteins including laminins, collagens, and fibronectin. Cells have the ability to sense ambient mechanical environment and cytoskeleton plays an important role in responding to the external forces. The term mechanotransduction encompasses overall process of how cells detect a mechanical stimulus and translate it to intracellular biochemical response [140]. Cells interact with ECM proteins using integrins during mechanotransduction to stimulate downstream signaling. For example, in smooth muscle cells, RhoA- regulation of the actin cytoskeleton selectively controls SMC differentiation marker gene expression by influencing serum response factor mediated transcription [141]. Similarly, when MSCs are cultured on stiff substrates, SMA accumulates at stress fibers and transfers the forces to the nuclear membrane via direct physical signaling from linkage proteins and results in upregulated lamin-A, which is associated with increase in osteogenesis [142]. Mechanosensors, YAP/TAZ also localize to nucleus on stiff substrates resulting in upregulation of genes responsible for osteogenic differentiation. YAP/TAZ act as mediators of actin induced downstream signaling as shown in a study where inducing α-SMA overexpression resulted in YAP translocation to the nucleus, while knockdown of YAP rescued the reduced adipogenesis [143]. Liu et al. demonstrated that actin cytoskeleton can influence nuclear mechanics via SUN1, a component of LINC complex (linker of nucleocytoskeleton and cytoskeleton) by physical pairing of nucleus with the cytoskeleton. In the paper, disruption of actin with cytochalasin D led to reduced nuclear area and stiffness, while stabilizing with jasplakinolide had the inverse effect, and SUN-1 was found to play an important role in cell migration [144].

The principles of mechanotransduction mediated by actin cytoskeleton can be dissected in detail through the use of engineered biomaterials. By varying nanotube dimensions of self-assembled TiO_2 nanotube arrays on Ti substrates, Oh et al. were able to promote cell adhesion and elongated stem cells showed increase in cytoskeletal stress fibers and osteoblastic differentiation [145]. When cultured on nanoscaled surface patterns, ESCs increased proliferation and colony formation, and the size of 200-280nm patterns drastically promoted cardiomyocyte differentiation and expressed early cardiac marker gene Mesp1 and cardiomyocytes. These patterned ESCs elicited vinculin and p-cofilin-mediated cytoskeleton reorganization, showing a strong involvement of the cytoskeletal dynamics [146]. Similarly, when cultured on groove ridge structures with periodicity in micrometer range, iPSCs elongate and rearrange the actin filaments. Subsequent, BMP-4 induced differentiation was enhanced in elongated colonies, and led to spatial modulation of YAP/TAZ (mechanosensors) activity upon induction [147]. *In vitro* cultures of human pluripotent stem cells are marked by the actin fence encircling the colony, which exerts extensive Rho-ROCK-myosin-dependent mechanical stress to instruct colony morphology, pluripotency, compaction, and mitotic spindle orientation [148]. Interestingly, engagement of mechanotransduction pathways by cytoskeletal manipulation is also capable of reprogramming HEK293 cells, simply by culture on soft substrate without using transcription factors, then after replating on glass (rigid surface), led to redifferentiation, i.e. cells showed close association of stemness to actin tension [149]. Understanding the importance of actin cytoskeleton and mechanotransduction is particularly important in selecting biomaterials for promoting therapeutic efficiency of MSCs. For instance, Abdeen et al. performed single cell micropatterning to prime MSCs, within 2 days, activated cells showed elevated pericyte markers and association with endothelial cells in co-culture [150]. Understanding mechanotransduction principles is

important for developing tissue culture protocols and platforms for MSC applications, for instance, cell culture on rigid tissue culture ware shows limited myogenic differentiation (1-2% positive for desmin and myosin heavy chain proteins) [58]. Biomaterials can be used to closely mimic mechanical microenvironment. Ferlin et al. described a dynamic stem cell culture platform by combining a biomimetic scaffold with a perfusion bioreactor where scaffold chemistry and stiffness is changeable [151]. New culture systems have started to focus on involving actin cytoskeleton modulation to control MSC differentiation. Sart et al. harnessed gelatin-based microcarriers to control actin cytoskeleton during MSC expansion and achieved efficient MSC differentiation demonstrating promise for this approach in a microcarrier based bioreactor [152]. Realizing the importance of instructive mechanical environment, new high throughput hydrogel arrays have been reported with 3D configuration and adoptable stiffness in a high throughput design [153]. Our lab has published several studies that involved mechanotransductive biomaterials to alter cytoskeleton. When cultured on polymer films with varied polyethelyene glycol composition, the cells reorganized their cytoskeleton in a distinct manner. Furthermore, cell culture on more hydrophilic self-assembled monolayer resulted in loss of stem cell marker (CD90) and concurrent increase in adipogenic differentiation[154]. In another study, we engineered micropatterned substrates in collaboration with Kohn laboratory (Rutgers University), where cells on co-continuous patterns that enabled cell spreading showed increased osteogenesis whereas discontinuous islands led to reduced MSC differentiation[155]. Therefore, altering surface geometry engages mechanosensory mechanisms in cells primarily via actin cytoskeleton modulation.

1.4.3 Actin in aging

Actin cytoskeleton has been reported widely to be altered during the course of aging in cells. Gourlay et al. reported that an increase in actin dynamics by genetic manipulation

resulted in increase in cellular lifespan by over 65% while decreased actin dynamics resulted in compromised mitochondrial membrane, increased ROS production and increased cell death [156]. In human skeletal muscle, β-actin levels were found to decline as a result of aging [157]. Cells derived from aged animals also showed decline in actin dynamics, abnormal ABPs and Rho signaling. Old liver-specific p38α MAPK knock out mice displayed decreased F-actin polymerization along with a marked deterioration of actin cytoskeleton. This was linked with unusually high activity of RhoA and Cdc42 GTPases. Prolonged p38α deficit resulted in inactivation of HSP27, causing actin cytoskeleton damage, manifesting in decreased number and length of actin filaments in isolated hepatocytes [158]. Even in budding yeast, increase in retrograde actin cable flow promoted mitochondrial and cellular fitness and extended lifespan, therefore, actin dynamics influence mitochondrial quality control during aging [159]. Aging induced neurodegeneration has been associated with altered actin cytoskeleton. Rat hippocampal cultures showed abnormal cofilin-actin aggregates which disrupted dendritic microtubule integrity, by blocking intracellular transportation of both mitochondria and early endosomes [160]. Furthermore, cofilin rods were detected in aging rat brains suggesting that cofilin aggregation may lead to neurodegeneration and brain aging by impeding intracellular trafficking and inducing synapse loss [160].

Lastly, Kasper et al. harnessed functional annotation clustering to reveal that age-affected biomolecular signals are connected with cytoskeleton organization and antioxidant function. These proteome screening results were in agreement with lowered actin turnover and antioxidant power in aged MSCs. Therefore, aging related cytoskeletal aberrations resulted in diminished sensitivity to biomechanical signals due to a less dynamic actin cytoskeleton. Since MSCs are susceptible to senescence *in vitro*, and

involvement of actin cytoskeleton has ample evidence [161], we specifically explored how actin dynamics changes during *in vitro* aging of MSCs.

Thesis overview

Chief among the barriers to the widespread use of stem cells in therapy and tissue engineering are the poor characterization of these cells in their living state and the single cell heterogeneity inherent to their functionality. MSC populations display heterogeneity at multiple levels: intra-population, intra-clonal, inter-donor. This raises an important question: how to predict the behavior of MSCs in culture and after large scale expansion prior to clinical applications? Unfortunately, most of the standard methods to determine the biological properties of MSCs are terminal assays that overlook population level variations among the cells. Further, due to inherent heterogeneity of stem cell sub-populations, cellular response to extracellular cues (growth factors, mechanical cues etc.) remains non-uniform, with each cell following a different chronological trajectory towards the ultimate desired phenotype. Thus, there is an urgent need to develop innovative assays that enable continuous monitoring of live cells to illustrate distinct cellular states. To this end, we have advanced a novel fluorescence imaging-based platform that is straightforward by design yet enriched with temporal data to generate a comprehensive profiling tool-box for dissecting phenotypes and functions of evolving stem cell populations. Our method employs probing of dynamic changes via an F-actin specific probe, sir-actin, which offers a unique opportunity to use actin turnover as a marker. Prior to this work, the majority of literature pertaining to stem cell research has focused primarily on visualizing cytoskeleton after fixing the cells that allowed data acquisition at discrete time-interval. The question that largely remains unaddressed is, what new

insights, ideas, and regenerative strategies can emanate from the live imaging of actin cytoskeleton in stem cell research?

Actin cytoskeleton and associated signaling pathways are clearly involved in determining stem cell behavior during differentiation, mechanotransduction and immunomodulation. All these factors govern the translatability of stem cells for clinical usage. We believe that by describing early phenotypic divergence during stem cell specialization towards a tissue phenotype, it might be possible to forecast their behavior much earlier compared to traditional time-consuming and end-point biochemical assays. We hypothesized that temporal characterization of actin dynamics can be used as a surrogate marker to track function specific kinetic changes in cells. For example, previously, our laboratory utilized high content image analysis using multiple cyto-nuclear markers such as SC35 (serine/arginine rich splicing factor 35)[37, 162], NuMA (nuclear mitotic apparatus, protein)[163, 164] and histone epigenetic marks[165] along with actin[84, 154, 164]. Despite the progressive advances in our ability to gain early insights into the evolution of cell states, the earliest we could reliably discern the differentiating cells from the naïve cells was after 24 hours of stimulation to the soluble cues. The cytoskeletal dynamics based imaging approach that this thesis proposes can shrink the time window further. In chapter 3, we were able to demonstrate the effect of cell state transition in response to soluble cues as early as few minutes. Another hurdle for stem cell applications (particularly for MSCs) is the issue of ongoing *in vitro* senescence. Here again, actin turnover probing allowed us to parse aged cells from young cells within one-hour. In chapter 4, we conducted deeper studies to establish the relationship between actin turnover and gene expression during lineage divergence. In addition to MSCs, even iPSCs showed co-occurrence of change in actin turnover along with the lineage specific markers. To our knowledge, actin dynamics have yet to be used as a determinant to isolate

phenotypically variant stem cells. Using sir-actin, we were able to collect cells on the basis of their inherent actin turnover which allowed us to investigate the role of cytoskeletal dynamics in determining MSC differentiation potential. A concerted insight from our studies is the concept of “cytoskeletal memory” in the sorted cells, where even after passaging, the cells retained the elevated differentiation potential compared to the heterogeneous populations.

The approach of fluorescence labeling of actin for live-cell probing is amenable to several fluorescence-based assays such as live-cell imaging, multiplex immunolabeling, flow cytometry and cell sorting. This thesis supports the use of actin-turnover as a versatile marker by adding the temporal dimension to stem cell phenotypic analysis.

Chapter 2: Dynamic fluorolabeling of cytonuclear mechanoreporters for temporal profiling of live cells

2.1 Abstract

In recent decades, stem cells have widely examined for their functional versatility in therapeutic applications. The traditional methods used for characterization of cellular functions, such as differentiation, are inadequate as they rely on assays that are not suitable for live cells and fail to capture the intrinsic heterogeneity among the cell populations. To address these limitations, we examined the feasibility of various live-cell compatible fluororeporters to monitor dynamic changes in single cells. This approach would be particularly useful to the characterization of mesenchymal stem cells whose early kinetics of the lineage specific changes are still unexplored. To this end, plasmid constructs were genetically manipulated to produce fluorescently labeled panel of nuclear (HP1α and SC35) and cytoplasmic (actin, YAP, TAZ) reporters in a regulated manner to generate a rich data set for high content image analysis. The constructs were successfully delivered via lentiviral vectors. Following lentivirus mediated transgene insertion in cells, we were able to eliminate non-transduced cells by puromycin selection to select only the fluororeporter expressing cells. Despite the successful generation of stable fluororeporter expressing cells, we observed that the lentiviral treatment interfered with MSC differentiation. Still, the platform developed could be useful in other applications involving mechanobiological pathways.

2.2 Introduction

Mesenchymal stem cells (MSCs) are stromal cells that have the ability to self-renew and exhibit multi-lineage differentiation potential. Although there is a lack of consensus for defining MSCs from various sources, yet the widely accepted minimum criteria of MSCs include: i) plastic adherence during standard culture conditions; ii) expression of CD105, CD73 and CD90, and lack expression of CD45, CD34, CD14 or CD11b, CD79alpha or CD19 and HLA-DR surface molecules; and iii) ability to differentiate to osteoblasts, adipocytes and chondroblasts *in vitro* [24]. MSCs could be expanded *ex vivo* and induced, either *in vitro* or *in vivo*, to differentiate to other lineages namely tenocytes, myotubes, neural cells and hematopoietic-supporting stroma as well [166, 167]. The ease of harvesting and expansion of MSCs from these sources make them highly suitable for *in vitro* research and clinical applications [167]. MSC based therapeutics in tissue engineering is also supported because of their paracrine, immunosuppressive, pro-angiogenic and immunomodulatory effects [168, 169]. MSCs have been employed extensively for transplantation studies in animals and clinical trials for regenerative medicine [170]. By definition, MSCs should demonstrate clonogenicity and tripotency, but only a small subset exhibits multipotency, indicating that MSCs are comprised of a heterogeneous population [26].

The classical methods for phenotypic evaluation of MSC differentiation include: alcian blue staining for chondrogenesis, ALP and alizarin red S staining for osteoblasts, and oil red O staining for adipocytes [66]. The protein expression level of differentiation related genes could be assayed by immunostaining [67, 68]. The transcriptional activation of differentiation related genes could be assessed by quantitative qPCR with common osteogenic (such as RUNX2, ALP), adipogenic (e.g., PPARγ, CEBPα), chondrogenic (COL2A1, SOX9) genes [66, 171]. Quantitative biochemical assays are also available for

various lineages: osteogenesis (ALP enzyme activity) [172], chondrogenesis (sulfated glycosaminoglycan) [173] and adipogenesis (triglyceride accumulation) [174]. These methods have several limitations. qPCR is destructive, reagent intensive and tedious. Immunostaining is qualitative in nature and requires expensive antibodies. All of these assays require 1-4 weeks of growth factor mediated induction in cell culture which adds to the overall cost [175, 176]. Moreover, these classical methods are end-point assays so the MSCs cannot be recovered for further testing. Thus, there is a need to develop new methods for assessment of MSC differentiation to overcome these challenges.

Our research group has published multiple studies on a high content image informatics based platform of key protein reporters to track the state of single cells at early time points in response to extracellular cues [37, 84, 163, 165, 177]. In spite of the insights these investigations enabled, all these studies were performed with fixed cells, which limits the data informatics to discrete timepoints. We hypothesized that a diverse array of reporters compatible with live cells might be better suited for dynamic assessment of stem cell behavior and cell states during differentiation. To this end, we designed lentiviral particles to introduce fluorescently labeled panel of reporter proteins to MSCs. Lentiviral vectors are a type of retrovirus that possess the capacity to efficiently infect non-dividing cells, carry large coding sequences, and provide stable long-term transgene expression making them suitable for gene delivery [178].

The candidate reporters used in this study included mechano-sensory proteins such as, actin, SC-35, YAP, TAZ, , and HP1α. The dynamics and organization of cytoskeletal actin network are well known to play a role in cell differentiation [179]. YAP (Yes-associated protein) and TAZ (transcriptional coactivator with PDZ-binding motif) act as

sensors and mediators of mechanical cues instructed by cellular microenvironment during MSC differentiation [117]. Splicing factor, SC-35, is a sub-nuclear protein that possess organizational domains with textural attributes that could be used for classifying emergent stem cell phenotype during MSC differentiation [37]. HP1α (Heterochromatin protein-1α) is an important epigenetic regulator of heterochromatin-mediated gene silencing and differentiation specific transcriptional activation [180]. These fluororeporters were genetically synthesized and lentiviral particles were generated. The lentiviral vectors were successful in generating fluororeporter expressing cell lines. The fluororeporter expression array was further characterized during lineage divergence in MSCs, however the transduced cells showed a decline in cell differentiation. Nonetheless, our array of reporters showed promise to monitor phenotypic organizational changes in live cells.

2.3 Material and Methods

2.3.1 Generating inducible tet-on plasmid system

The inducible plasmid system was engineered by cloning TRE (Tet Response Element) from GenScript on to the plasmids carrying the reporters SC35, HP1α, YAP and TAZ within the MyoD-T2A-dsRedExpress2 backbone (Courtesy of Dr. Rick Cohen and Dr. Anandika Dhaliwal, Rutgers University). Briefly, 3 μg TRE (Tet Response Element) sequence carrying plasmid from GenScript was restriction digested with XhoI and NheI, and the resulting linearized fragment was run on 1% agarose gel prepared in Tris/Borate/EDTA (TBE) buffer. The fragment was extracted from the gel. The TRE sequence was ligated on the plasmid carrying the MyoD backbone. The resulting product was transformed in One Shot™ Stbl3™ Chemically Competent E. coli and plated on agar plates in the presence of Carbenicillin antibiotic overnight. Single colonies were picked and plasmids were isolated using QIAGEN Miniprep Kits. The final fluororeporter

construct was validated by sequencing from Macrogen using two primers specific to all 4 plasmids: CMV-MM-P-F (5'-atccacgctgttttgacctc-3') and TURBOGFP-R (5'-GATGCGGCACTCGATCTC-3) [Integrated DNA Technologies].

2.3.2 Cell culture

Human mesenchymal stem cells (hMSCs) were obtained from Texas A&M University (College Station, TX). Cells were cultured in the presence of 5% CO_2 at 37 ^oC. The cells were maintained in basal growth media (BA) [Minimal Essential Media alpha (MEM, ThermoFisher Scientific), 10% Fetal Bovine Serum (Atlanta Biologicals), 0.1% Penicillin-streptomycin (Gibco™)]. Cells were received at passage 1 and used for up to 8 passages. Cells were sub-cultured upon reaching 70-80% confluence by lifting the cell monolayer with trypsin and seeded at 2000-3000 cells/cm^2 for maintenance. For differentiation studies, a density of 10,000 cells/cm^2 was used in 96 well dish. Cells were allowed to attach overnight, then stimulated with differentiation media for up to 14 days unless specified otherwise. Adipogenic media was prepared by supplementing BA with insulin, dexamethasone, indomethacin, and 3-isobutyl-1-methyl-xanthine. Osteogenic media was formulated from BA supplemented with dexamethasone, L-ascorbic acid-2-phosphate, and β -glycerophosphate.

HEK293 cells [293FT, Invitrogen, gift from Dr. Cohen, Rutgers University] were cultured in Dulbecco's Modified Eagle Medium (Gibco™), supplemented with 10% fetal bovine serum, 1X non-essential amino acids (Gibco™), 1% Penicillin-streptomycin (Gibco™) and 500μg/mL G418, Geneticin (ThermoFisher Scientific). Upon reaching 70-80% confluence, the cell monolayer was disrupted by trypsin and cells were passaged at the seeding density of 20,000-50,000 cells/cm^2 in T-75 cm^2 flask.

2.3.2 Preparing lentivirus particles carrying the inducible reporter system

Lentiviral particles were generated by co-transfecting lentiviral components along with the inducible reporter system in Human embryonic kidney 293 (HEK293) cells. We used a 2nd generation lentiviral system consisting of psPAX (packaging plasmid), pMD2.G (envelope plasmid), and pCEP4-TAT (transcription transactivator plasmid). After transfections, the supernatant carrying the lentivirus was harvested for 2 consecutive days. Successful transduction of difficult to transduce cells (such as MSCs) require preparation of highly concentrated viral stocks [181]. The lentiviral particles were concentrated 100-fold by pooling the supernatants from the two time-points and subjected to ultra-centrifugation [181]. The lentiviral particles were frozen and stored at -80 degrees until further use.

2.3.3 Lentiviral transduction of cells

HEK293 and MSCs were seeded their respective growth media as mentioned in "cell culture" and allowed to attach overnight. Viral infections were performed in Opti-MEM™ (Gibco™) for HEK293 cells or serum free media without antibiotics for MSCs for 8-12 hours. Then regular growth media was added on top for another 12 hours to ensure high transduction efficiency. The TET-on fluororeporter expression was induced by adding 1 μg/mL doxycycline (tetracycline derivative[182]) for 48 hours. For late MSC differentiation studies (14 days), doxycycline was added one day prior to imaging (13th day) to get optimal fluororeporter expression. Stably transduced cells were selected by supplementing the growth media with 1 μg/mL puromycin.

2.3.4 Cell viability assay

The CellTiter 96® AQueous One Solution Cell Proliferation Assay (Promega) was conducted to evaluate the effect of lentiviral transduction on MSC viability. Briefly, cells were cultured at a density of 10,000 cells/cm^2 in a 96 well plate and transduced with lentiviral particles via introduction to the growth media as described previously. The 4 test groups included virus +doxycycline, virus-doxycycline, doxycycline only and untreated cells. Cell viability was assessed by adding Aqueous One Solution in each well after 1, 2 and 3 weeks of initial treatment and incubated for 1 hour. Subsequently, the absorbance was measured with a multi-well plate reader at 490 nm.

2.4 Results

2.4.1 Engineering inducible plasmid system for live-cell profiling

Our objective was to express mechano-sensitive fluororeporters in a regulated manner to study temporal organizational changes in live cells. Tetracycline-inducible plasmid constructs were created that express fluororeporter upon addition of tetracycline (TET-ON). The reporters used in this study included actin, YAP, TAZ, SC-35, and HP1α. As described previously, the aforementioned diverse panel of mechanosensitive proteins possess the potential to be a dynamic marker for induced differentiation and cytoskeleton tension in hMSCs. To engineer the constructs, each reporter plasmid was cloned on human MyoD-T2A-dsRedExpress2 backbone (Courtesy Dr. Rick Cohen and Dr. Anandika Dhaliwal, Rutgers University). To add the TET-ON sequence, TRE (Tet Response Element) carrying plasmid from GenScript was restriction digested and cloned on to each reporter plasmid. Fig. 2.1 depicts the general construct synthesized for each reporter. The final construct was RFP labeled for one of the four reporters: YAP, TAZ, SC35 and HP1α along with Lifeact-TurboGFP for actin. The plasmids were expanded by maxi-preps and sequencing was conducted with fluororeporter specific primers to ensure the correct

sequence of the constructs. Furthermore, an insert specific restriction digestion reaction was performed with NheI and the resulting products were run on gel to validate the constructs.

2.4.2. Generating inducible fluororeporter expressing cells for live-cell imaging

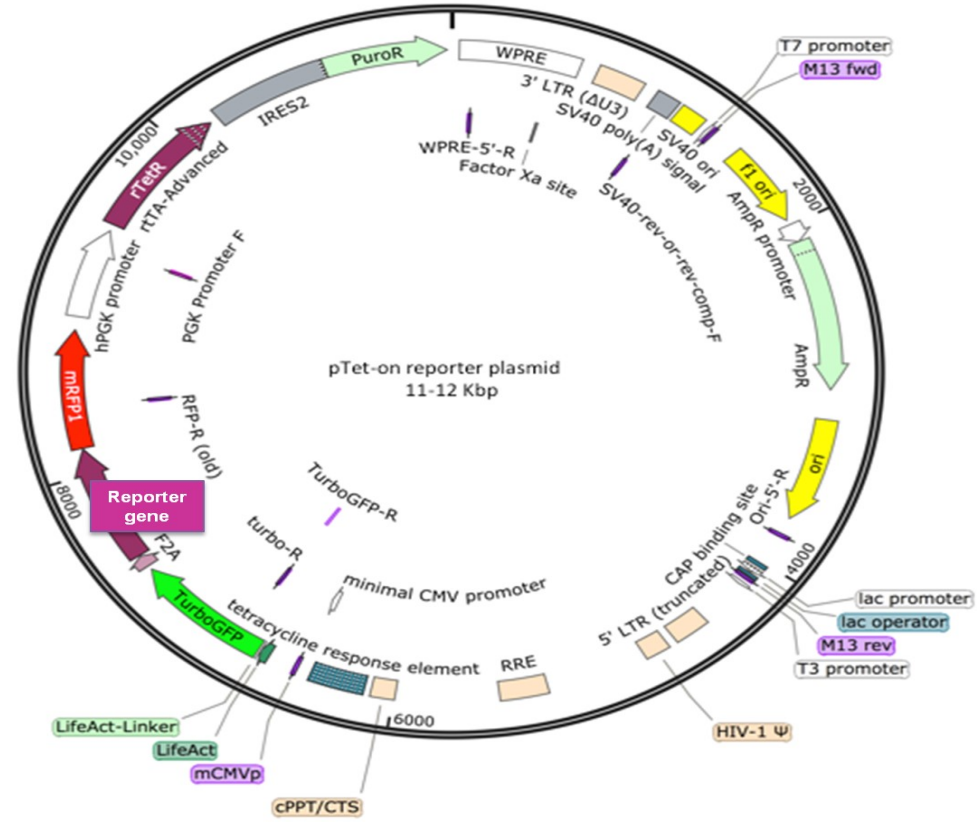

Fig. 2.1. Design of Tet-inducible construct for reporter genes: the plasmid consists of sequence for LifeAct-TurboGFP and one of the four mRFP-reporter genes (SC-35, HP1α, YAP or TAZ). The expression of fluororeporters was dependent on Tetracycline Response Element (TRE) that requires tetracycline to turn on gene expression. Puromycin resistance was imparted by PuroR fragment that could be used for stable cell selection.

Initial validation of the fluororeporter expression of the lentiviral constructs was conducted with HEK293 cells. After 24 h of lentivirus infection, the reporter transgene was activated by doxycycline (DOX) stimulation, and fluorescent images were taken after 2 days of stimulation [Fig.2.2]. In the preliminary study, we used same titers of the

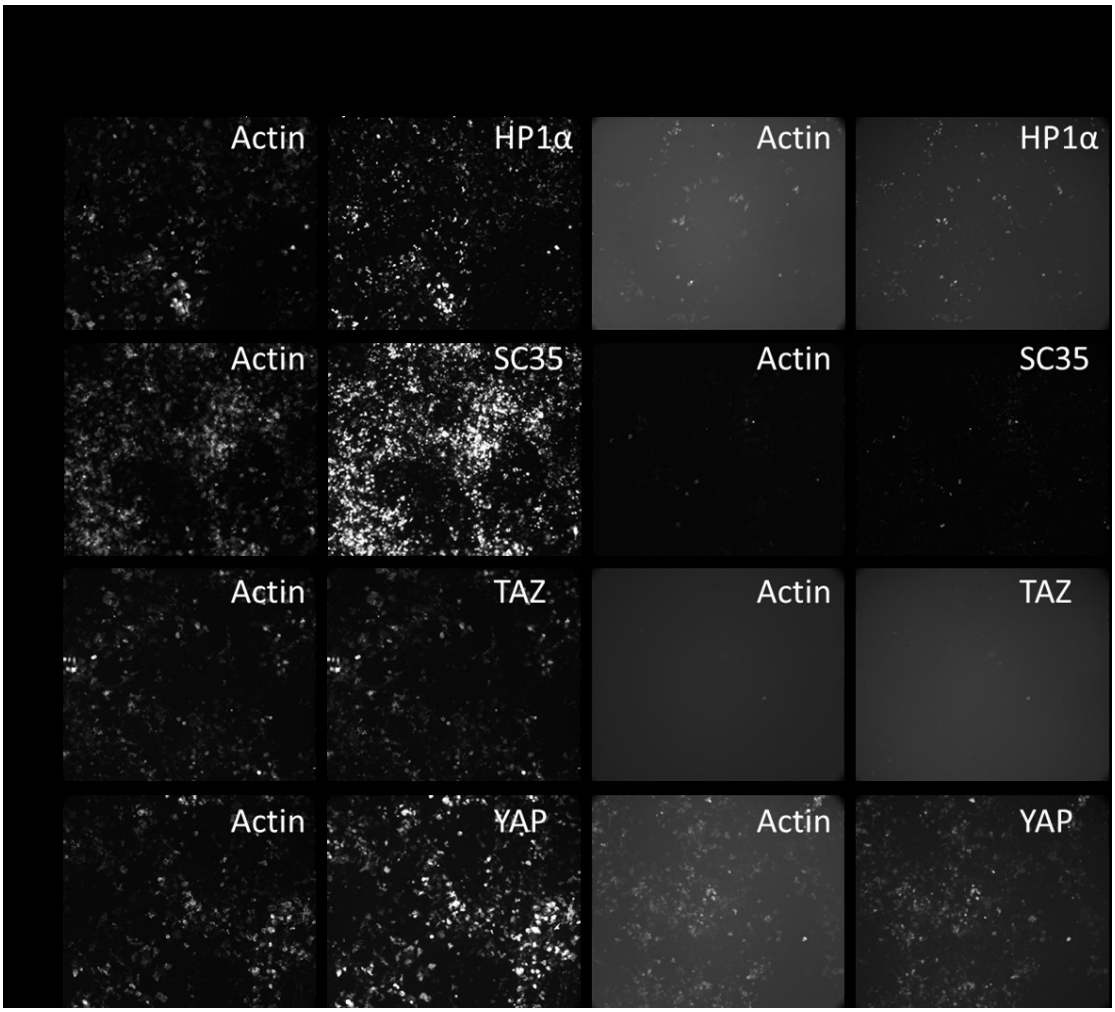

Fig. 2.2. Inducible fluororeporter expression in HEK293 cells: HEK293 cells were transduced with RFP labeled HP1α (A), SC-35(B), TAZ(C), or YAP (D) and LifeAct-TurboGFP was present in all reporters. The panel show fluororeporter expression with or without doxycycline treatment for 48 hours.

concentrated virus to determine the relative expression of each fluororeporter. SC35 and YAP showed brighter fluororeporter expression compared to HP1α and TAZ after DOX

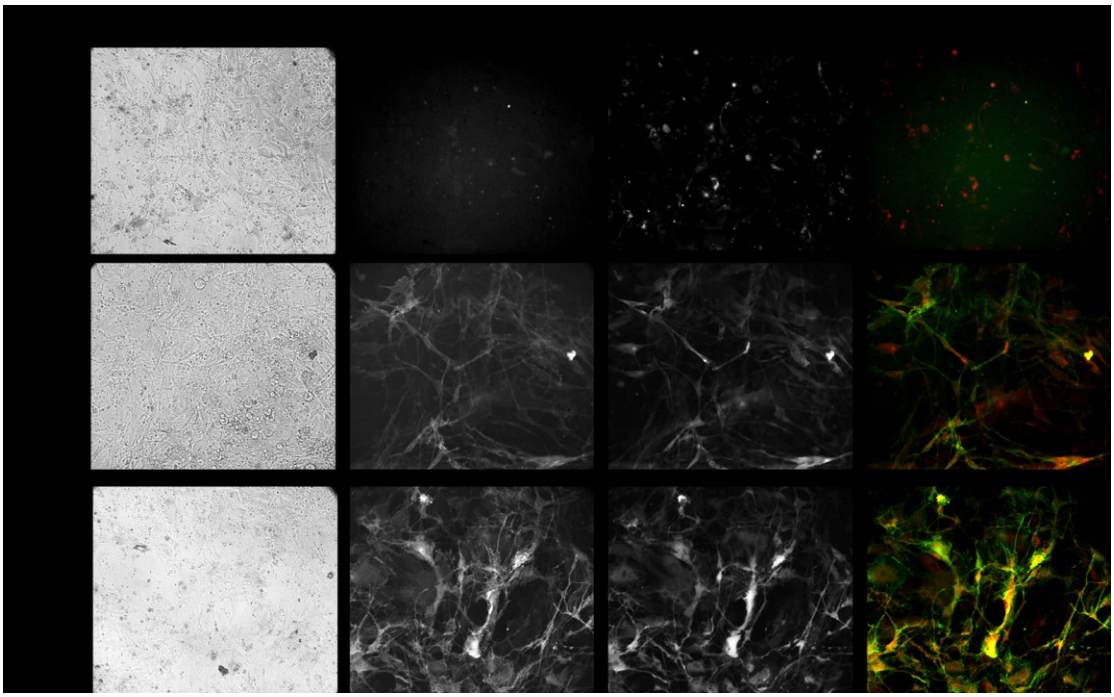

Fig. 2.3. Fluororeporter expression in MSCs after puromycin selection: Representative images showing fluororeporter expression (LifeAct-TurboGFP in green, YAP-RFP in red) in puromycin selected MSCs after Doxycycline stimulation for 48 hours.

treatment. The expression of Lifeact-TurboGFP (actin) was lower compared to all other fluororeporters. The cells without DOX treatment showed basal level expression of the fluororeporter, but overall, a comparison of the basal expression compared to +DOX group showing the successful generation of inducible reporter system for live cells. The cells with integrated lentiviral expression were subsequently selected by cell culture in the presence of 1μg/mL puromycin containing media. The puromycin selected cells upon

stimulation with DOX showed stable expression of fluororeporters demonstrating the successful generation of a stable fluororeporter cell line [Supplementary Fig 2.1].

After successful generation of stable HEK293 cell line that stably expressed the fluororeporters, we sought to create analogous transgene expressing human Mesenchymal

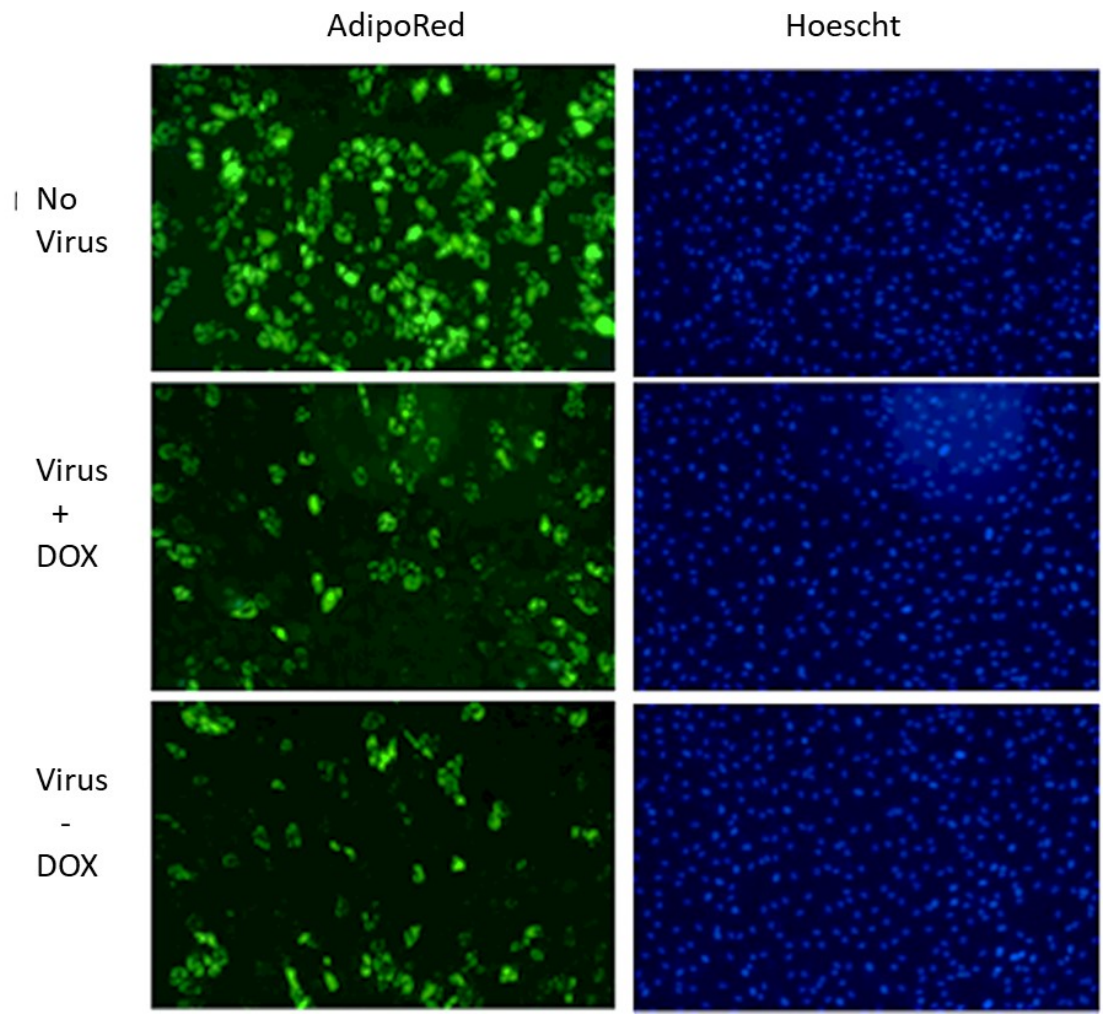

Fig 2.4. Adipogenic differentiation following lentiviral transduction: Representative images showing AdipoRed stained cells to mark adipocytes after 14 days of cell culture in AD media following lentiviral transduction. Regardless of fluororeporter transgene activation by doxycycline, diminished adipogenesis was observed after transduction.

stem cells (MSCs). After lentiviral infections, the MSCs were cultured in the presence of puromycin (1 μg/mL), which resulted in extensive cell death. The surviving cells were maintained in growth media to acquire adequate cells for future experiments. However, after reaching the density of 70-80% confluence, the cells were unable to expand any further. In addition, the cells had a distorted morphology indicative of senescence [183]. Doxycycline stimulation resulted in expression of the fluororeporters, but these cells were not used for subsequent experiments as they failed to proliferate. Therefore, the subsequent live cell studies were conducted after transient lentiviral infections without puromycin selection.

2.4.3. Dynamic cell profiling during MSC differentiation after lentiviral infections

The primary objective of this study was to characterize the dynamic changes in the mechanotransducive reporters to characterize temporal changes in cell states during cellular processes, particularly during lineage stratification. As mentioned in the above section, the stable cell lines failed to grow, so we focused on transient transfection of lentiviral particles prior to initiation of cell differentiation. Cell viability after viral transduction was assessed by MTS assay after 1, 2 and 3 weeks of transgene activation by DOX treatment [Supplementary Fig. 2.2]. The later timepoints showed slightly reduced cell viability in the cells with lentiviral particles but the viability was still >75% compared to untreated control cells. Next, the influence of lentiviral particles on MSC differentiation was assessed. Cells were exposed to the viral particles for 24 hours, then cells were cultured in BA, AD or OS media for 2 weeks. The adipogenic differentiation was assessed by AdipoRed staining which labels the lipid droplets in the adipocytes. Both virus+DOX or virus only groups showed reduced number of cells with lipid droplet accumulation

compared to the uninfected group. Given that adipogenic differentiation is favored by high cell density, reduced cell number after 2 week of lentiviral treatment might also have contributed towards reduced adipogenesis (Fig. 2.4) [184]. Fluorescent imaging showed lack of expression of HP1α and actin in the cells with lipid droplet accumulation [Supplementary Fig. 2.3], suggesting that successful lentiviral infection of MSCs interfered with adipogenesis. Additionally, osteogenic differentiation was assessed after fast blue staining to mark the osteoblasts. Qualitatively, all experimental groups had similar fast blue staining, however no overlap between fast blue staining and the expression of Lifeact-TurboGFP was observed (Fig. 2.5). Typically, osteogenic differentiation is expected to

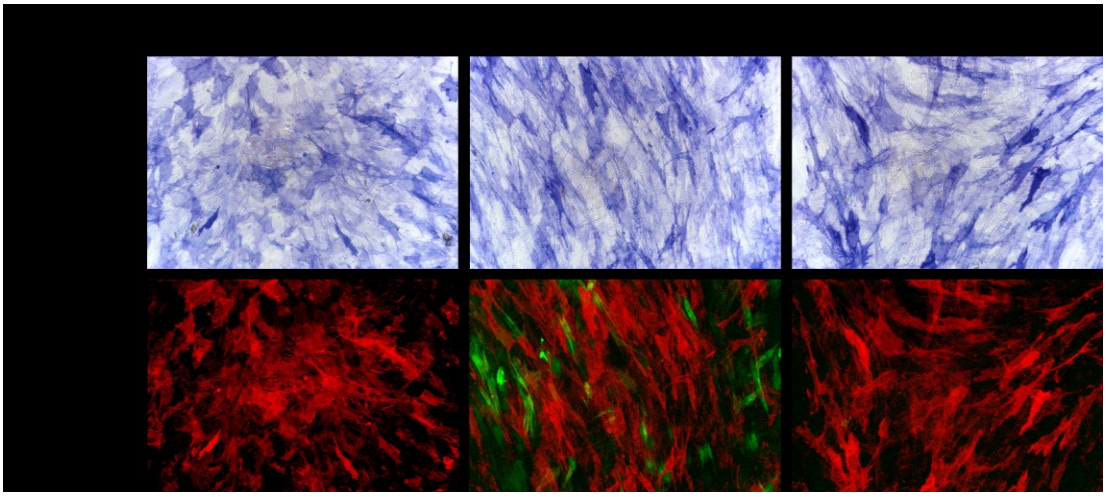

Fig. 2.5. Osteogenic differentiation following lentiviral transduction: Representative images showing Fast blue stained cells to mark alkaline phosphatase positive cells (osteoblast marker) after 14 days of cell culture in OS media following lentiviral transduction. The brightfield images shows the actual fast blue staining. In the bottom panel fast blue image was inverted and pseudocolored in red, while lentiviral LifeAct-TurboGFP reporter is shown in green. The lack of co-occurrence of the two reporters suggest that successful expression of lentiviral reporter interfered with osteogenesis.

demonstrate extensive network of intertwined actin fibers [185]. Similarly, other lentiviral reporters also showed no overlap with fast blue staining cells (data not shown). The lack of fluororeporter and fast blue co-staining demonstrated that MSCs that were stably infected by the lentivirus lost their ability to undergo osteogenic differentiation.

2.5 Discussion

In this study, our objective was to develop a live cell fluororeporter platform that would lend itself to a cell-fate predictive system capable of tracking temporal change in cell states. Our approach involved design and introduction of fluorescence tagged mechanosensory panel of reporters via lentiviral mediated transgene integration in MSCs. To this end, we were able to create stably transduced cell lines for HEK293 and MSCs. The modified MSCs were subsequently characterized for live-cell imaging during lineage stratification.

We developed a robust live cell profiling platform with several desirable features attributed to the inducible fluororeporter expression. Usually, stromal cells such as MSCs are considered difficult to transfect [186], but with our system we were able to achieve high levels of fluororeporter expression. Previously, our first generation of lentiviral constructs were designed sans the inducible element, which led to overexpression of the reporter proteins that negatively affected the cells. The modified TET-on lentiviruses allowed a regulated expression of the reporter proteins, which was found to be inducible for at least up to 3 weeks in live cells (data not shown). These reporters had the potential to monitor the morphometric temporal changes in the mechanosensory reporters from immediate early stages during differentiation up to a lineage committed cell state. During live-imaging, photobleaching of the fluororeporter presents a challenge during prolonged imaging, but our platform overcame this limitation as reinduction with doxycycline allowed expression of the fluororeporter at will. Our lentiviral particles were able to

successfully integrate within the host cells, and the cells could be selected by puromycin treatment as demonstrated by two different cell lines in this study, HEK293 and MSCs, showing that they could be used in other human cells as well.

We report that the array of inducible lentiviral particles used in this study interfered with MSC differentiation. One of the possible reasons could be that our viral transduction protocol involved Polybrene (hexadimethrine bromide), a cationic polymer, a widely used chemical to increase the efficiency of retroviral transduction [187]. Lin et al. reported that polybrene severely inhibits MSC proliferation, even with growth factor supplementation and also potentially hinder MSC differentiation [188]. Without polybrene, transduction efficiency is reduced [188]. Therefore, alternative transduction protocol or an alternative chemical to aid transduction could potentially alleviate reduced MSC differentiation. A few studies have reported that doxycycline could influence *in vitro* differentiation. For instance, doxycycline treatment was found to antagonize BMP2-mediated osteogenesis with human periodontal ligament cells [189]. Another study harnessed microarray analysis after doxycycline treatment to report upregulation of differentiation but downregulation of proliferation genes [190]. In our study, the expression of transgenes was observed at detectable levels even after 7 days of withdrawal of doxycycline under the microscope. It is possible that an improved system capable of de-inducing the fluororeporter expression sooner might be better for MSC differentiation. But, even without doxycycline stimulation, we observed a decline in MSC differentiation (Fig. 2.4). Lastly, the integration of viral gene fragments in MSCs could pose a genetic hindrance to differentiation. Perhaps, optimizing our lentiviral protocol by titrating the viral dosage, doxycycline concentration and polybrene might improve MSC differentiation overall, but the absence of fluororeporter expression in differentiated cells provided little

impetus to use this platform any further for dynamic profiling of MSCs during differentiation.

As an alternative to the inducible lentiviral reporter system, a pilot study was undertaken to explore the use of fluorescently labeled antigen-binding fragments (Fabs) to visualize endogenous histone modifications in MSCs [191]. Previously, our lab demonstrated that the phenotypic divergence in stem cells is associated with alteration of gene organizational domains which can be detected and quantified to forecast lineage specific changes in MSCs. The two co-occurring epigenetic markers in that study were trimethylations of lysine residues 4 and 27 on histone 3 (H3K4K27me3)[165]. We have previously shown that these epimarks have the predictive ability to forecast stem cell differentiation. The levels of the bivalent epimarks was able to distinguish naïve cells from differentiated MSCs [165]. We hypothesized that Fab-conjugate labeling of live cells would allow to develop a more sensitive and comprehensive image informatics platform to show different textures emerging during MSC differentiation compared to our previous study conducted with fixed cells. We obtained the fluorescent Fabs as a gift from Dr. Hiroshi Kimura (Tokyo Institute of Technology, Japan). The Fabs were introduced in live cells using the glass-bead loading method as described in [191]. We expected fluorescent labeling of the epimarks within nuclei, but confocal imaging revealed that the localization of reporters showed a high background due to non-specific cytoplasmic localization (Supplementary fig. 2.4). In addition, the glass bead loading method was found to perturb cell morphology and resulted in reduced the cell numbers which could potentially influence MSC differentiation. Therefore, we decided not to pursue this method any further for live-cell profiling.

2.6 Conclusion

The primary objective of this study was to engineer MSCs for dynamic profiling via fluorolabeled mechanosensitive proteins associated with differentiation. To this end, inducible plasmids were constructed for expression of fluorescent actin, HP1α, SC35, YAP, and TAZ by molecular cloning. We generated lentiviral particles capable for genetic introduction of the constructs. These constructs allowed generation of stable cell lines with HEK293 and MSCs after puromycin selection. However, successfully transduced MSCs demonstrated hampered differentiation, therefore our lentiviral array was not used any further for this project. Genomic analysis of the site of the transgene insertion and concurrent pathway analysis might help to determine the cause of MSC differentiation impediment.

2.7 Supplementary Figures

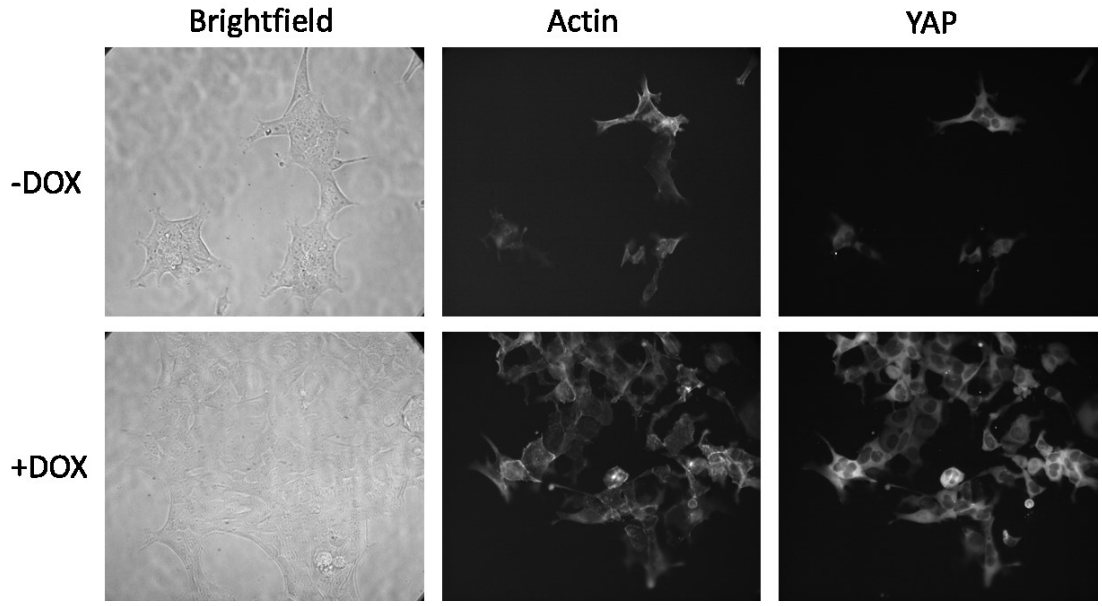

Supplementary Fig 2.1. Fluororeporter expression in HEK293 cells after puromycin selection: Following lentiviral transduction, HEK293 cells were cultured in puromycin to select cells with integrated transgene expression. The cells were found to possess doxycycline inducible fluororeporter expression of LifeAct-GFP and RFP-labeled reporter (YAP in this figure). The panel shows fluororeporter expression with or without doxycycline treatment for 48 hours.

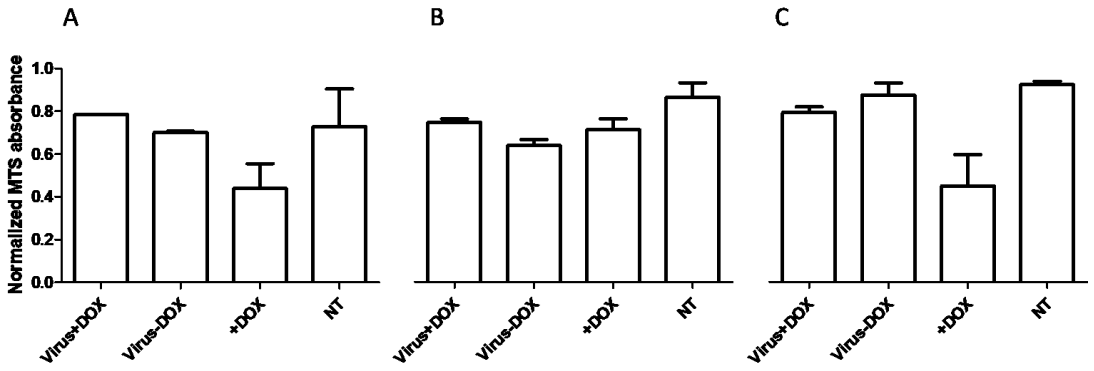

Supplementary Fig. 2.2. MTS assay to assess cell viability after lentiviral transduction and doxycycline stimulation: MSCs were transduced with lentivirus and after doxycycline treatment, and the cell viability was assessed by MTS assay after 7 (A), 14 (B) or 21 (C) days. The experimental groups were: Virus+DOX (TET-on group), Virus-DOX (Tet-off group), DOX (no virus, but DOX added), NT (no treatment control).

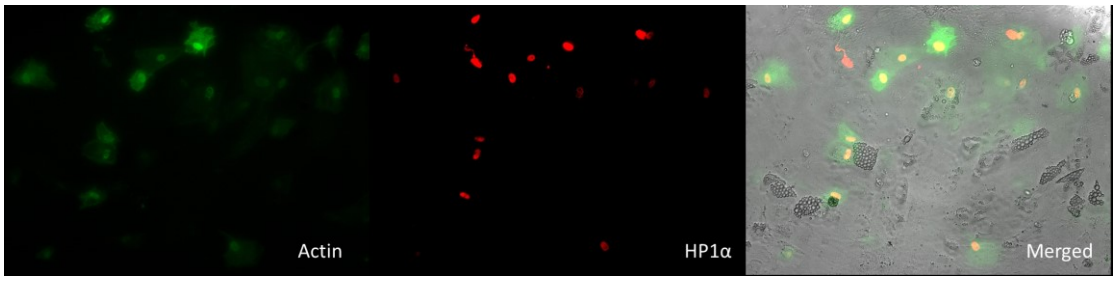

Supplementary Fig. 2.3. Lentiviral fluororeporter expressing cells showed no accumulation of lipid droplets: upon adipogenic differentiation the cells accumulate lipid droplets. Representative images showed lack of co-expression of fluororeporters (LifeAct-TurboGFP in green, RFP-HP1α in red) within adipocytes.

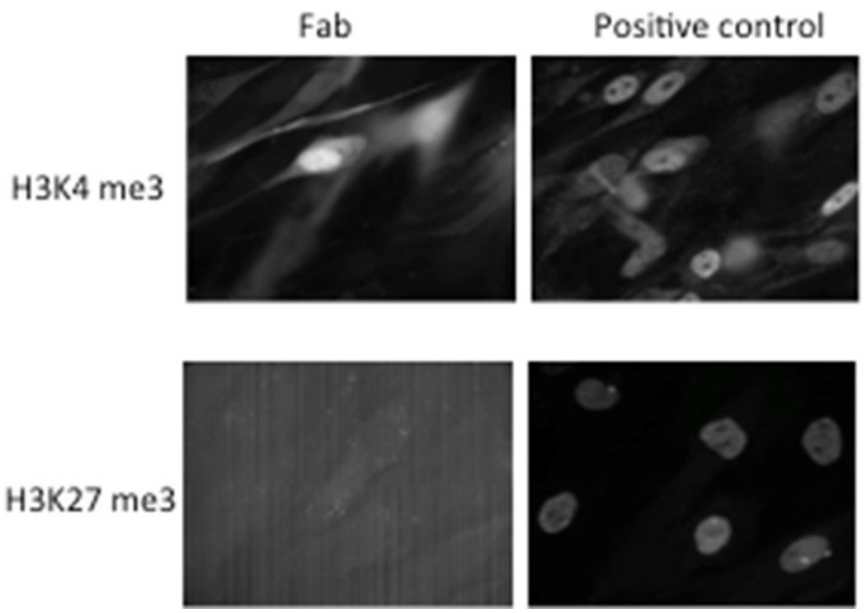

Supplementary Fig. 2.4. Live cell Fab-labeling of histone epimarks: Live MSCs were labeled with fluorescently labeled H3K4me3 or H3K27me3 following glass bead loading method [36]. We observed a high background indicating non-specific labeling (H3K4me3) or poor labeling (H3K27me3) with this method. As a positive control, cells were fixed and immunostained with the appropriate antibodies to show the benchmark labeling for developing a live-cell image informatics platform.

Chapter 3: Fluorescence Imaging of Actin Turnover Parses Early Stem Cell Lineage Divergence and Senescence

*Note: this chapter has been reproduced from the following publication:

Prakhar Mishra, Daniel C. Martin, Ioannis P. Androulakis, Prabhas V. Moghe. Fluorescence Imaging of Actin Turnover Parses Early Stem Cell Lineage Divergence and Senescence. Scientific Reports 2019 Jul 17;9(1):10377.

3.1 Abstract

This study describes a new approach to discern early divergence in stem cell lineage progression via temporal dynamics of the cytoskeletal protein, F-actin. The approach involves real-time labeling of human mesenchymal stem cells (MSCs) and longitudinal tracking of the turnover dynamics of a fluorogenic F-actin specific probe, SiR-actin (SA). Cells cultured in media with distinct lineage factors and labeled with SA showed lineage specific reduction in the actin turnover shortly after adipogenic (few minutes) and chondrogenic (3-4 hours) commitment in contrast to osteogenic and basal cultured conditions. Next, composite staining of SA along with the competing F-actin specific fluorescent conjugate, phalloidin, and high-content image analysis of the complementary labels showed clear phenotypic parsing of the sub-populations as early as 1-hour post-induction across all three lineages. Lastly, the potential of SA-based actin turnover analysis to distinguish cellular aging was explored. In-vitro aged cells were found to have reduced actin turnover within 1-hour of simultaneous analysis in comparison to cells of earlier passage. In summary, SiR-actin fluorescent reporter imaging offers a new platform to sensitively monitor emergent lineage phenotypes during differentiation and aging and resolve some of the earliest evident differences in actin turnover dynamics.

3.2 Introduction

Mesenchymal stem cells (MSCs) have been widely used for their ability to self-renew and differentiate into cells of distinct lineages including adipocytes, osteoblasts, and chondrocytes [192]. As a cell type that can be harvested from multiple sources and are easily expanded in-vitro, MSCs have become a valuable tool for experimental and clinical cell based regenerative applications [167]. One of the challenges for using cells with multi-lineage potential is the ability to track and control their lineage-specific differentiation. Given the possible heterogeneity that a population of MSCs adopts, methods to distinguish single cell lineage staging within a population would be extremely advantageous for selecting cells that have potential utility in regenerative medicine.

MSC differentiation is accompanied by a significant degree of reorganization of the intracellular cytoskeleton [179, 193-195]. Both the dynamics and architecture of the actin network play a vital role in differentiation [179]. Disrupting actin cytoskeleton by cytochalasin D (actin polymerization inhibitor) results in reduced osteogenesis but increased adipogenesis and chondrogenesis [195, 196]. Sliogeryte et al. reported that MSC differentiation led to overall increase in actin organization and slower turnover after 7 days of induction [197]. Actin cytoskeletal organization and dynamics play a determining role in regulating MSC differentiation and could be used as a marker for assessment of stem cell behavior. Treiser et al. used organizational features of F-actin to forecast emergent MSC lineages based on high-content image analysis [84]. Despite the new insights these reports reveal about the heterogeneity of the cytoskeleton in lineage diverging culture conditions, these studies were based on phalloidin staining of fixed cells, and thus were largely restricted to static comparisons of cell phenotypes and long-range shifts in these

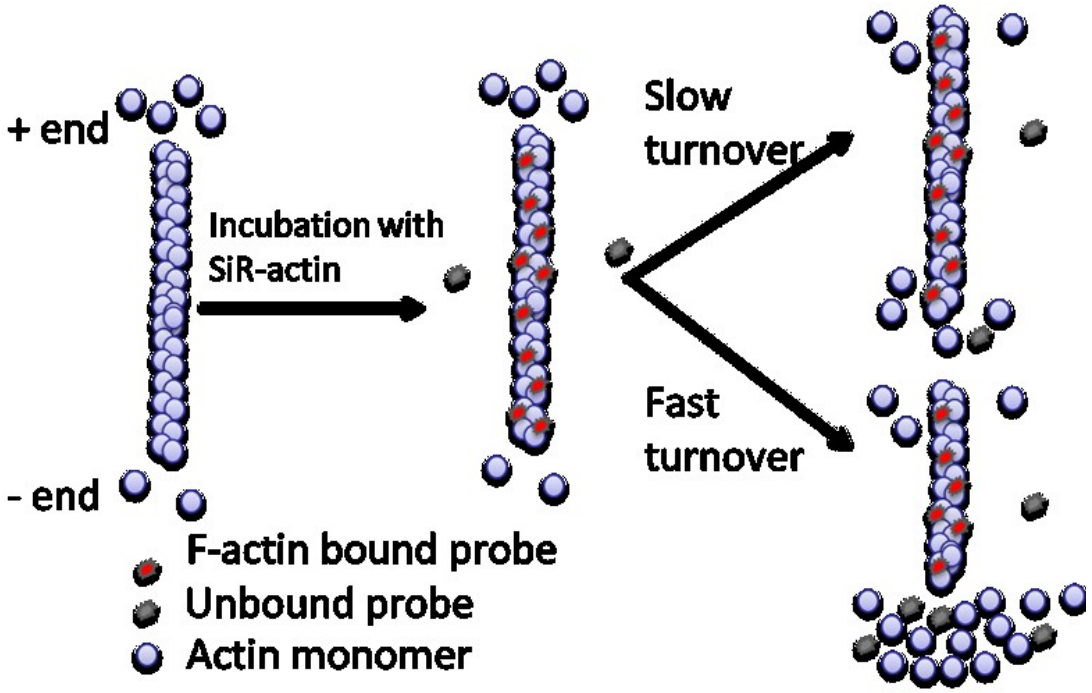

Fig. 3.1. Schematic showing F-actin interaction with SiR-actin (SA): SA is a cell permeable probe that fluoresces when bound to F-actin. Actin monomers are assembled/disassembled at either ends of the filament with different rates creating the fast growing "+" end and the slow growing "–" end. SA binds F-actin with high specificity, but upon removal from the filament due to actin turnover, the probe loses >100 fold in fluorescence. Probe binding is inversely correlated with actin turnover[6] .

phenotypes (over days). Some of the earliest known changes in the cytoskeletal morphology during MSC differentiation to date have been described as early as 24 hours post-induction even with flow cytometric analysis [84, 185]. Little is known about the dynamic changes in the actin cytoskeleton during the initial, emergent stages of lineage divergence. We propose that early reorganization of actin precede the lineage specific morphological changes. Therefore, the dynamics of the actin network could act as a sensitive marker of lineage divergence.

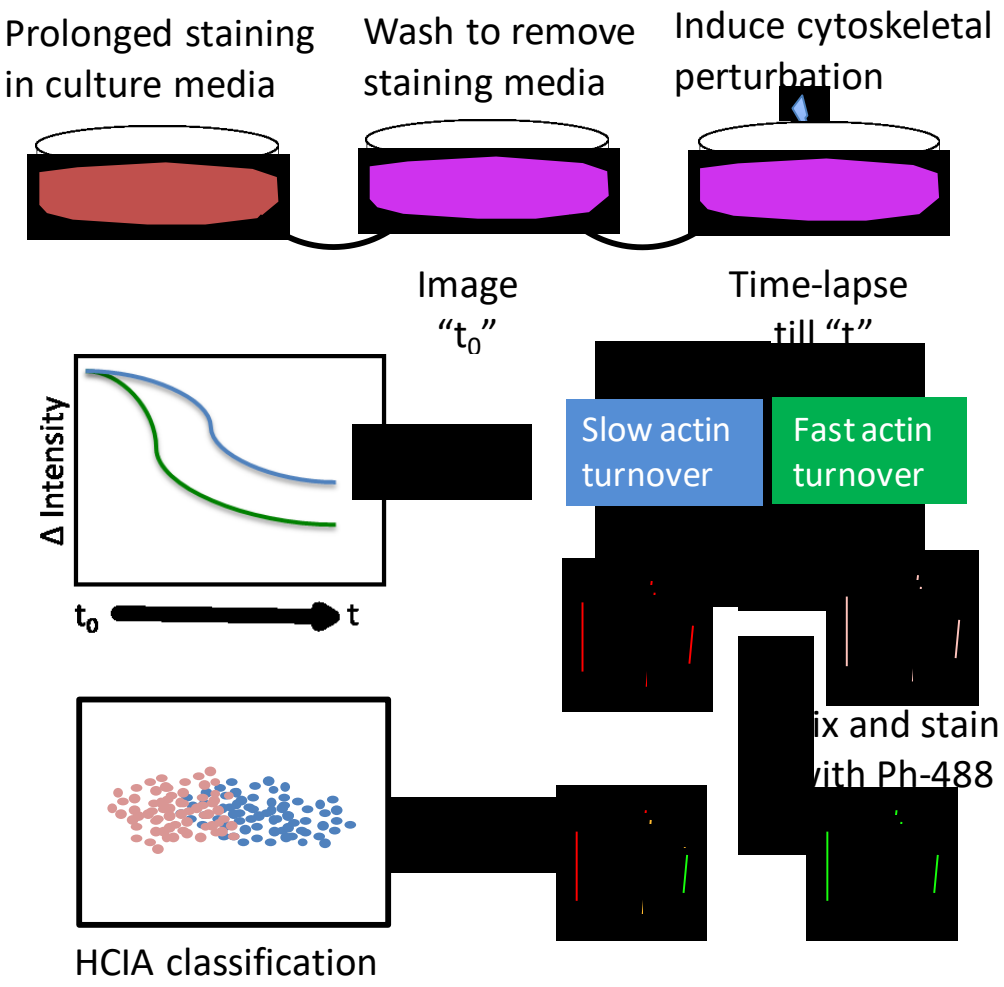

Fig. 3.2. Probing altered actin dynamics in live-cells based on an F-actin specific fluorogenic probe: SiR-Actin based Measurement of Actin Turnover (SMAT) involves prolonged live cell staining in the growth media with SA, removal of staining media, addition of cytoskeleton influencing cues and simultaneous time-lapse imaging. The loss of SA due to altered actin dynamics is quantified via the ratiometric decay of intensity in the image series captured during time "t" and normalized to the first timepoint (t_0). Further, subtle phenotypic variations in the actin cytoskeleton are parsed via high content image analysis (HCIA), based on dual imaging of SA and F-actin specific fluorescent probe, phalloidin (ph-488).

MSCs require in-vitro expansion to generate adequate cell numbers for most clinical or research-based applications. Unfortunately, MSCs are susceptible to senescence during prolonged cell culture leading to reduced proliferation, and differentiation potential [198]. MSC aging also results in altered expression of actin-associated proteins and decreased actin [199]. Similar to MSC differentiation, actin reorganization plays a role in aging as well, therefore it is important to elucidate the kinetics of actin turnover in both differentiation and senescence phenomena.

In this study, we employed an F-actin specific cell permeable probe, SiR-actin (SA), for real-time assessment of the kinetics of actin turnover during early stages of differentiation and cellular aging. The highly dynamic actin filaments undergo the addition or removal of the monomers (G-actin) at unequal rates on either end (Fig. 3.1). The addition of G-actin is favored at the more dynamic plus end, while the monomers are turned over at the minus end [200]. Milroy et al. proposed that SA binds F-actin only at the sites with three contiguous G-actin monomers, and the rate of actin turnover is faster than the rate of SA binding. Therefore SA incorporation is favored at the F-actin sites with slow dynamics (Fig. 3.1) [6]. Detachment of SA from its binding site due to filament turnover results in 100-fold decline in the fluorescence [201]. Because of this property, the highly dynamic actin structures (such as lamellipodia or filopodia) are weakly stained by SA while the more complex and long lived structures (such as ventral stress fibers and transversal arcs) are strongly labeled with SA (Fig. 3.1) [6].

The key premise for this paper is that distinct actin turnover rates can be resolved and quantified through imaging of SiR-actin probe binding behaviors, a method we call

SiR-actin based measurement of actin turnover (abbreviated as “SMAT”). The SMAT workflow (Fig. 3.2) involves prolonged incubation of cells in SA supplemented growth media, wash/removal of the staining media, introduction of the cytoskeleton-perturbing cue, time-lapse epifluorescence/confocal fluorescence imaging and image processing and data analysis and modeling. Change in actin turnover exhibits altered SA staining, which can be measured as a function of time by ratiometric intensity plot of the image series. Morphological reorganization of the cytoskeleton can be further benchmarked against F-actin specific probes, such as Phalloidin (P). SA stained cells (red) with more dynamic F-actin regions offer more binding sites to enable P binding (green) and show increased green color intensity compared to the less dynamic regions. This dual SiR-actin-Phalloidin (S-P) imaging protocol was used in conjunction with high-content image analysis to elucidate temporal lineage specific alterations in actin cytoskeleton during lineage progression (Fig. 3.2).

The focus of this paper was to first calibrate SMAT with cytoskeletal drugs to validate actin turnover dependent loss of SA staining. Next, we characterized and quantitatively modeled the temporal profiling of MSC lineage divergence to identify actin turnover with lineage specific kinetics. We also developed a composite staining framework with competing F-actin probes to further profile, via high content imaging, minute phenotypic changes in the actin cytoskeleton underlying the lineage specific changes. Lastly, as a potential application to regenerative medicine, SMAT was deployed to discern between later and earlier passaged cells.

3.3. Materials and methods

3.3.1 Mathematical model for SA decay kinetics

SA binding with F-actin sites is dependent on the actin dynamics. The observed change in intensity of the SA probe in the time-lapse images can be illustrated using a ligand-receptor binding model, where the unbound probe (ligand, L) associates with the F-actin site (Receptor, R) resulting in 100-fold increase in fluorescence of the probe (C) in a reversible manner.

$$L + R \leftrightarrow C$$

k_f and k_r represent the rate constants for forward and backward reaction. C_0 is the initial total fluorescent probe bound with F-actin. Due to the inherent actin dynamics, there is a net dissociation of SA probe as it comes off from F-actin and loses fluorescence by 100 fold. But, the rate constants k_f and k_r dependent on the lineage progression towards AD, OS or CH. Hence, we observed different lineage specific decay rates. The decay kinetics in Fig. 3.4a can be described as follows:

$$\frac{dC}{dt} = k_f R_T (C_0 - C) - k_r C$$

Where $C_0 - C$ denotes the concentration of free ligands while the available binding sites are denoted by R_T and are assumed to be in excess. Fitting the dissociation kinetics enabled us to deconvolute the values of the parameters: k_r and $k_f^d = k_f R_T$

On the other hand, Fig. 3.4b describes a scenario where the net effect is the association of SA resulting in increase in the intensity with time. Now, we assume L_T, the total number of probe molecules, to be constant. The association kinetics, assuming an excess on unbound ligands (L_T), in Fig. 3.4b can be described as follows:

$$\frac{dC}{dt} = k_f R_T L_T - k_r C$$

The effective rate of association, $k_f^a = k_f^d L_T$, depends on the media to reduce actin turnover. Therefore, using the association data we can estimate L_T. The SA association described in Fig. 3.4b initiates with the abundant availability of the SA ligand, which results in rapid increase in C.

The model parameters were successively estimated using the dissociation data. We determined k_f^d and k_r^d and subsequently using the association data we determined L_T. Fig. 3.6 shows the plots of estimated and the experimental data, except CH in the association study, the estimated plots corroborated with the observed data. The ratio of kr/kf could be used as a parameter to describe the simulated dissociation kinetics of SA at equilibrium.

3.3.2 Cell culture

Human bone-marrow derived MSCs were a kind gift from Dr. Rick Cohen (BME, Rutgers University). Cells were cultured in Corning® T-75 tissue culture flasks in humidity-controlled 5% CO2 atmosphere at 37 °C. After the initial expansion of the cells in the peprotech media, cells were maintained in the basal growth media (BA) composed of Gibco Minimum essential medium α (MEMα) supplemented with 10% premium-select fetal bovine serum (Atlanta Biologicals), and penicillin-streptomycin 0.1% v/v (Lonza). Cells were received at passage 3 and were used till passage 8 unless specified otherwise. The growth media was changed every third day and cells were passaged when the monolayer reached 70-80% confluence. For dissociating the cells, TrypLE™ express enzyme (Gibco) was used and seeding density for maintenance was typically 3,000-4000 cells per cm^2. Adipogenic media (AD) was prepared by supplementing BA with final concentrations of 1μM dexamethasone, 10μg/mL insulin, 500μM isobutyl-1-methyl-

xanthine and 200μM indomethacine. Osteogenic media (OS) were prepared by supplementing BA with 500μM L-ascorbic acid-2phosphate, 1μM dexamethasone, and 10nM b-glycerophosphate. Chondrogenic media bullet kit was obtained from Lonza. For inducing differentiation, cells were passaged to 96-well dish, allowed to attach overnight and induction media was added next day and subsequently changed every third day. The cytoskeletal drugs, jasplakinolide and cytochalasin D were purchased from Cayman chemicals, and nocodazole from Sigma Aldrich.

3.3.3 Live cell staining with SA and imaging

MSCs were seeded on 96 well tissue culture treated imaging dishes (Corning) and allowed to attach for 2 hours. Then 100nM SiR-actin (Cytoskeleton, Inc.) was added to the BA media for overnight staining of live cells. For time-lapse imaging, Zeiss LSM780 laser scanning confocal microscope was used. The tissue culture dish was placed on the microscope equipped with a stage-top incubator and staining media was aspirated, followed by quick media change to remove residual SiR-actin. Immediately, the first image-set was taken for all the test conditions as base intensity reference picture. The cells were then treated based on the experimental setup and time-lapse imaging was performed to capture the same fields at multiple time points. Imaging was done with the 10x objective in triplicates for all test conditions and 4 distinct fields were imaged in each replicate.

3.3.4 Measurement of intensity and data analysis

After image acquisition, the intensity of SiR-actin was quantified by measuring mean gray value on ImageJ. The mean gray value for all the image sets for a specific field of view were normalized to the first timepoint, and the values were averaged by the number of replicates and fields of view for each condition. The averaged mean gray value was plotted with time to quantify actin dynamics using SMAT.

3.3.5 F-actin dual staining based high content image analysis

Following prolonged SA staining in BA, the cells were stimulated with AD, OS or CH media and stained with phalloidin-488 (Ph). 10x 10 Tile scans of single cells were generated with the 20x objective with the confocal microscope. The images were analyzed on CellProfiler, and single cells were identified based on Hoescht as reference; while the cytoskeletal segmentation was performed based on Otsu thresholding. 41 morphometric features describing the cell shape, intensity of the fluorophores (s-p) and texture (Haralick features) of the cytoskeleton were obtained for each cell. The descriptors are listed in Supplementary table 1. Linear discriminant analysis (LDA) was performed on JMP software for dimensional reduction to categorize the differentiating cells. Briefly, linear combination of 41 variables were used to derive canonical variables that represent the variations among BA, AD, OS and CH groups (Supplementary table 1). The percent of correctly classified cells was calculated based on the specified data set. In the canonical plot, an ellipse that contains 50% of the data sets were drawn where the center represents the 95% confidence region for the means of the canonical variables. Wilk's Lambda test was performed to compare the means of the covariates (41 features) across groups. In addition, the Predictor screening platform on JMP was utilized to identify the significant predictors of differentiating cells based on bootstrap forest model.

3.3.6 Phalloidin staining

MSCs were fixed with 4% paraformaldehyde (Electron Microscopy Sciences) for 15 minutes, permeabilized with 0.1% Triton X-100 (Sigma) in PBS. To visualize F-actin, Alexa Fluor™ 488 Phalloidin (Life technologies) was used after dilution in PBS.

3.3.7 Cell differentiation assay

After 14 days of induction with differentiation media, the cells were fixed and stained with fast blue RR (Sigma) and AdipoRed (Lonza) reagents to stain for alkaline phosphatase

(osteoblast) and intracellular triglycerides (adipocyte). AdipoRed and fast blue were quantified on the Tecan microplate reader by measuring fluorescence with excitation at 485 and emission at 535nm. Fast blue absorbance was measured at 572nm.

3.3.8 Cell proliferation assays

The CellTiter 96® AQueous One Solution Cell Proliferation Assay (Promega) was performed to assess the effect of SA staining on cell viability. Briefly, cells were cultured at a density of 10,000 cells/cm2 in a 96 well plate and labeled with 100nM SA in either complete basal media (BA) or serum deprived media (SDM) for 18 hours. After overnight staining, the media was replaced with fresh media and the assay was performed along with unstained cells after 24 or 48 hours of initiation of SA labeling. To assess cell viability, Aqueous One Solution was added in each well to be assayed and incubated for 1 hour. The absorbance was measured using a plate reader at 490 nm.

3.3.9 Immunofluorescence analysis of ki67

The expression of ki67 in MSCs was quantified by immunofluorescence. Cells were cultured at a density of 3,000 cells/cm2 in 96 well plate and labeled with 100nM SA in either complete basal media (BA) or serum deprived media (SDM) for 18 hours. After overnight staining, the media was replaced with fresh media and the cells were fixed with 4% paraformaldehyde in PBS for 10 minutes after 24 or 48 hours of initiation of SA labeling. Fixed cells were incubated in the blocking buffer (10% normal goat serum, 1% BSA, 0.1% Triton-X100 in PBS) for one hour at room temperature. Cells were incubated in the primary antibody for ki67 (Abcam:15580) overnight at 1:200 dilution in 4 degrees, followed by three 5 minute washes. Subsequent, secondary antibody (Invitrogen, A-11010) staining was done at dilution of 1:500 for 1 hour at room temperature. After three 5 minute washes, nuclei was stained with Hoescht in PBS for 5 minutes. For quantification

of ki67 expression in single cells, confocal imaging was performed. Nuclei was used to designate ROI for ki67, intensity was measured with ImageJ.

3.3.10 Statistical analysis

Statistical analysis for SMAT data was done with GraphPad 5 software. The analysis of the changing probe intensity from live-imaging was performed by two-way ANOVA followed by Bonferroni post-hoc correction of p-values. While, with the fixed cells, one-way repeated measures ANOVA was done followed by Turkey's multiple comparison test. Asterisks were used to show the significance with the following p-values: $p<0.05$, $**p<0.01$, $***p<0.001$. Statistical analysis for LDA was done on JMP software as described above using the Wilks' Lambda test to compare the means of the covariates (41 features) across groups (BA, AD, OS and CH) based on the approximate p-values, p^F.

3.4 Results

3.4.1 Validation of SiR-Actin Labeling for quantification of actin turnover with cytoskeleton-perturbing drugs

The cytoskeletal drugs with known effects on actin dynamics were used to validate the SiR-Actin labeling. Initially, the effect of cytoskeletal drugs on actin morphology was determined. The three drugs were, cytochalasin D (CYTO, actin polymerization inhibitor), nocodazole (NOC, microtubule polymerization inhibitor) and jasplakinolide (JASP, actin polymerization promoter). Typically, MSCs are elongated spindle-shaped with defined stress fibers. SA stained cells treated with the high dose of cytoskeletal drugs demonstrated distorted actin cytoskeleton after two hours (Fig. 3.3a). Treatment with 8 uM NOC diminished the cell size, but the SA staining was intact and appeared similar to untreated cells. Both 1uM CYTO and 1uM JASP treatments disrupted the actin

cytoskeleton to an amorphous mass with no stress fibers. However, CYTO treated cells preserved the SA stain in the collapsed cytoskeleton, while JASP treated cells lost the SA

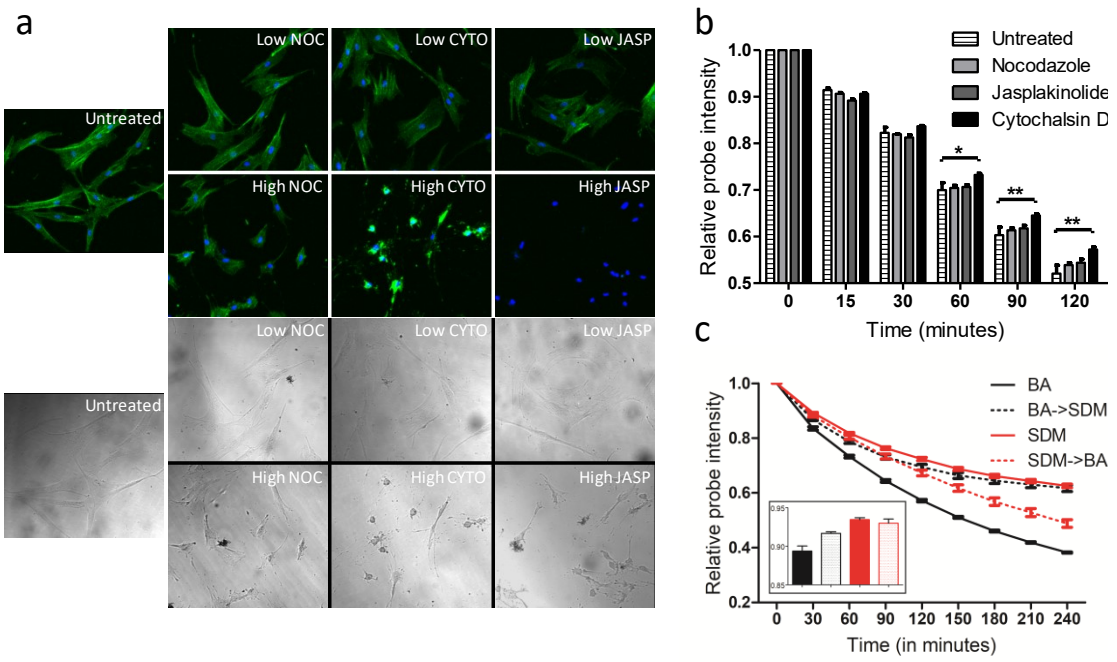

Fig. 3.3. Characterizing the influence of cytoskeletal perturbations on SiR-actin staining: A. Change in actin morphology 2 hours of treatment with low or high dose of drugs. Conditions include: untreated, nocodazole (8nM, 8uM; NOC), cytochalasin D (1nM, 1uM; CYTO) and jasplakinolide (1nM, 1uM; JASP) B. Change in SA staining due to altered actin turnover by low dose of cytoskeletal drugs. For each group, values are mean+standard error (n=3). *p<0.05, **p<0.01, ***p<0.001 vs the untreated group. C. Change in SA staining due to serum deprivation. BA: basal media, SDM: serum deprived media, BA->SDM: SA staining performed in BA, then switched to SDM, SDM->BA: SA staining performed in SDM, then switched to BA. Inset: SA intensity at 15 minutes. For each group, values are mean ±standard error (n=3). ***p<0.005 for BA vs SDM, ***p<0.01 for SDM-> BA vs SDM, *p<0.05 for BA vs BA->SDM, n.s. for BA->SDM vs SDM after 120 min.

staining entirely (Fig. 3.3a). This pronounced effect on SA staining stems from the differences in the mechanisms of action of the two drugs. CYTO induced actin cytoskeleton collapse preserved the SA bound on actin filaments, whereas JASP, owing to its structural similarities to SA, liberated the probe during cytoskeletal collapse. These observations provided the evidence for actin dynamics-dependent SA staining.

In order to test the sensitivity of the SMAT pipeline, very small doses of cytoskeletal drugs were identified to alter actin turnover without any apparent changes in the cell shape. For SMAT analysis, the lowest drug concentrations that led to no gross changes in actin morphology were 1:1000 dilution of the drugs (1nM CYTO, 1nM JASP, 8nM NOC) (Fig. 3.3a, Supplementary Fig. 3.1). 1nM CYTO showed slower decay of SA intensity which emerged after 30 minutes of treatment, then reached significance after 1 hour ($p<0.05$), while JASP and NOC showed no statistical significance compared to untreated cells (Fig. 3.3b). These results are in agreement with the observations in Fig. 3.3a with 1uM CYTO treatment, because 1nM CYTO interfered with actin turnover resulting in prolonged SA staining. Interestingly, SMAT analysis discerned changes in the actin turnover caused by low dose of cytoskeletal drugs even with no apparent changes in actin morphology (Supplementary Fig. 3.1).

As another approach to explore our workflow for dynamic assessment of actin turnover, SMAT was performed with cells cultured in serum deprived media (SDM) (Fig. 3.3c). Serum depletion during cell culture is known to induce a cell growth arrest along with actin depolymerization [202]. Indeed, SMAT analysis showed that cells in SDM showed significantly slower SA decay compared to the complete basal (BA) media (SDM vs BA: $p<0.001$ at 30 min). The serum induced growth arrest can be reversed by reintroduction of serum in the culture media causing an increased actin polymerization [202]. Reintroducing serum containing BA in cells (SDM->BA), resulted in rapid decline

in SA intensity due to accelerated actin turnover (SDM vs SDM->BA, $p<0.001$ at 120 min). Similarly, initiation of serum deprivation showed concurrent reduction in SA decay rate (BA->SDM vs BA, $p<0.05$ at 30 min). High sensitivity of SMAT to the changing actin turnover was demonstrated by early emergence of differences in SA intensity among the groups as early as 15 minutes (Fig. 3.3c, inset). In summary, SMAT analysis demonstrated the ability to monitor dynamics of actin turnover.

3.4.2 Live-profiling of differentiation induced cytoskeletal reorganization

MSC differentiation invokes extensive cytoskeletal reorganization in response to the soluble cues [179]. Previously, our lab demonstrated that higher order organizational features of actin cytoskeleton could be used to distinguish cells in adipogenic or osteogenic media after 72 hours of initial exposure [84]. We hypothesized that evaluation of kinetics of actin turnover via SMAT would enable faster temporal resolution of distinct cell fates. SA-stained cells in basal growth media (BA) were stimulated with adipogenic (AD), osteogenic (OS) or chondrogenic (CH) media and subsequently imaged for ~15 hours. All soluble cues demonstrated a unique SA decay profile due to slow down of actin turnover albeit at different times (Fig. 3.4a). AD demonstrated slowest probe decay compared to all other conditions and reached significance within minutes, followed by CH and OS (Fig. 3.3a). Therefore, SMAT enabled parsing the live MSCs undergoing differentiation within minutes to few hours. The SMAT approach entails SA based dissociation (off-rate) and imaging-based profiling. We also undertook a complementary SA association kinetics approach by initiating the live-imaging with unstained cells and subsequent addition of BA, AD, OS and CH supplemented with SA. Here, the increase in SA staining indicates slower actin turnover while the dynamic actin sites are poorly stained as mentioned earlier. Similar to SMAT analysis, the SA kinetics followed an exponential behavior. Again,

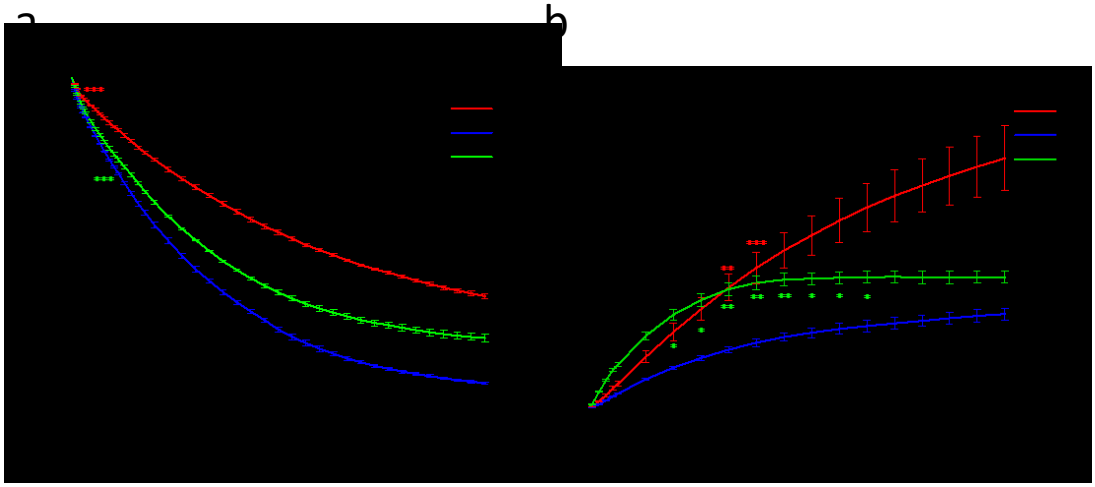

Fig. 3.4. Temporal profiling of actin turnover in MSCs in response to differentiation: A. SMAT analysis enabled early parsing of MSCs exposed to adipogenic (AD), chondrogenic (CH), and osteogenic (OS) from basal (BA) growth media. For each group, values are ratiometric mean± standard error of SA intensity normalized to the first timepoint within the respective group. *p<0.05, **p<0.01, ***p<0.001 vs the BA group (n=3). **B.** Alternative approach to SMAT with unstained MSCs showed distinguished rates of increase in SA intensity when introduced with BA, AD, OS and CH media. The statistical analysis was done similar to A.

AD showed the slowest actin turnover, with more rapid kinetics in CH and OS conditions (Fig. 3.4b). The SA kinetics showed variations and did not resolve the trendlines for OS and CH from BA. Therefore, the dissociation kinetics approach in SMAT was found to be more sensitive for re solving changes in actin turnover.

3.4.3 Determining temporal responsiveness of actin cytoskeleton by switching soluble cues

Initiation of differentiation leads to extensive changes in the cytoskeletal organization. But the cytoskeletal plasticity during the course of MSC differentiation is not well understood. Next, we explored the temporal responsiveness of the cytoskeleton to the lineage specific

cues by swapping the medias with concurrent SMAT analysis. SA stained cells were induced with AD for 3.5 h, which showed similar trends as seen previously (Fig. 3.4a). The

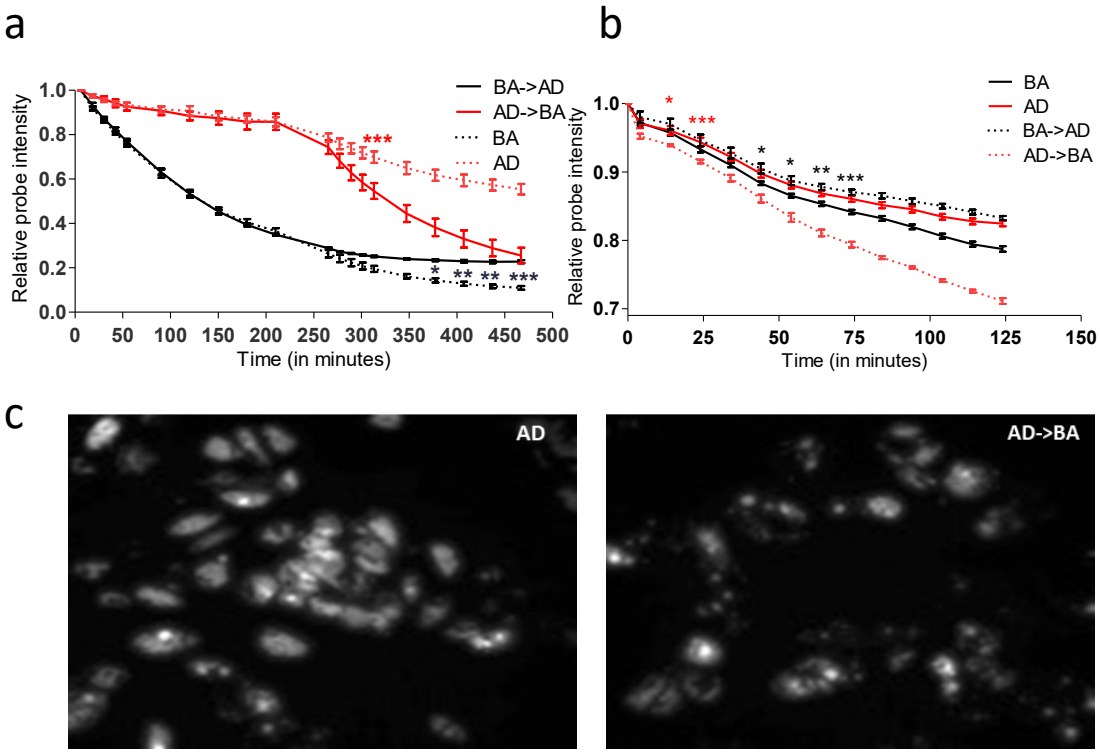

Fig. 3.5. Temporal profiling of actin turnover in lineage committed MSCs: **A.** SMAT analysis showed temporal sensitivity of cytoskeleton during media switch. After 4 hours of initial induction with AD, media swap resulted in switched probe decay profiles within minutes. For each group, values are ratiometric mean± standard error of SA intensity normalized to the first timepoint within the respective group. P values were calculated after the media switch. *p<0.05, ***p<0.001 BA vs BA->AD and **p<0.01, ***p<0.001 BA vs BA->AD group (n=3) **B.** SMAT analysis demonstrates cytoskeletal plasticity after lineage commitment: after 15 days of adipogenic induction switching to BA resulted in faster SA decay. P values were calculated similar to A. **C.** Adipored stained cells showed a reduction in the number of adipocytes after 3 days of media swapping from AD to BA (15+3 days)

media was swapped at 4 h timepoint and imaging was done from 4 to 8 h. The switch from AD->BA showed significantly faster SA decay compared to the AD group ($p<0.01$ after 32 minutes of media switch), while BA->AD switch showed slower actin turnover vs BA ($p<0.05$ after 120 minutes of media switch) (Fig. 3.5a). Also, SMAT analysis remained sensitive to the change in actin turnover over the course of this study, particularly for BA vs BA-> AD group, which had already lost most of the SA at the media switch. A similar longer-term media swap experiment and SMAT analysis was done after 14 days of adipogenic induction. Several cells with intracellular lipid droplets were seen under the bright field microscope in AD (data not shown), while cells in BA were mostly elongated and spindle shaped. At Day 14, cells were stained with SA and the media switch was performed on the following day. BA->AD showed significantly slower SA decay compared to the BA group (BA vs BA->AD $p<0.05$ at 44 min), while AD->BA showed faster SA decay compared to the AD group ($p<0.05$ at 14 min) [Fig. 3.5b]. The rapid response from BA->AD and AD->BA groups shows that the cytoskeleton remains plastic and responds instantly to the soluble cues even in lineage committed cells. After the media switch, cells were cultured for 3 more days. On 18^{th} day, the cells were fixed and stained with adipored.

BA->AD group showed emergence of lipid droplets and AD->BA group showed reduction in the number of adipocytes compared to the AD group (Fig. 3.5c). While other groups have described dedifferentiation for MSCs[203], here we have demonstrated that the actin cytoskeleton remains plastic and responds rapidly to the lineage specific soluble cues, even with lineage committed MSCs.

3.4.4 F-actin composite staining based high content image analysis for assessment of morphological changes during lineage progression

SA staining of single stem cells also enables higher content analysis of the temporal progression of the cytoskeleton morphology during differentiation. A single cell morphometric approach was employed to quantitatively profile cytoskeletal changes during the early lineage divergence. The workflow as described in Fig. 3.6 involved differentiation induction of SA-stained cells, followed by complementary Phalloidin staining and confocal imaging. Single cell images were analyzed and high content image informatics (HCIA) was performed to allow classification of single cells in BA, AD, OS and CH groups using linear discriminant analysis (LDA) (Fig. 3.6). Each point on the plot represents the data from a single cell, the contour plots envelope roughly 50 % of the cell

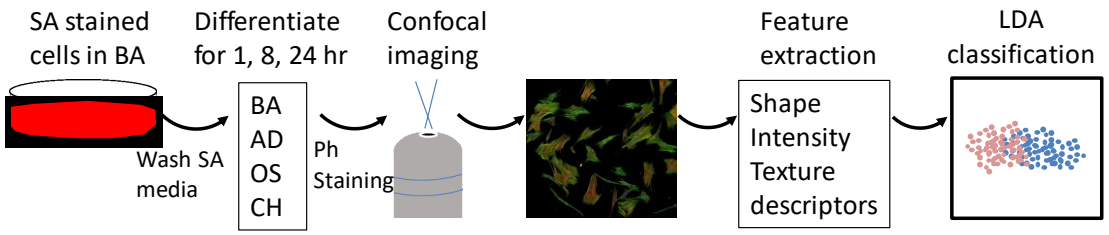

Fig. 3.6. Workflow describing F-actin dual staining based high-content image analysis: SA stained cells were cultured in AD, OS or CH media for 1, 8, or 24 hours. The cells were fixed and stained with a competing F-actin stain, phalloidin (Ph) and images were acquired using confocal microscopy. A total of 41 shape, intensity and texture-based features were extracted from single cells. These features or descriptors were used as the input to derive canonical covariates using linear discriminant analysis (LDA) to classify the individual cells.

population, and the center of the contours approximates the mean values of the canonical variables (Fig. 3.7a, b). Examination of tri-lineage progression showed temporal divergence in the cytoskeleton (Fig. 3.7a). After 1 h of induction, all medias had largely

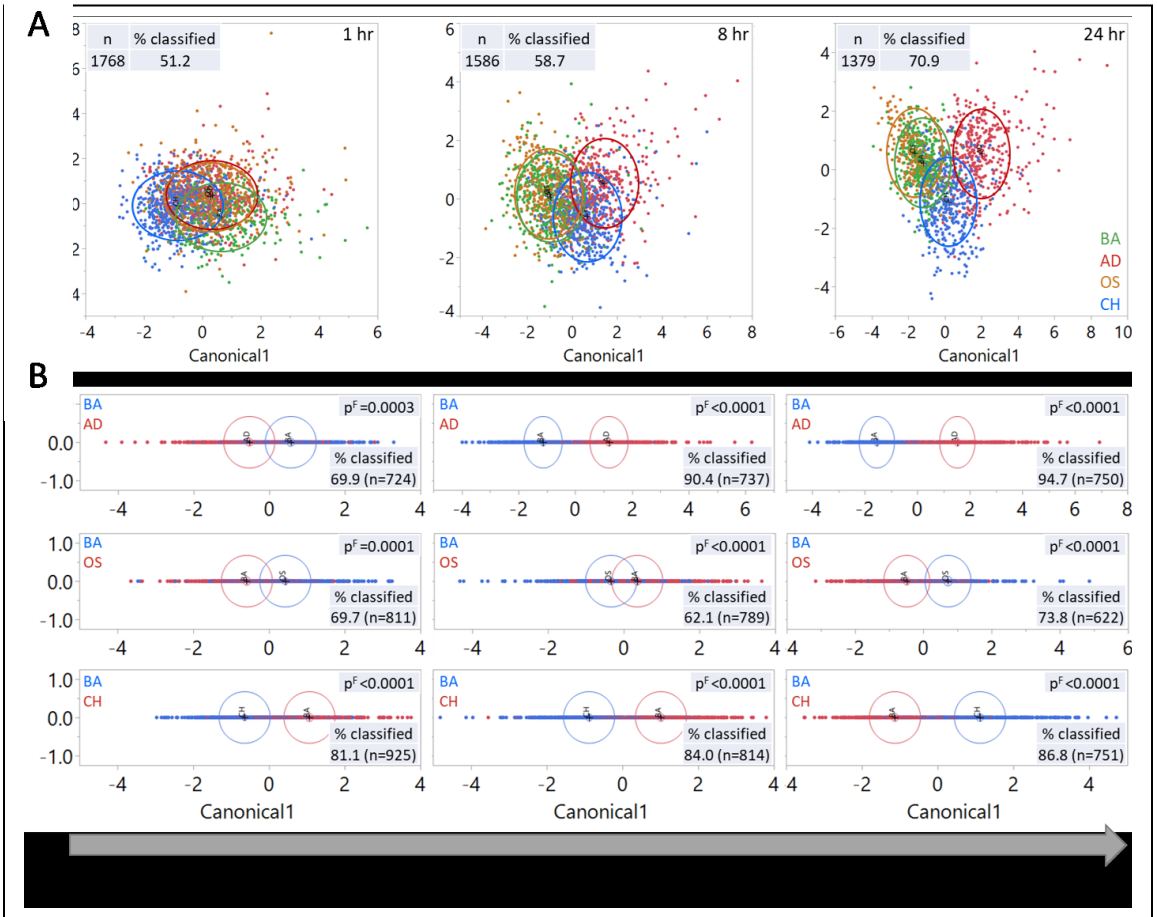

Fig. 3.7. F-actin dual staining coupled with high-content analysis for parsing MSC differentiation: A. Simultaneous comparison of cells cultured in AD, OS and CH media to show early divergence in the cytoskeleton during differentiation. Each point represents a cell. Contour plot encompasses roughly 50% of the cells in a given media, while its center approximates the mean canonical values. B. Binary classification of cells highlight temporal divergence of cytoskeleton during differentiation. Wilks' lambda test was employed to calculate the p-value, p^F to compare the means of the covariates among the groups.

overlapping contour plots, and the number of correctly classified cells was 51.2%. The data from 8 h timepoint demonstrated increased separation of the contours with improved classification of 58.7%. After 24 h, the contour plots were more separated, as evidenced by improved classification of 70.9%. These results demonstrate that the early stage cytoskeletal changes during MSC differentiation can discern lineages within 24 h in a lineage specific manner. In the interest of decluttering the data, each lineage was also individually compared with the basal condition (Fig. 3.7b). 70-80% of the cells were correctly classified with significant differences in the mean values of the covariates as early as 1 h. At 8 h, the cells clustered more distinctly except in the OS media. At 24 h, ~95%, 74%, 87% of the cells were classified in separate lineage groups, AD, OS and CH, respectively. Note that the difference in the mean canonical values were significant in all conditions at all timepoints, while the single cell classification was a function of time. The high-content image analysis demonstrated that MSC differentiation involves temporal morphometric changes in the actin cytoskeleton, which are evident as early as one-hour post-induction.

3.4.5 Quantifying altered actin dynamics in MSCs following aging in culture

Cellular aging is a complex phenomenon which is associated with reduced telomere length, altered transcriptional profile, DNA damage and epigenetic deregulation[204]. Aging in MSCs leads to a reduction in the proliferative capacity and differentiation potential. Since we were able to detect subtle changes in actin turnover in response to the lineage specific cues, we hypothesized that SMAT could be harnessed to detect changes in the actin turnover due to *in vitro* aging. The effect of *in vitro* cellular aging on actin turnover was evaluated by simultaneous SMAT profiling with early (P5) and late (P12) passage MSCs. P12 cells exhibited slower SA decay compared to the P5 cells, and the data

reached statistical significance after 1 h ($p<0.01$ at 62 min, $p<0.001$ at 77 min after SiR-actin removal) (Fig. 3.8a). In a parallel study, P5 and P12 cells were evaluated for adipogenesis and osteogenesis for 14 days. P12 cells showed significantly reduced adipocytes (cells with lipid droplet accumulation) and osteoblasts (fast blue stained cells) compared to P5 cells (Fig. 3.8 b,c). Therefore, SA decay could be used as a marker to evaluate and forecast diminished differentiation potential in MSCs due to *in vitro* senescence.

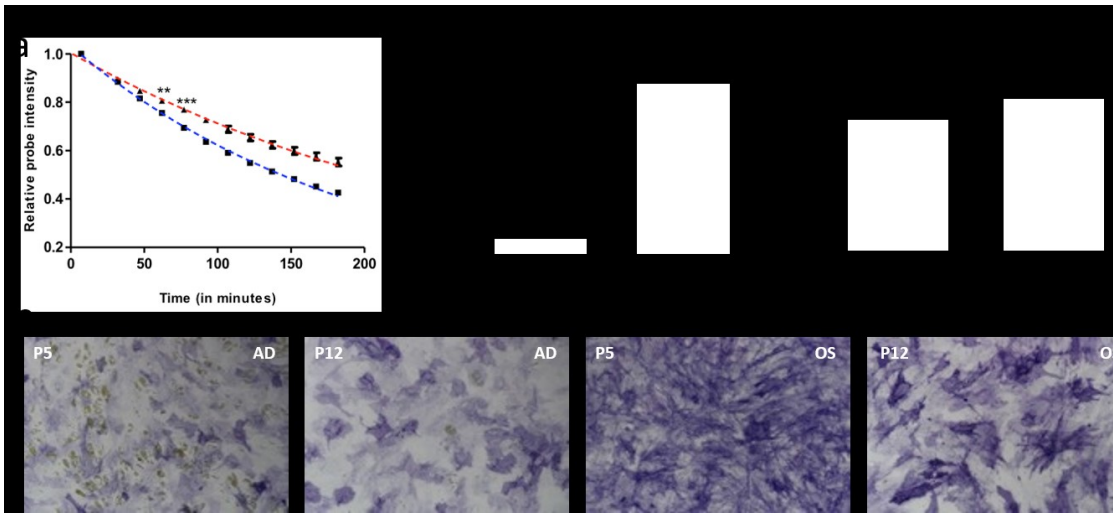

Fig. 3.8. Assessment of altered actin turnover kinetics and differentiation due to in-vitro aging: A. SMAT analysis discerned early passage cells (P5, blue curve) from late passage (P12, red curve) cells. Values are ratiometric mean± standard error of SA intensity normalized to the first timepoint within the respective group. **$p<0.01$, ***$p<0.001$ vs the P5 group (n=3). B. Quantification of Fast Blue (FB) and Adipored (AR) from B. For each group, values are mean+ standard error of AR or FB normalized to Hoechst staining. *$p<0.05$, **$p<0.01$ vs the P5 group (n=3). C. Late passage (P12) cells showed minimal lipid droplet accumulation after adipogenic induction (AD) and reduced fast blue staining after osteogenic induction (OS) compared to early passage cells (P12).

Discussion

The actin cytoskeleton plays a pivotal role in guiding MSC differentiation [179, 194]. The mechanobiology, signaling pathways, and morphology of the actin cytoskeleton have been extensively studied in the context of MSC differentiation [119, 194, 205-207] but the kinetics of the actin reorganization are mostly unexplored. We reasoned that change in cell shape begins by a highly organized and complex restructuring of the network of actin filaments. Given that actin reorganization is accompanied by a change in actin turnover [202, 208, 209], the actin turnover has the potential to be a real-time indicator of the inherent cytoskeletal dynamics. In this study we developed a novel approach to monitor the actin turnover and parsed the kinetics of actin turnover during chemically induced MSC differentiation and in-vitro senescence. The key reagent for the proposed method is a fluorogenic probe, SA, which binds select F-actin sites depending on in situ cellular dynamic states[201].

Initial validation of SA based quantification of changing actin turnover was conducted with the cytoskeletal drugs that are known to perturb the actin cytoskeleton. NOC was used as a negative control as it induces depolymerization of microtubules without interfering with actin assembly*[210-212]*. At high dose (8uM), NOC resulted in reduced cell size, but had no effect on SA staining. Treatment with actin perturbing drugs showed more dramatic effects on SA staining. CYTO binds the plus end of F-actin, thereby interferes with addition of G-actin leading to arrested actin dynamics*[213-215]*. At high dose (1uM), CYTO caused the cytoskeleton to collapse, whereas SA was retained due to encumbered actin turnover. In contrast, high dose (1uM) of JASP caused rapid decline in

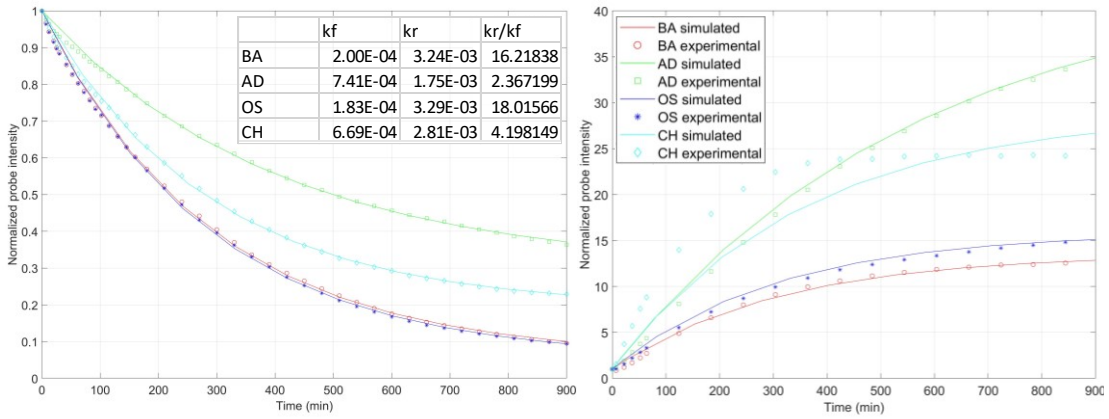

Fig. 3.9. The lineage-specific divergence of normalized SA kinetics was modeled in live MSCs: Kinetic data for SA decay (Fig. 3.4a), and SA association (Fig. 3.4b), were plotted in the LEFT and RIGHT panels, respectively, and denoted using varied symbols for different treatment conditions above (BA: basal; AD: adipogenic; OS: osteogenic; CH: chondrogenic). Kinetic parameters were estimated using a simple ligand-receptor binding model to fit the data and used to generate simulated kinetics (bold curves). The table in the left panel shows the values of the two rate constants, kr(dissociation) and kf (association). The ratio kr/kf indicates lineage specific dissociation kinetics for SA. [See materials and methods for details].

SA staining by promoting de novo filament formation and possibly due to the structural similarity with the probe *[216]*. Treatment with low drug dose showed that SA staining is capable of detecting actin cytoskeletal perturbations even without any observed change in cell shape. Furthermore, we also investigated the influence of serum deprived media (SDM) on SA staining. We were able to detect changes in actin turnover during both serum reintroduction (SDM->BA) and initiation of serum deprivation in the complete media (BA->SDM) (Fig. 3.3c) as early as 15 minutes.

The primary goal of this study was to discern possible temporal changes in actin turnover during MSC differentiation. Using imaging of SA actin-based turnover (abbreviated as SMAT) and dual-staining based HCIA, we report altered actin dynamics and organization much earlier than seen using conventional methods. The earliest changes in the cytoskeleton during differentiation have been reported based on mechanobiology (Change in young's moduli at day 10[217], morphometric descriptors (after 1 day [84]) and phalloidin intensity (after 1 day; flow cytometry [185]). With SMAT, we discerned changes in actin turnover as early as few minutes upon the induction of lineage differentiation. To establish that the observed change in actin turnover is related to the lineage commitment, we employed a converse approach by inducing dedifferentiation. Within minutes of a differentiation media swap (by removing lineage differentiation factors), we observed a switch in the SA decay rate, as lineage committed cells assumed decay profiles of cells in basal media, which subsequently led to reduction in the number of adipocytes compared to the group with no media change (Fig. 3.5b, c). The media swap study provided evidence for high responsiveness and plasticity of the actin cytoskeleton. Therefore, SMAT has the potential to be used as a robust early indicator for actin turnover, and the tested cells can be used for subsequent assays to verify the functionality. As a potential application, we showed a correlation between a down-tick in actin turnover with MSC differentiation due to in-vitro aging (Fig. 3.8).

Using the SMAT profiling, we could effectively discern between AD, OS and CH lineages, but the differences between BA and OS remained insignificant. This could be potentially due to similar actin dynamics of BA and OS during the time course study. Previously, we employed high content informatics to parse BA from OS by 24 hours but on fibronectin coated surfaces that are conducive to osteogenesis. While, with uncoated

surface, it took 48 hours to discern the two [84]. The analogous approach to our 2009 paper in this study is the s-p dual staining based descriptor analysis where unlike SMAT we could extract an array of descriptors that enabled us to correctly classify osteogenic cells with ~70% accuracy as early as one hour of induction [Fig. 3.7b]. Due to dual chromatics of phalloidin and SiR-actin, we generated more richer descriptors that enabled an earlier classification. Simultaneous staining with complementary probes, SA and Ph, provides a new strategy by which the F-actin sites can be labeled based on the inherent turnover dynamics. After removing the SA media, the residual SA stain represents the F-actin sites that were not turned over. Subsequent staining with Ph will specifically highlight the unoccupied F-actin sites. We also confirmed the competitive nature of the probes in a dose response study (Supplementary Fig. 3.3b). The dual-actin image informatics demonstrated the temporal drift of single cells during lineage progression that eventually was able to cluster cells in all 3 lineages (AD, OS, and CH) simultaneously after 24 hours of induction. A binary juxtaposition of each lineage with the basal condition improved the correct classification, and also displayed the actin structural divergence that accompanies lineage progression. The features that enabled the classification of cells were identified by a predictor screening on JMP to rank the features. SA intensity and haralick features were the top 5 predictors across all conditions [Supplementary Table 2], while notably the shape descriptors did not feature as the influential ones. Therefore, high content image informatics enabled identification of phenotypic variations in the cytoskeleton in advance of the role of the cell shape. High content image informatics-based parsing improved with time, indicating that the cytoskeleton undergoes progressive reorganization during lineage commitment. Unlike SMAT which is based on a unidimensional analysis, high content image informatics benefits from multi-variate approach that enables better classification. However, the two major limitations of high

content informatics are that it is based on discreet timepoints and requires complex data analysis. On the other hand, SMAT is suitable for dynamic profiling of actin turnover for prolonged duration.

In an attempt to explain the observed SA kinetics during lineage progression we proposed a simple ligand-receptor equilibrium model simulating the observed data (Fig. 3.6). First, the kinetic parameters were fitted to the SA dissociation kinetics in Fig. 3.4a, and then used to determine the SA association in Fig. 3.4b (Fig. 3.6), showing that both association and dissociation can be adequately described by a consistent set of kinetics parameters. The proposed model supports a ligand-receptor interaction model of SA with F-actin (Fig. 3.6). After removal of SA from the growth media, the initial fast decay is likely the result of rapid loss of SA primarily from the dynamic structures within the actin cytoskeleton, such as podosomes and filopodia. On the contrary, stress fibers show SA staining even after several hours. We suggest that the least dynamic regions are primarily responsible for lineage specific changes in the turnover, as they are the prime sites responsible for the change in SA. The SMAT analysis of early changes during adipogenic and chondrogenic differentiation show a major decrease in actin turnover, whereas osteogenic differentiation is accompanied with a rapid actin turnover. This observation is supported by the previous findings where osteogenic differentiation leads to extensive reorganization of actin filaments to create a disordered mesh with thick stress fibers [179]. In contrast, adipogenic differentiation showed disrupted network, which may be the result of arrested actin dynamics [194, 218]. The proposed model suggests the need in the future for a more detailed biophysical analysis of the interaction of SA with F-actin during MSC lineage progression, and the overall role of actin cytoskeleton during immediate early stages of MSC differentiation.

MSCs possess the ability to proliferate and differentiate, but because of their low frequency, it is necessary to expand them *in vitro* for clinical applications. During *in vitro* expansion, these cells are susceptible to a decline in the proliferative capacity along with reduced differentiation potential [7]. Given that increasing passage number leads to an altered cell morphology we hypothesized that SA label could be used as a dynamic function for evaluation of change in actin turnover due to *in vitro* aging [198]. Using SMAT, we could detect altered actin turnover in late passage cells within one hour of the assay. Thus, SA decay-based evaluation of actin turnover could be used as a potential tool for benchmarking the actin turnover to evaluate *in vitro* aged MSCs or from aged donors to predict their differentiation potential.

The influence of SA on MSC morphology and differentiation was also examined (Supplementary Fig. 3.2, 3.3). Complex structures within the actin cytoskeleton with slow actin turnover (such as stress fibers) showed bright staining unlike the dynamic regions towards cellular periphery that are involved in motility (Supplementary Fig. 3.3a). Due to structural similarity with JASP, SA has the potential to influence actin dynamics and morphology[201]. We compared the area of SA stained and unstained cells after fixing and independent phalloidin staining (Supplementary Fig. 3.3c). At 100nM, SA treated cells displayed increased cell area but the difference was not significant. However, a higher SA dose (500nM) resulted in distinct change of cell shape from elongated spindle to a rounded morphology along with more pronounced stress fibers in comparison with the low SA dose (100nM) (Supplementary Fig. 3.3a, c). Therefore, low SA dose was found to be suitable for the live imaging of MSCs. Thus, SMAT has the potential to assess actin turnover over the course of several hours with a simple low magnification imaging

protocol. Further, SMAT analysis may be suitable for bulk cell populations where single cell segmentation analysis may be challenging. Most of the conventional methods for *in vitro* MSC quality control, such as analyzing the gene expression [219], differentiation[23], immunostaining [220] and senescence [221], are difficult to implement with live MSCs, and thus cannot be used in preparative processing of cells prior to therapy. At low dose (100nM), transient labeling with SA, is suitable for live characterization of MSC behaviors without adversely affecting the innate MSC ability to proliferate or differentiate (Supplementary Fig. 3.2, 3.4). We note the caveat that at higher concentrations, SA staining could induce cytoskeletal reorganization, and as such, the effect of labeling should be independently investigated to determine its influence on cytoskeletal dynamics and other cellular functions. Additionally, supplementation of 100nM SA with verapamil, a broad-spectrum efflux pump inhibitor recommended by the SA manufacturer to improve signal, caused prolonged retention of the probe resulting in poor or delayed resolution of decay plots, and hence was not used in this study.

Most of the information about actin dynamics in live cells has come from assays based on FRAP (fluorescence recovery after photobleaching) based experiments [49]. The recovery of fluorescence is driven by intrinsic diffusion kinetics of depolymerization of bleached monomers and addition of new non-bleached monomers on the filaments [222][50]. On the other hand, the SMAT approach is primarily driven by SA dissociation from F-actin sites during depolymerization and a slow association rate of the probe, leading to a net temporal decline in number of labeled actin sites[6]. While both methods measure actin turnover, these approaches could offer complementary information about the actin dynamics. FRAP is well characterized for monitoring specific region of interest within a single cell for short duration (up to few minutes), while SMAT could be used to

monitor the global actin dynamics of cell populations for long-term (several hours). In addition, due to the low magnification imaging protocol and ease of data analysis, SMAT could be readily applied for high-throughput analysis of multiple cell populations.

This study revealed the early changes in the kinetics and organization of actin turnover in response to differentiation induction and *in vitro* aging. The earliest reported change during adipogenic differentiation involved altered expression of 46 genes as early as 30 minutes[223]. Subsequent analysis in the same paper and other studies have also demonstrated upregulation of adipogenic transcription factors in the C/EBP family and MYC [224, 225]. Notably, using imaging of the SA turnover, we observed an even earlier decrease in actin turnover during cell culture in the adipogenic media. This raises the question about the causality i.e. whether the change in actin dynamics is a result of altered transcriptional profile or whether the actin dynamics initiate MSC differentiation via downstream signaling. In the latter scenario, actin might influence the immediate-early gene expression with integrin, Rho and YAP/TAZ signaling pathways [220, 226]. Actin monomers have been shown to be a part of the transcriptional apparatus that modulate gene expression[227]. Also, the proportion of G to F actin determines the activity of a transcription cofactor, serum response factor (SRF) along with its cofactor MKL1 [228], which have been shown to be an important regulator of MSC differentiation. On the other hand, if the actin-transforming signal emanates from the nucleus then the focus would be on immediate early genes that have been reported to be associated with both MSC differentiation and the cytoskeleton. Our previous gene expression analysis shows several clusters of genes upregulated early during lineage divergence, including cell cycle genes and nuclear splicing factor genes, especially Nuclear mitotic apparatus protein,

NuMA[164]. Morphotextural descriptors of NuMa were able to distinguish phenotypes with greater efficacy when combined with descriptors for actin filaments in MSCs[163].

In summary, we have described an approach to study actin turnover and organizational features using the probe, SA. First, we validated SA dissociation turnover dynamics by quantifying the early effects of cytoskeletal perturbation on actin turnover. Next, we found that MSC differentiation involves change in actin turnover that precedes change in the cell shape and has the potential to be used as a dynamic reporter of lineage progression. A single-cell F-actin dual-staining based high content image informatics approach enabled parsing emergent phenotypes much earlier than the previously reported studies. Finally, as a potential application, we applied the SA turnover image analysis to detect slow actin turnover as a result of in-vitro aging, which could be a potential discriminant of early aging effects in stem cell cultures.

Supplementary Figures

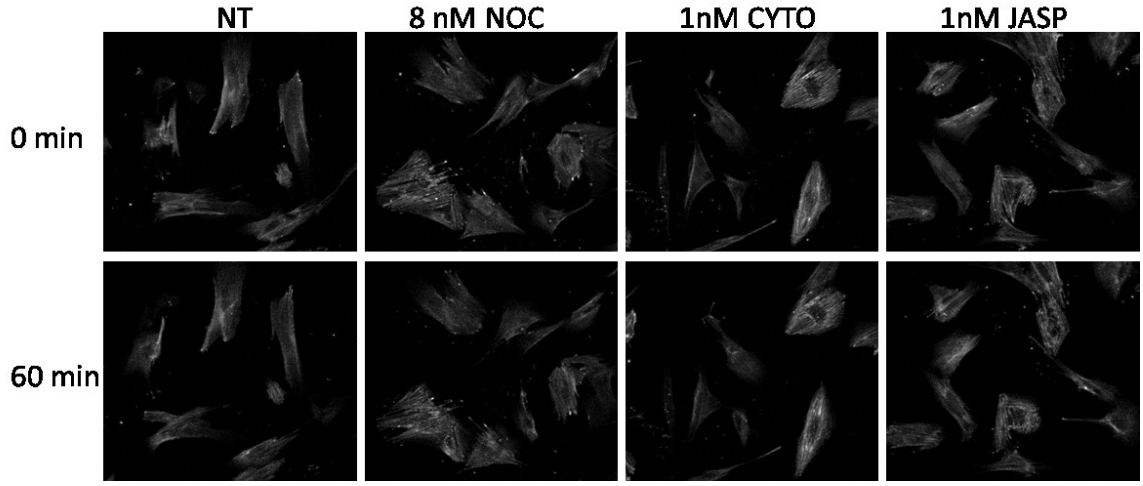

Supplementary Fig. 3.1. Cytoskeletal drug treatment at low dosage had no appreciable effect on cell morphology: SA stained cells were treated with the cytoskeletal drugs NOC, CYTO and JASP after washing off the staining media and imaged for 60 minutes.

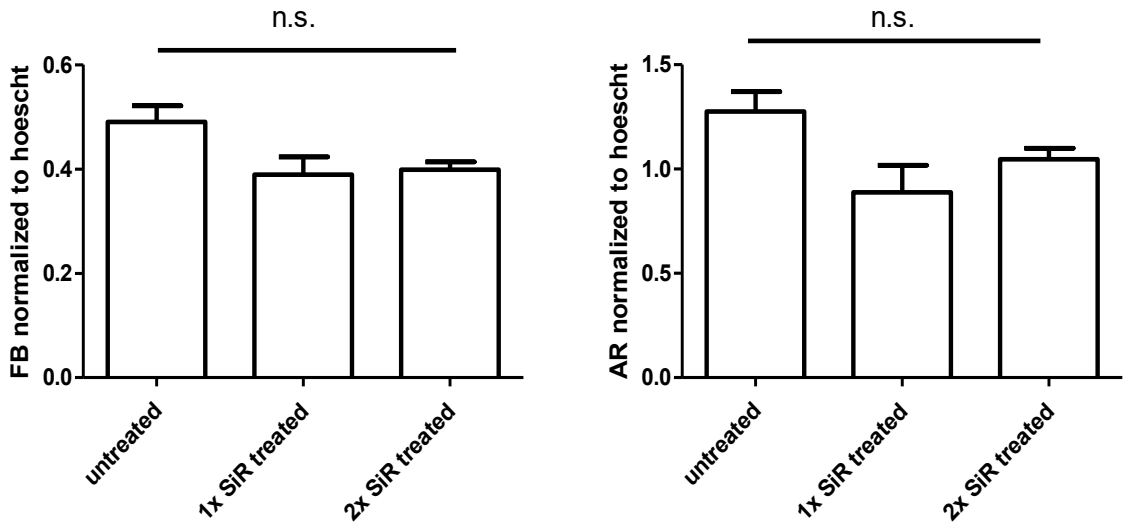

Supplementary Fig. 3.2. Effect of SA staining on MSC differentiation: Cells were either stained once (day 0) or twice (day 0 and 7) overnight during 14 days of AD or OS differentiation. Adipogenesis (adipored) and osteogenesis (fast blue) were compared vs unstained group. For each group, values are mean +standard error (n=3).

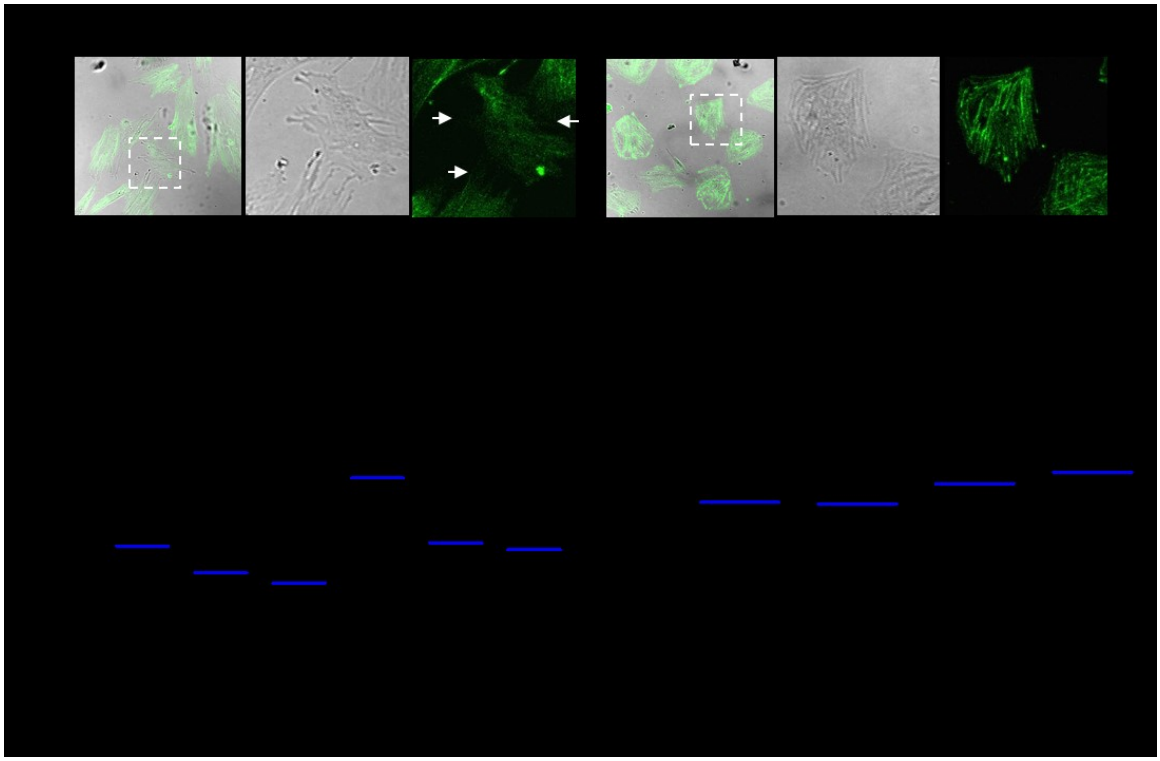

Supplementary Fig. 3.3. Characterization of the effect of SA on actin morphology and co-staining with Phalloidin: **(A)** Live cell images after staining with SA (green) at 100nM and 500nM. 100nM SA showed poor staining of protrusive dynamic structures such as filopodia (white arrows) but brighter staining of stress fibers. The dashed rectangle is the zoomed-in region to show single cells. 500nM SA stained cells affected the cell morphology accompanied by increase in stress fibers. **(B)** Phalloidin (P) staining is inversely correlated with SA. Cells stained with high(500nM) or low (100nM) SA were subsequently stained with high (132nM) or low (26.4nM) concentration of P. The mean intensity of P + standard error shown in blue bars. ***p<0.001 vs the single stained group (n=130-170) **(C)** SA labeling led to increase in cell area, but the differences were not significant at 100nM. For each group, mean area± standard error is shown in blue bars. **p<0.01 was calculated within groups with Turkey's multiple comparison test (n=130-170)

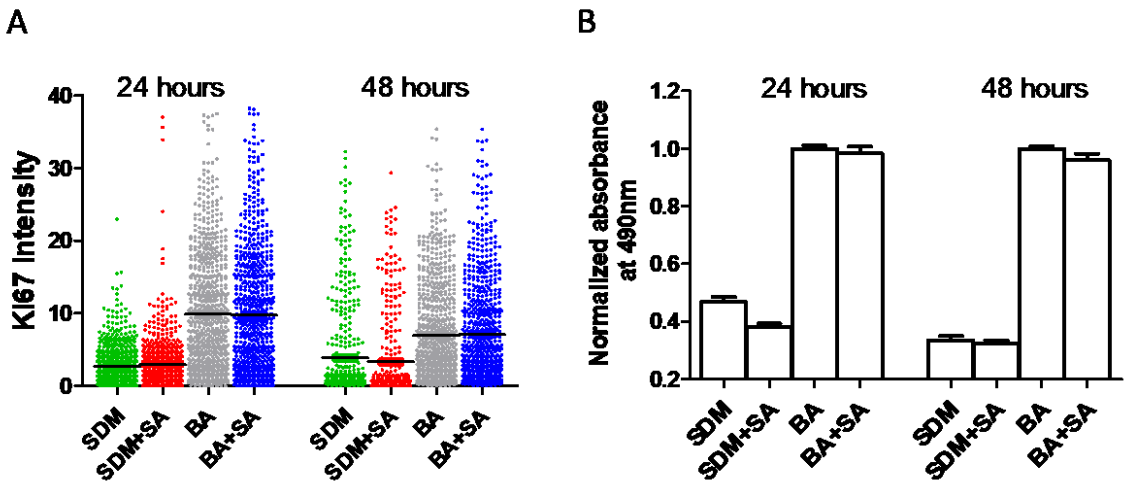

Supplementary Fig. 3.4: Effect of SA staining on cell proliferation:

Cells were stained with SA for 18 hours in either basal media (BA+SA) or serum deprived media (SDM+SA). Cell proliferation and viability were assessed by comparing **(A)** ki67 expression and **(B)** MTS assay respectively, with unstained cells (BA or SDM) after 24 and 48 hours of initial staining. Cells in serum deprived media (SDM) were used as negative control. No significant differences were observed in either assays due to SA labeling in either media. Mean Ki67 intensity (black bars) was higher in both BA and BA+SA as determined by one-way ANOVA ($p<0.001$ vs SDM or SDM+SA, n=400-742 cells). Similar results were obtained with MTS assay ($p<0.001$ vs SDM or SDM+SA, n=5)

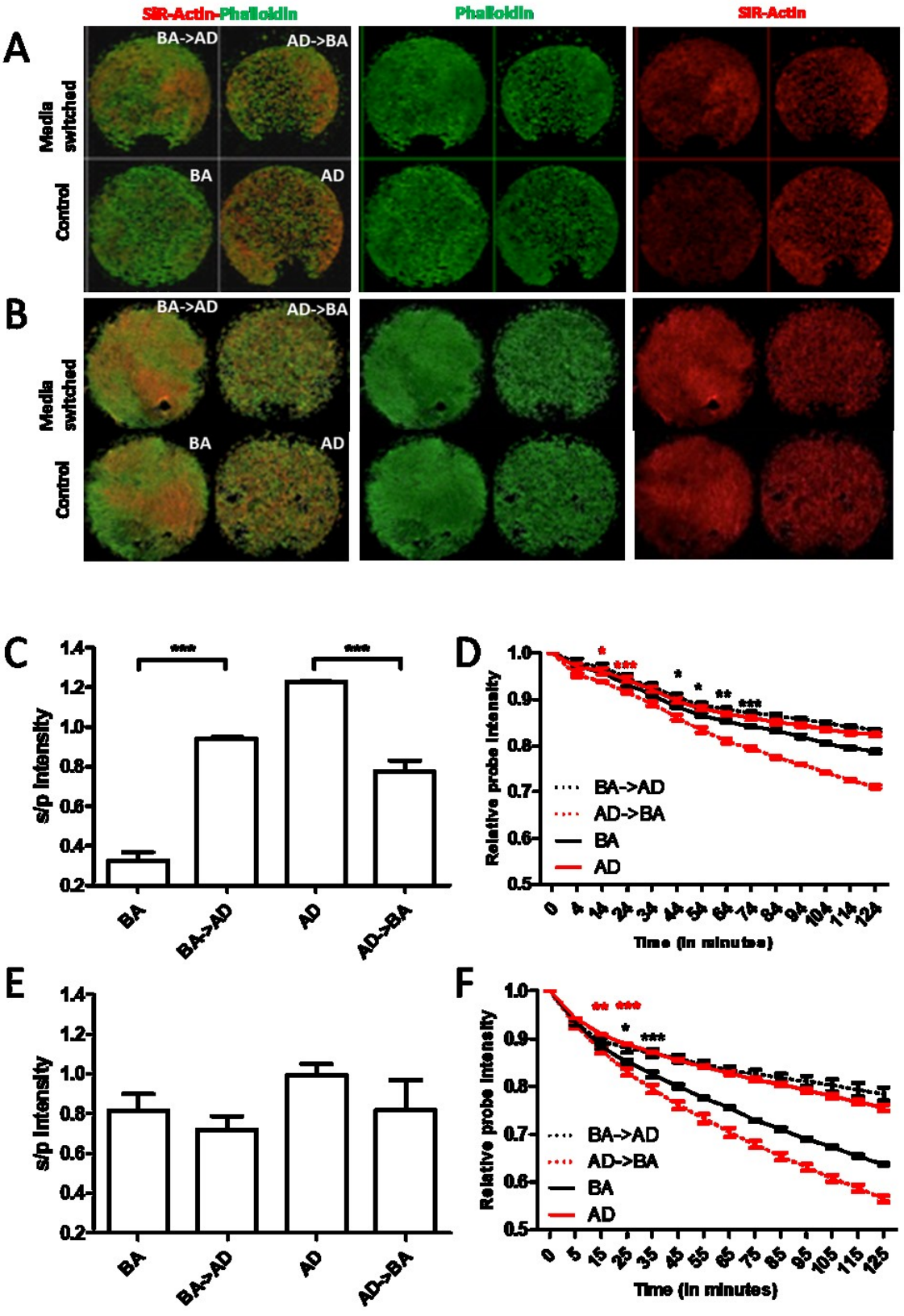
SiR-Actin-Phalloidin
Phalloidin
SiR-Actin
A
B
Media switched
Control
BA->AD
AD->BA
BA
AD
C
s/p Intensity
BA
BA->AD
AD
AD->BA
D
Relative probe intensity
Time (in minutes)
E
F

Supplementary Fig. 3.5. SA vs. Phalloidin (s/p) staining demonstrates cytoskeletal plasticity after media switch during MSC differentiation:

Cells were cultured in basal (BA) or adipogenic media (AD) for 3 or 14 days prior to media switch. A night before the media switch, cells were stained with SA and after 3 hours of media switch cells were fixed and stained with phalloidin.

A, B. s-p dual stained cells after 3 days (A) or 14 days of induction (B)

C, E. S/P intensity ratio for figures A and B respectively. For each group, values are mean +standard error (n=3). ***p<0.001 within groups with Turkey's multiple comparison test

D, F. SMAT analysis after media switch at 3 days (C), and 14 days (F) post-differentiation induction. For each group, values are ratiometric mean ± standard error of SA intensity normalized to the first timepoint within the respective group. *p<0.05, **p<0.01, ***p<0.001 vs the BA group (n=3).

Category	Feature	Canon1	Canon2	Canon3
Shape	Area	-0.0921	0.638692	0.07808
	Compactness	0.15783	0.194831	0.243956
	Major Axis Length	-0.3228	0.231322	-0.68679
	Max Feret Diameter	0.13517	-0.82015	0.766212
	Min Feret Diameter	0.03169	-1.0574	0.975473
	Minor Axis Length	-0.2893	0.964815	-0.90758
	Perimeter	0.11993	0.517484	-0.26398
	Solidity	-0.0592	0.171664	0.230162
Intensity	Manders_Correlation	-0.0014	0.038961	0.185267
	Integrated Intensity_ph	0.13481	-0.47987	0.825335
	Integrated Intensity_sir	-0.3033	-0.58467	-0.51118
	Mean Intensity_ph	-0.5487	0.161539	-0.33304
	Mean Intensity_sir	1.23095	0.556185	0.286562
Haralick texture features	Angular Second Moment_ph	-0.1563	-0.89925	-1.60342
	Angular Second Moment_sir	-1.016	-0.79401	3.917558
	Contrast_ph	0.2882	0.856925	0.295049
	Contrast_sir	1.41222	-0.3294	-3.03077
	Correlation_ph	0.39667	0.348032	-0.15778
	Correlation_sir	0.22622	-0.30291	0.718908
	Difference Entropy_ph	-0.115	-0.17024	1.3306
	Difference Entropy_sir	1.61033	-1.57163	-2.69159
	Difference Variance_ph	0.22155	-0.17868	-0.73826
	Difference Variance_sir	-0.9047	0.872723	4.074608
	Entropy_ph	1.50682	1.96433	-1.98281
	Entropy_sir	1.20014	-2.43656	-0.53744
	Gabor_ph	0.07984	-0.06236	-0.1117
	Gabor_sir	-0.085	0.111228	0.10126
	Info Meas1_ph	-0.1352	0.675782	-0.24977
	Info Meas1_sir	0.12777	0.235886	0.471895
	Info Meas2_ph	-0.8357	0.557415	0.293982
	Info Meas2_sir	0.36221	0.981438	-0.11777
	Inverse Difference Moment_ph	2.51235	1.488451	-0.44691
	Inverse Difference Moment_sir	0.94972	-0.39215	-1.72053
	Sum Average_ph	-0.2489	0.442019	1.445709
	Sum Average_sir	0.63978	0.760079	-0.07606
	Sum Entropy_ph	0.84754	-2.19042	-2.93634
	Sum Entropy_sir	-3.4428	1.624043	6.033163
	Sum Variance_ph	0.03547	-0.25562	-0.03139
	Sum Variance_sir	-0.5988	-0.97964	-1.37346
	Variance_ph	-0.0363	-0.18666	0.96231
	Variance_sir	-0.078	0.091542	-0.39858

Supplementary Table 3.1: A list of 41 features along with a set of example canonical covariates used for LDA based classification of s-p dual stained MSCs after 24 hours of BA, AD, OS and CH (Fig. 3.4b).

Predictor	Portion	Rank
Mean Intensity_sir	0.3195	1
Integrated Intensity_sir	0.1389	2
Difference Entropy_sir	0.0379	3
Info Meas2_sir	0.0331	4
Info Meas1_sir	0.0286	5
Entropy_sir	0.0286	6
Integrated Intensity_ph	0.0254	7
Area	0.0226	8
Sum Entropy_sir	0.0214	9
Max Feret Diameter	0.0192	10
Manders_Correlation	0.0179	11
Info Meas1_ph	0.0174	12
Correlation_sir	0.0173	13
Angular Second Moment_sir	0.0167	14
Solidity	0.016	15
Mean Intensity_ph	0.0154	16
Compactness	0.0154	17
Info Meas2_ph	0.0147	18
Correlation_ph	0.0145	19
Difference Variance_sir	0.0141	20
Major Axis Length	0.0139	21
Min Feret Diameter	0.012	22
Minor Axis Length	0.0118	23
Contrast_sir	0.011	24
Sum Average_sir	0.0102	25
Difference Variance_ph	0.0099	26
Variance_sir	0.0098	27
Inverse Difference Moment_sir	0.0093	28
Gabor_sir	0.0086	29
Sum Variance_sir	0.0075	30
Variance_ph	0.0075	31
Perimeter	0.0072	32
Sum Variance_ph	0.0063	33
Sum Average_ph	0.0062	34
Gabor_ph	0.0059	35
Difference Entropy_ph	0.0059	36
Inverse Difference Moment_ph	0.0056	37
Contrast_ph	0.005	38
Sum Entropy_ph	0.0049	39
Angular Second Moment_ph	0.0036	40
Entropy_ph	0.0033	41

Supplementary Table 3.2: Predictor screening analysis to show the contribution of individual features for lineage classification. Data shown only for 24 hr timepoint (Fig 3.4b). SA intensity and texture features were in the top 5, but not the shape descriptors for parsing the cells

Chapter 4: Fluorescence-based actin turnover dynamics of stem cells as a profiling method for stem cell functional evolution, heterogeneity and phenotypic lineage parsing

Note: This chapter has been reproduced from the following publication:

Prakhar Mishra, Rick I. Cohen, Nanxia Zhao, Prabhas V. Moghe. Fluorescence-based Actin Turnover Dynamics of Stem Cells as a Profiling Method for Stem Cell Functional Evolution, Heterogeneity and Phenotypic Lineage Parsing.

Methods. 2020 May 28;S1046-2023(20)30026-8. doi: 10.1016/j.ymeth.2020.05.020. Online ahead of print.

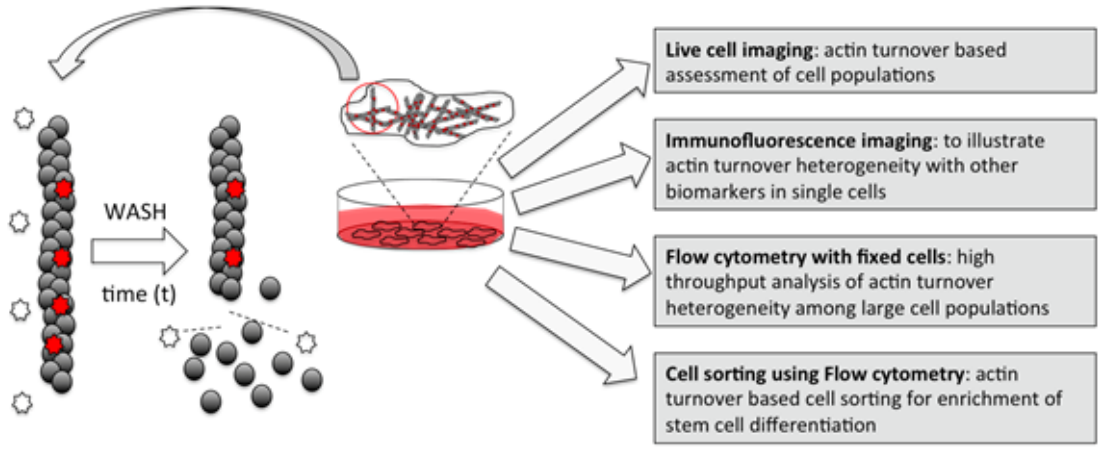

Graphic Summary of chapter 4: Multiple methods to employ SiR-actin (SA) labeling of actin cytoskeleton in live cells: SA is a fluorogenic actin filament specific probe that can be used as a surrogate marker of live-cell actin dynamics. Fluoro-labeled cells can be assayed in several ways, including: live cell imaging (quantification of actin turnover), Immunofluorescence (high content image analysis to correlate actin turnover with other cellular processes), Flow Cytometry (rapid analysis of cell population distribution of actin turnover along with other biomarkers), Cell Sorting (isolation of cell sub-populations based on actin turnover).

4.1 Abstract

Stem cells are widely explored in regenerative medicine as a source to produce diverse cell types. Despite the wide usage of stem cells like mesenchymal stem cells (MSCs) and induced pluripotent stem cells (iPSCs), there is a lack of robust methods to rapidly discern the phenotypic and functional heterogeneity of stem cells. The organization of actin cytoskeleton has been previously used to discern divergent stem cell differentiation pathways. In this paper, we highlight the versatility of a cell profiling method for actin turnover dynamics. Actin filaments in live stem cells are labeled using SiR-actin, a cell permeable fluorogenic probe, to determine the endogenous actin turnover. Live MSC imaging after days of induction successfully demonstrated lineage specific change in actin turnover. Next, we highlighted the differences in the cellular heterogeneity of actin dynamics during adipogenic or osteogenic MSC differentiation. Next, we applied the method to differentiating iPSCs in culture, and detected a progressive slowdown in actin turnover during differentiation upon stimulation with neural or cardiac media. Finally, as a proof of concept, the actin dynamic profiling was used to isolate MSCs via flow cytometry prior to sorting into three distinct sub-populations with low, intermediate or high actin dynamics. A greater fraction of MSCs with more rapid actin dynamics demonstrated increased inclination for adipogenesis, whereas, slower actin dynamics correlated with increased osteogenesis. Together, these results show that actin turnover can serve as a versatile biomarker to not only track cellular phenotypic heterogeneity but also harvest live cells with potential for differential phenotypic fates.

4.2 Introduction

Mesenchymal stem cells (MSCs) have been widely explored for cell based regenerative applications. Knowhow and control of differentiated MSCs are integral to the cell therapeutic efficacy following cell transplantation but the clinical outcomes can be challenged by the innate heterogeneity and lineage propensity of MSCs. Typically, the phenotypic classification of MSCs is defined by their ability to demonstrate plastic adherence, self-renewal and tri-lineage differentiation potential, along with expression of CD105, CD90, CD73 and lack of CD45 [24]. However, several studies have recommended the consideration of novel surface markers such as CD146, CD271 given that these biomarkers correlated with increased differentiation or proliferation capacity [229, 230]. Yet, the expression of these newly reported markers varies depending on the donor or the tissue of origin, and the relevance of these markers during dynamic cycles of lineage differentiation and dedifferentiation remains to be fully validated. Thus, there is a need to identify a robust and universal phenotypic determinant to simplify the processability of MSC characterization.

The cytoskeleton has been shown to possess the ability to both influence and correlate with MSC differentiation [194]. Naïve MSCs have a fibroblastic spindle shape morphology with actin cytoskeleton organized as thin, parallel microfilaments spread across the cytoplasm [179]. When naïve MSCs differentiate, they undergo distinct cytoskeletal changes depending on the final cell type [84, 179, 193]. Osteogenic differentiation results in increased actin polymerization leading to an intertwined patterning of actin filaments with thickened stress fibers [179, 193]. In contrast, adipogenic differentiation results in a rounded cell morphology, with reduced focal

adhesions and a disrupted actin network [185, 231]. Differentiation induced actin reorganization takes place over the course of several days to attain a distinct lineage specific cell shape. Interestingly, much before the appearance of gross morphological changes in the differentiated cells, higher order variations in cell shape and cytoskeletal organization have been shown to have the ability to forecast the lineage fates in MSCs within few hours of induction [84, 164]. In addition to being a morphological marker of differentiation, the actin cytoskeleton actively regulates differentiation. In their seminal study, Mcbeath et al. demonstrated that manipulation of cytoskeletal morphology conveyed mechanical cues that influenced lineage commitment of MSCs. Furthermore, several studies have also shown that disruption of actin cytoskeleton can modify cell differentiation [119, 179, 206, 232]. For instance, modulation of actin network using cytoskeletal drugs results in downregulation of osteogenesis [232], while the inhibition of actin polymerization results in promotion of adipogenesis [232].

Another major stem cell source for cell-based therapies are human pluripotent stem cells. These include but are not limited to human embryonic stem cells (hESC) and induced pluripotent stem cells (iPSC) [233-238]. Many protocols have been advanced to optimize the differentiation process to generate cells belonging to the three possible lineages: endoderm, ectoderm, and mesoderm (reviewed in selected publications: [239-248]). However, a major challenge is the ability to establish a highly differentiated population of cells without significant phenotypic heterogeneity. Cytoskeletal markers, such as alpha and beta tubulins, are among the earliest proteins that emerge during iPSCs differentiation to become cardiomyocytes or neurons [133]. Similarly, proteins including alpha- and beta- MHC appear when IPSCs adopt cardiac phenotype [249]. Several retrospective studies have more broadly investigated cytoskeletal changes [133, 136, 249-

253]. The role of the immediate morphological changes and the relation to differentiation has also been examined with greater focus [251]. While these studies will help understand how spontaneous differentiation, or particular signals alter the cytoskeleton and associated pathways, they do not afford the ability to address the heterogeneity within a cell population during differentiation.

The actin cytoskeleton has been largely studied as a static marker in the context of stem cell differentiation, as exemplified by the gold standard F-actin probe, phalloidin, which requires cell fixation. For visualization of actin in live cells, some of the widely used methods involve administration of fluorescent actin-binding proteins (e.g. LifeAct), actin-directed nanobodies (e.g. Actin-Chromobody) or fluorescent-labeled actin (e.g. GFP-actin derivatives) in live cells [254]. Recently, we showed a new approach to benchmark actin turnover using SiR-actin (SA), a fluorogenic live-cell F-actin specific probe [255]. Unlike the aforementioned live F-actin reporters, SA offers a unique feature since its fluorescent labeling correlates with the endogenous filament actin turnover in live cells. Therefore, cells with high levels of actin polymerization or pronounced stress fibers demonstrate brighter staining with SA, whereas cells with low actin polymerization level or high actin turnover display dimmer probe labeling. Quantitative image analysis of the changing SA fluorescence intensity as a result of actin reorganization could be used as a metric of the real-time actin turnover [255].

In this study, we highlight the use of SA intensity based live stem cell profiling method in terms of harnessing actin turnover in multiple ways, from assessing stem cells during differentiation to isolating MSC sub-populations to achieve enhanced differentiation. By using SA imaging, we found a correlation between actin turnover and

differentiation in a heterogenous cell population. Similarly, SA labeling was found to correlate with the expression of lineage specific markers when differentiating to cardiomyocyte or neuronal lineages. Lastly, we employed cell sorting to isolate and characterize MSC sub-populations for their inclination to differentiate. Given the universal nature of actin cytoskeleton, we suggest that our method could serve as a proxy marker for probing live cell differentiation or for selective enhancement of stem cell differentiation.

4.3 Materials and methods

4.3.1 MSC culture

Human bone-marrow derived MSCs were provided by Dr. Rick Cohen (Rutgers University). Cells were maintained in VWR™ T-75 or Corning® T-175 tissue culture flasks. After the initial expansion of the cells in Peptrotech® MSC media, cells were cryopreserved at passage 3 (P3). Upon thawing, cells were maintained in basal growth media (BA) prepared with Gibco Minimum essential medium α (MEMα) supplemented with 10% Fetal Bovine Serum-premium select (Atlanta Biologicals™) and 0.1%v/v penicillin-streptomycin (Lonza). The growth media was changed every third day and passaged when 70-80% confluence was reached. For passaging, MSCs were dissociated with TrypLE™ Express (Gibco) and a seeding density of 3000-4000 cells/cm^2 was used. Flow cytometric isolation of cells based on actin turnover was conducted at P6 or P7 upon reaching cell count of at least 5 million cells. Post-sort cells were allowed to attach and grow. Subsequent proliferation and differentiation studies were done for 2 more passages.

Adipogenic media was prepared with BA media supplemented with 1 μM dexamethasone, 10 μg/mL insulin, 500 μM isobutyl-1-methyl-xanthine and 200 μM indomethacine. Osteogenic media was prepared by adding 500 μM L-ascorbic acid-2phosphate, 1 μM dexamethasone, and 10 nM b-glycerophosphate to the BA media. Chondrogenic media bullet kit was obtained from Lonza. Cell differentiation experiments were conducted on 96-well multi-well dish at 10,000 cells/cm^2 seeding density.

4.3.2 iPSC culture

Human foreskin Fibroblasts (HFFs) were derived from discarded tissue (CHTN) using the protocol similar to Bryne and coworkers using optimized media conditions to support the expansion of Skin Derived Precursors [256]. All cell culture is carried out in 5% O2, 5%CO2 atmosphere. The HFF cultures were electroporated (NEON, ThermoFisher) with a single EBNA1/Ori plasmid containing a polycistronic vector with Oct4, Sox2, KLF4, L-Myc and a fusion of mRFP and Blasticidin S Deaminase using conditions similar to Okita and coworkers [257]. iPSC colonies appeared within 30 days and were subcultured using standard enzyme free techniques onto vitronectin (PeproTech) coated plasticwear with albumin free low protein culture media (PeproTech). Under these conditions, the IPS cells were Oct4+/SSEA4+/SSEA1-, and Nanog+/Lin28+/Tra-1-60+, and found to reliably form both neurons [258] and cardiomyocytes (TnT1+, beating clusters) using standard protocols [259, 260]. A more detailed protocol is included in the supplementary material.

4.3.3 Immunostaining pre-SA labeled MSCs to determine actin turnover correlation with differentiating MSCs

MSCs were stained with 100 nM SA overnight in BA followed by 7 day culturing in BA, AD or OS media. Then cells were fixed in 4% PFA and permeabilized with 0.1% triton-X100.

PPARG and RUNX2 specific antibodies (Cell Signaling Technology, Inc.) were used as differentiation specific markers for AD and OS were labeled respectively [36, 261, 262]. To evaluate differentiation specific dynamics of actin turnover, cells in AD and OS were compared separately against cells in BA. For image analysis, Hoescht 33342, Invitrogen™ (nuclear stain) was used to mark single cells. For BA vs AD, PPARG intensity was plotted against SA after normalization using the highest value of SA and PPARG among both media. Similar approach was followed for BA vs OS, but with RUNX2 quantification instead of PPARG. Adipogenesis and osteogenesis were assessed by plotting PPARg or RUNX2 intensities respectively against SA after normalization using their highest intensity values and compared to BA media.

4.3.4 Flow cytometry for isolation of MSC sub-populations

MSCs were labeled with 100nM SA overnight, then transferred to the sorting buffer (2% fetal bovine serum, 0.5mM EDTA, 20 μg/mL DNaseI (Worthington Biochemical, Lakewood, NJ) in Dulbecco's Modified Eagle Medium/Nutrient Mixture F-12. Prior to sorting, cells were filtered through a 40um nylon mesh to eliminate cell aggregates. BD Biosciences Influx High Speed Cell Sorter equipped with 100μm nozzle was used for aseptic isolation of MSC sub-populations. 640nm solid-state laser was used to sort MSCs based on SA probe intensity. DAPI staining was done to determine the gating for excluding dead cells. The sorted cells were collected based on SA intensity gradation into 3 sub-populations: dim, intermediate and bright.

4.3.5 SA quantification based on live iPSC imaging

Live iPSCs were labeled with 100nM SA overnight in iPSC growth media (IGM) following the methodology described by 2019 Mishra et al. [255]. The SA staining media was aspirated, and a quick media change was done to remove residual SA. The cell culture dish was placed on Zeiss LSM780 laser scanning confocal microscope equipped with a stage-top incubator. The reference intensity images were captured for all test conditions. Time-lapse imaging was performed following induction with IGM, cardiac differentiation media (CDM) or neural differentiation media (NDM) for 4 hours. Imaging was done with the 10x objective in triplicates for all test conditions and 4 distinct fields were imaged in each replicate. Subsequent image analysis was done using ImageJ to measure the changing SA intensity of the cell populations compared to the reference images. The mean gray values of SA were plotted against time to quantify changing actin turnover.

4.3.6 Flow cytometry analysis to determine the correlation between SA and iPSC pluripotency/differentiation markers

iPSCs were labeled with 100nM SA overnight, then the cells were cultured in label free IGM, CDM or NDM for up to 3 days. At day 0, 2 and 3, cell monolayer was dissociated with TrypLE™ Express (Gibco) and cells were fixed using 2% paraformaldehyde in PBS. Subsequently, cells were permeabilized and immunostained with primary labeled SOX-1 (early neuronal or ectodermal marker) [263-265], SSEA-1 (general early differentiation marker) [266-269], OCT3/4 (stemness marker) [270] and BRACHYURY (early cardio or mesodermal marker) [271-273] antibodies (BioGems). The correlation between SA and iPSC markers was assessed by FACS analysis of the immunolabeled cells using BD Biosciences Influx High Speed Cell Sorter.

4.3.7 Differentiation assay for MSCs

MSCs were seeded at the density of 10,000 cells/cm^2 and allowed to attach overnight in 96-well dish. MSC differentiation were induced with adipogenic or osteogenic media for 7 or 14 days. The cells were fixed with 4% paraformaldehyde and stained with fast blue RR (Sigma) and AdipoRed (Lonza) reagents to stain for alkaline phosphatase (osteoblast) and intracellular triglycerides (adipocyte) respectively. For cellular enumeration, Hoechst dye (33342, Invitrogen) was used to label nuclei. Subsequently, to scan the entire wells, automated confocal images were taken of 3 wells per condition, and fast blue RR and AdipoRed fluorescence intensity signals were normalized to the number of cells in each well.

4.4 Results

4.4.1 Method for tracking actin dynamics during stem cell differentiation induction

Actin filaments (F-actin) are dynamic structures that rapidly polymerize and depolymerize, with the addition and detachment of actin monomers driven by ATP hydrolysis and several cellular factors [274]. SA binds F-actin at sites with 3 contiguous monomeric units and increases its brightness by 100-fold [201]. When the F-actin undergoes depolymerization, the bound probe comes off resulting in loss of fluorescence [6]. Our approach to assessment of actin turnover involves temporal analysis of changing SA labeling. A workflow for the method is illustrated in Fig. 4.1. Briefly, the F-actin in live cells is probed with SA in basal growth media overnight to allow maximal SA labeling in all cells. Subsequent removal of staining media followed by addition of a cytoskeletal

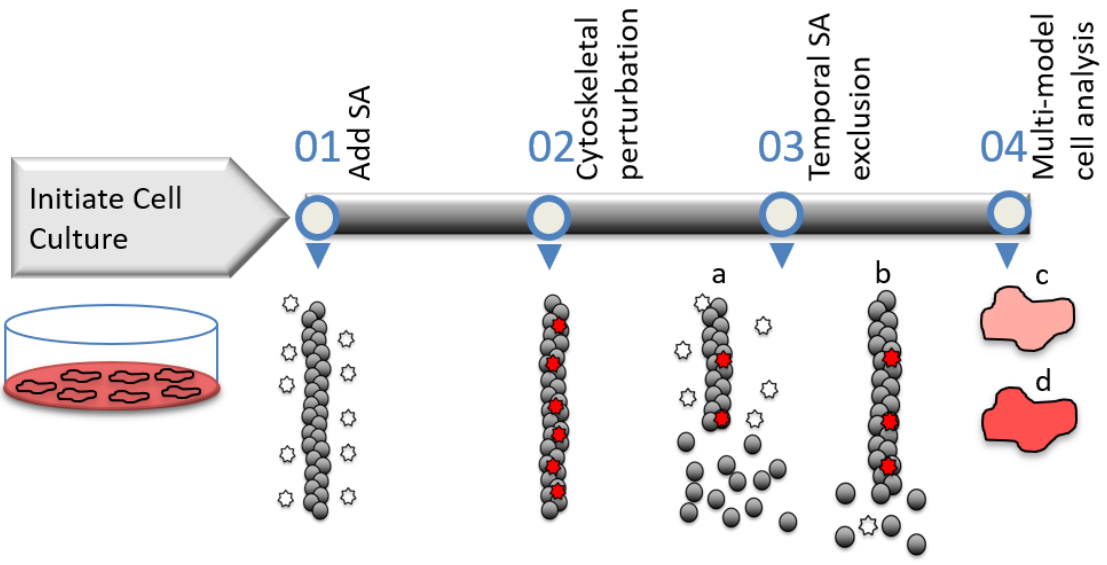

Fig. 4.1. Workflow for SiR-actin (SA) labeling protocol enables live cell actin turnover analysis and cellular profiling: 1) Cell seeding and adhesion in basal media, followed by SA labeling in basal media; 2) Repeated washes with basal media followed by introduction of cytoskeletal perturbation cues; 3) With time, cells with high actin turnover display lower SA fluorescence (a, c) compared to the cells with low actin turnover (b,d); 4) The variable SA labeling can be assessed qualitatively or quantitatively, and used as a basis for further cell analysis or cell sorting.

perturbation results in varying loss of SA from cells based on their actin turnover status. In this paper, the cytoskeletal perturbation was induced with differentiation media, but it is possible to influence cell dynamics in other ways as well. For instance, cytoskeleton perturbing drugs that arrest actin dynamics (e.g. cytochalasin D) result in prolonged retention of SA probes on actin filaments compared to untreated cells [255]. High SA label indicates a slow actin turnover and vice versa. SA labeled cells can be subsequently evaluated by various methods for qualitative or quantitative assessment of actin turnover in cell populations.

4.4.2 Live tracking of actin dynamics during MSC differentiation

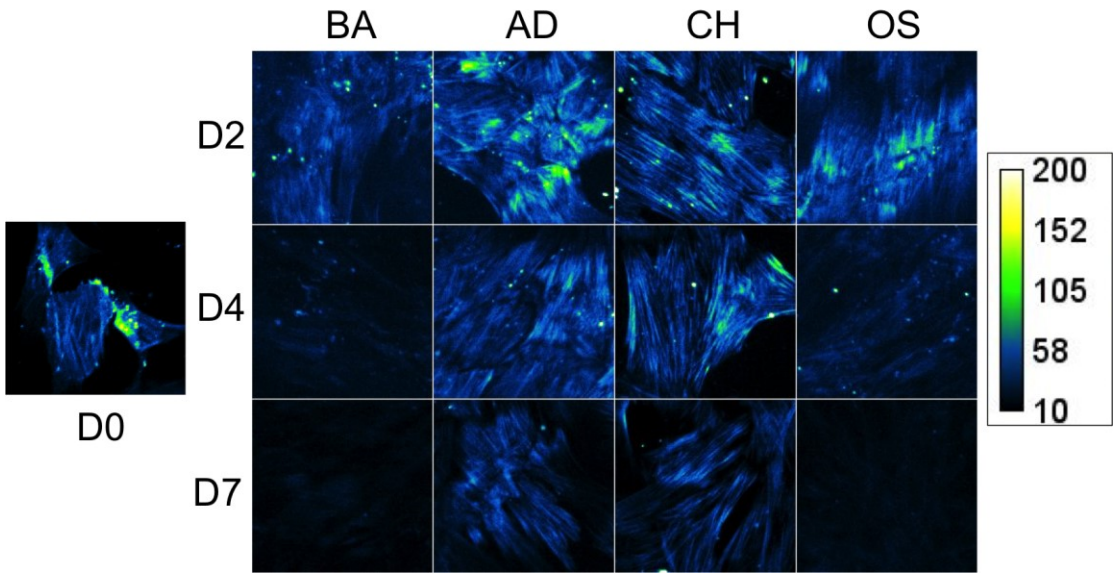

Fig. 4.2. Multiday live cells imaging of MSCs showed lineage specific changes in SA labeling: Representative images showing changing SA staining during induction for 7 days with basal (BA), adipogenic (AD), chondrogenic (CH) or osteogenic (OS) media. The imaging settings were kept consistent Day 2 onwards (calibration bar unit: mean gray value). Higher SA brightness indicates a slowdown in actin turnover.

In order to monitor how differentiating cells modulate their actin turnover, cells were stained with SA in basal media (BA) followed by stimulation with adipogenic (AD), osteogenic (OS) and chondrogenic (CH) media (Fig. 4.2). In BA, the cells demonstrated elongated spindle morphology with less defined stress fibers, indicating a dynamic actin cytoskeleton as this group demonstrated lowest SA intensity at all time-points. Adipogenic induction begins with dramatic reduction in actin turnover at day 2 as evident by the SA

brightness. The cells in AD continue to show slow actin turnover like the chondrogenic induction till day 7. Similar to AD, CH showed high retention of SA during 1 week of induction with relatively brighter staining of stress fibers indicating reduced actin turnover i.e. less dynamic cytoskeleton. OS induction demonstrated higher SA labeling of actin stress fibers compared to BA at day 2, but the subsequent loss of SA staining indicates a higher level of cytoskeletal reorganization unlike AD and CH.

4.4.3 Correlating changing actin turnover with differentiation specific markers to highlight heterogeneity of MSC states

After discerning an early slowdown in actin turnover in MSCs upon differentiation induction, next we sought to understand how actin turnover dynamics correlate with MSC differentiation. MSC differentiation was induced after initial overnight SA labeling in BA media, followed by cell culture in BA, AD or OS media for 7 days. After 7 days, the differentiated cells were fixed and immunostained for lineage specific reporters, PPARG (master regulator of adipogenesis[262]) or RUNX2 (master regulator of osteogenesis [36]). Cells in BA showed minimal expression of PPARG or RUNX2 (Fig. 4.3.1 A-D). To determine the correlation between SA labeling due to MSC differentiation markers, SA intensity was plotted against PPARG (AD marker) or RUNX2(OS marker). The intensity of fluorophores in single cells were normalized with the highest mean gray value within BA vs AD or BA vs OS groups. An ellipse was drawn encompassing all the datapoints in BA to define the basal level of reporter intensities for the undifferentiated cells (Fig. 4.3.2 A, C). In AD media, the average SA intensity was higher compared to BA (Fig 4.3.1 B, 4.3.2-A,-B,-E). $PPARG^{high}$ cells exhibited low levels of SA labeling (Fig. 4.3.2 B-ii). A possible explanation could be that adipogenic induction results in slowdown in actin-turnover (Fig.

4.2) but as the adipocytes mature, SA is eliminated due to the loss of actin filaments [185]. Cells in OS also showed elevated levels of SA labeling compared to BA (Fig. 4.3.2 D, F). either AD or OS lineages demonstrated a more uniform range of SA expression, while the

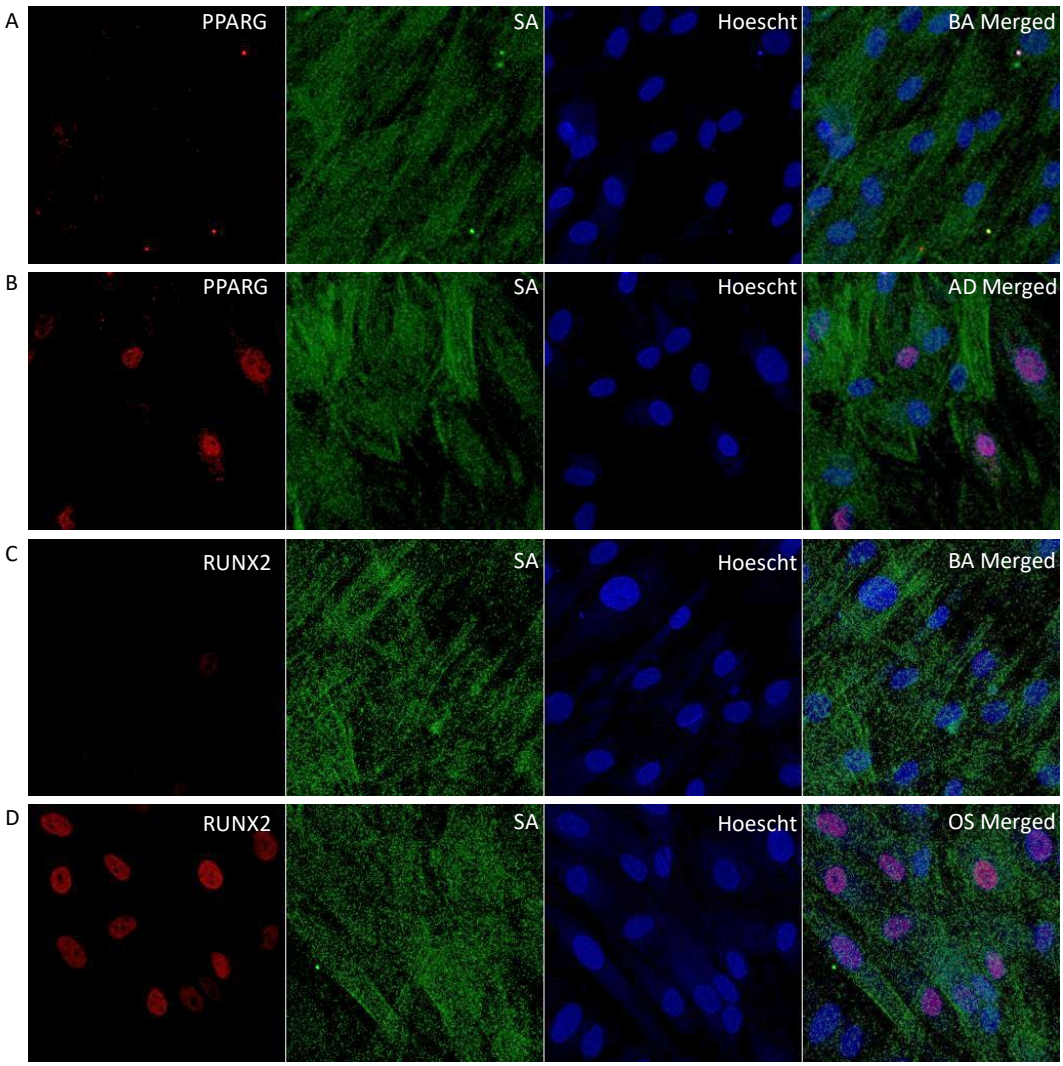

Fig. 4.3.1 Immunofluorescence based correlation of differentiation and actin turnover in MSCs: After SA labeling, MSCs were cultured for 7 days in BA, AD or OS media. Subsequently, cells were fixed and immunostained. The representative images show differences in expression of SA (actin turnover marker), Hoechst (nuclei), PPARG [adipogenic marker (A) BA media, (B) AD media) or RUNX2 (osteogenic marker (C) BA media, (D) OS media].

undifferentiated cells had a more variable SA labeling (Fig. 4.3.2 B, D). Taken together, the SA dynamics reveals actin turnover heterogeneity during MSC

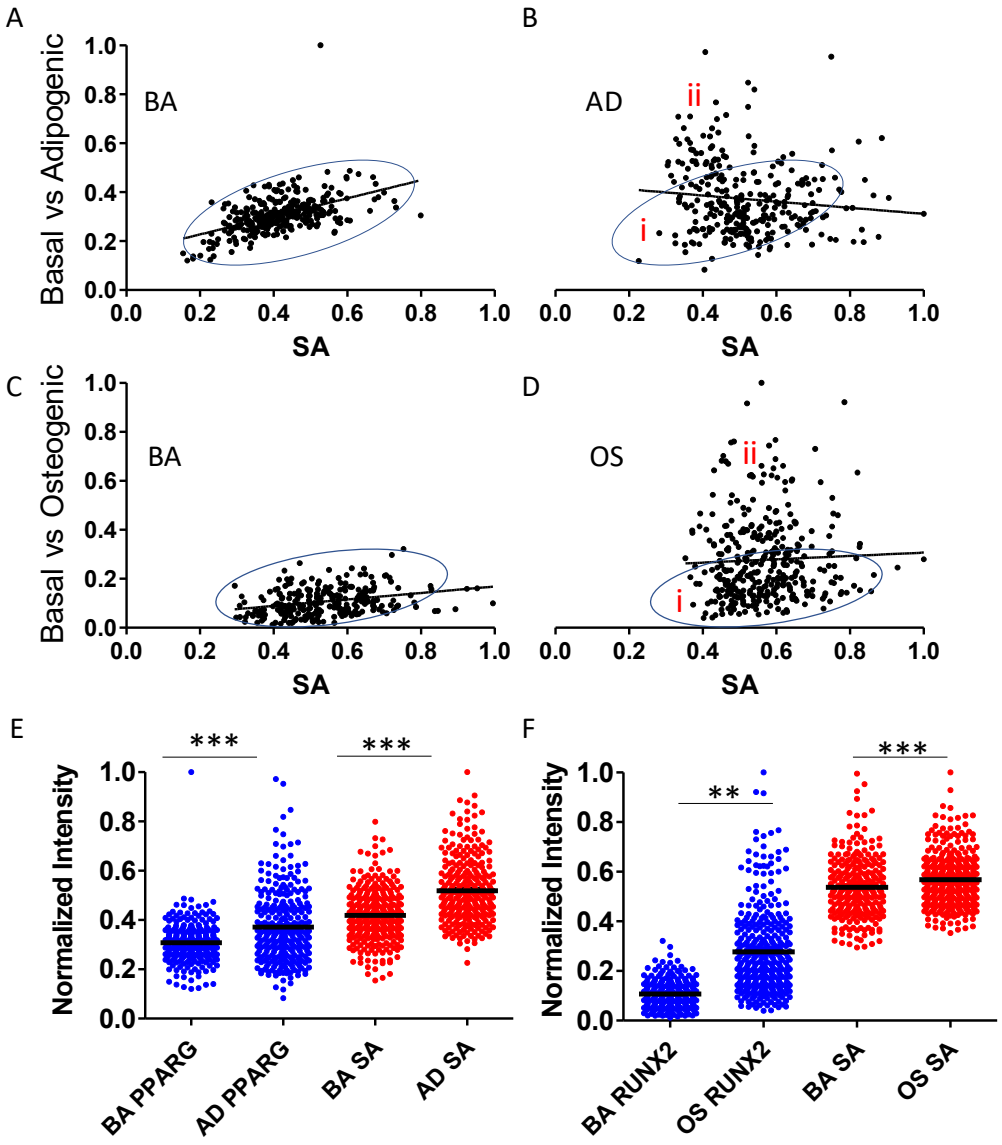

Fig. 4.3.2. Immunofluorescence based correlation of differentiation and actin turnover in MSCs: The correlation plots for PPARG (A, B) and RUNX2 (C, D) intensities are shown along with best-fit line. In addition, an elliptical region was marked for AD (A, B) and OS (C, D) based on corresponding BA plots to mark the undifferentiated cells. The single cell scatter plots for SA and PPARG (E) or RUNX2 (F) are also represented along with means to summarize differences among cell populations..... *Continued on next page*

Continued from previous page: ...during AD and OS differentiation respectively compared to BA. Two-tailed Pearson correlation test for A and C showed $p<0.001$, but n.s. for B and D. [n=315(A), 285 (B), 252 (C) and 350 (D)]. Comparison of means of BA vs AD or BA vs. OS of RUNX2, PPARG, and SA was done using unpaired student t-test method ($p<0.001$ ***, $p<0.01$ **).

differentiation. Thus, intrapopulation heterogeneity during lineage commitment based on actin dynamics.

4.4.4 Early cardiomyocyte or neuronal differentiation of iPSCs involve reduction in actin turnover

iPSC maturation towards distinct lineages involves extensive cytoskeletal reorganization [133, 249] but the early changes during differentiation are not reported. Therefore, the SA-labeling based approach was extended to assess the early changes in actin turnover during iPSC differentiation. The naïve cells were SA stained in iPSC growth media (IGM), followed by stimulation with either neural differentiation (NDM) or cardiac differentiation media (CDM). Differentiation induction resulted in elevated retention of SA staining in both NDM and CDM compared to the basal growth media (Fig. 4.4.1 A). After 2 days, cells cultured in CDM showed highest probe retention with well-defined actin filaments marking the periphery of cells but with diffused cortical actin. Cells cultured in NDM showed a more dispersed SA staining but at an elevated level compared to cells cultured in growth media (Fig. 4.4.1 B).

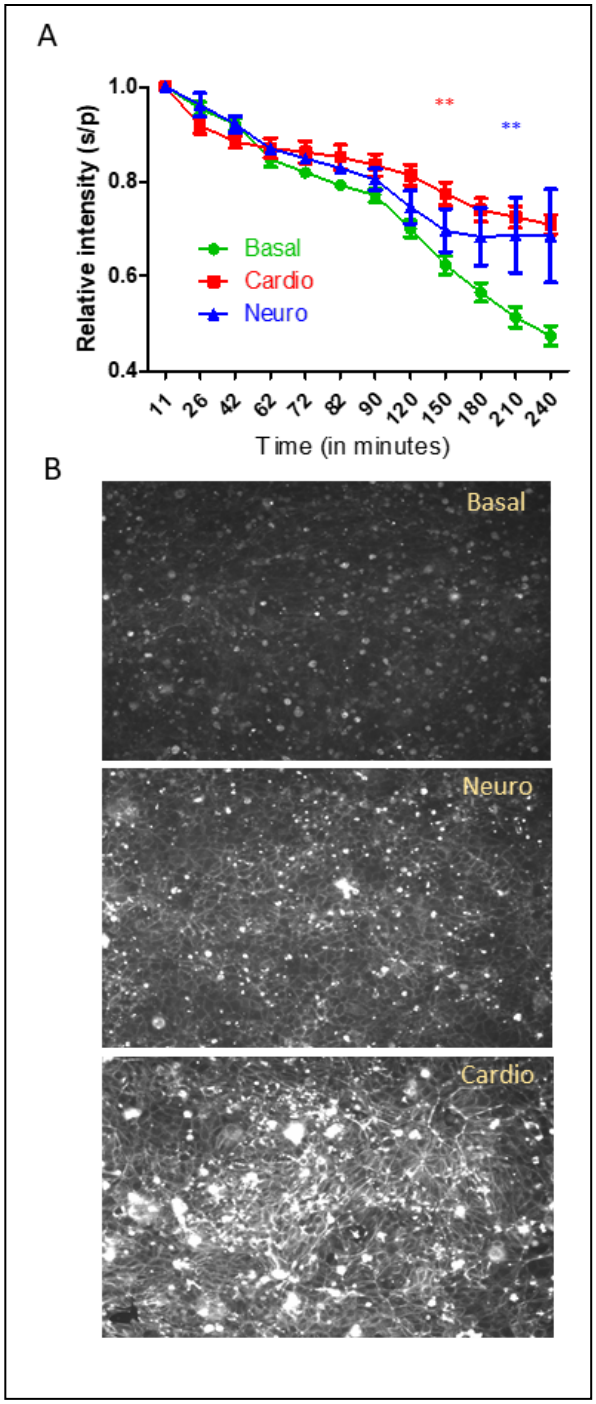

Fig. 4.4.1. Early changes in actin dynamics during iPSC differentiation. A. Intensity quantification of SA labeling during Cardiac and neural differentiation **B.** Representative images to show lineage specific SA retention after 2 days of stimulation following removal of SA staining media.

Next, FACS analysis was performed at different timepoints to assess the correlation between SA staining (actin dynamics) and early differentiation markers. Cells were cultured in NDM or CDM and fixed and immunostained at Day 0, 2, and 3. Day 1 was not included in this study as the expression early differentiation markers has not been reported previously [271]. As early as 2 days of stimulation, cells in NDM resolved into two populations and high SA expressing cells were found to be positive for Sox-1 (neuroprogenitor marker) and SSEA-1 (general differentiation marker). Oct-4 (pluripotency marker) expression declined after 2 days of stimulation compared to naïve

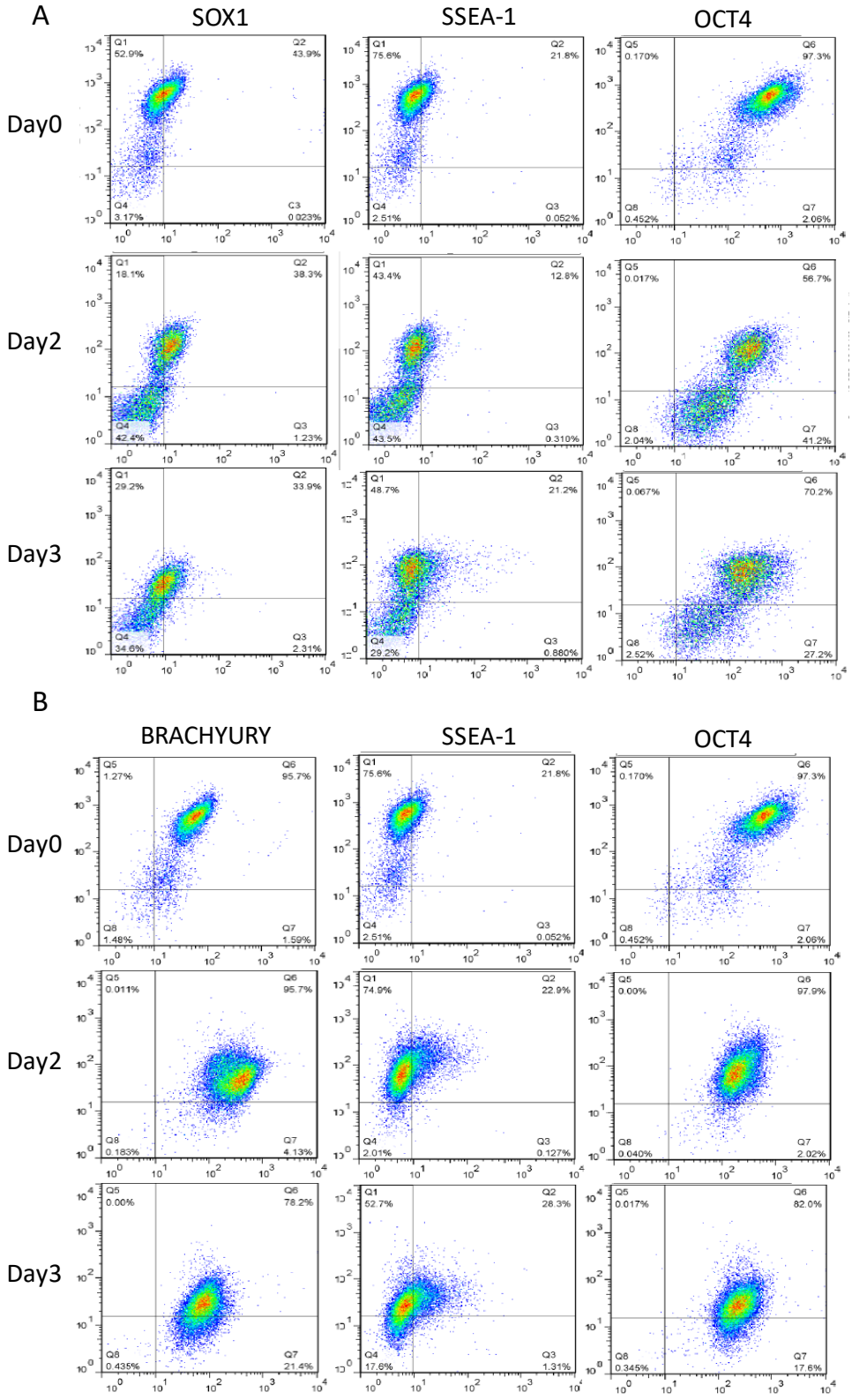

Figure Caption on next page

Fig. 4.4.2. Early changes in actin dynamics during iPSC differentiation: FACS analysis to show expression of stemness and differentiation markers for neural **(A)** and cardiac **(B)** lineages [x-axis: SiR-actin, y-axis: iPSC markers]

(Fig. 4.4.2 A). A possible explanation for 2 sub-populations could be that the initiation of neural differentiation induced a slowdown of actin turnover resulting in elevated SA levels while naïve cells lost more SA due to relatively higher actin dynamics. Upon stimulation with CDM, cells showed higher levels of SA compared to basal media or NDM indicating slower actin turnover. Unlike NDM, CDM did not resolve the iPSCs in 2 populations. However, at both timepoints (Day 2, 3), SA^{high} cells were found to have a higher expression of Brachyury (mesoderm marker, early cardiomyocyte) and SSEA-1 compared to IGM (Fig. 4.4.2 B). Interestingly, the expression of OCT-4 did not decline from day 2 to day 3. Therefore, SA labeling was found to correlate with the expression of early neural or cardiac markers indicating that iPSC differentiation initiates with slowing down of the actin turnover.

4.4.5 Actin turnover based sorting of MSCs results in sub-populations with distinct proclivities for differentiation

SA labeling is indicative of the actin cytoskeleton dynamics in live cells. Cells with more dynamic actin structures are poorly labeled while the cells with long-lived, less dynamic actin cytoskeleton demonstrate weak labeling [6, 201]. We hypothesized that the intensity of SA probe could be used as a predictive marker to isolate cells based on the dynamic status of the actin cytoskeleton. MSCs were stained with SA in basal growth media. Cell

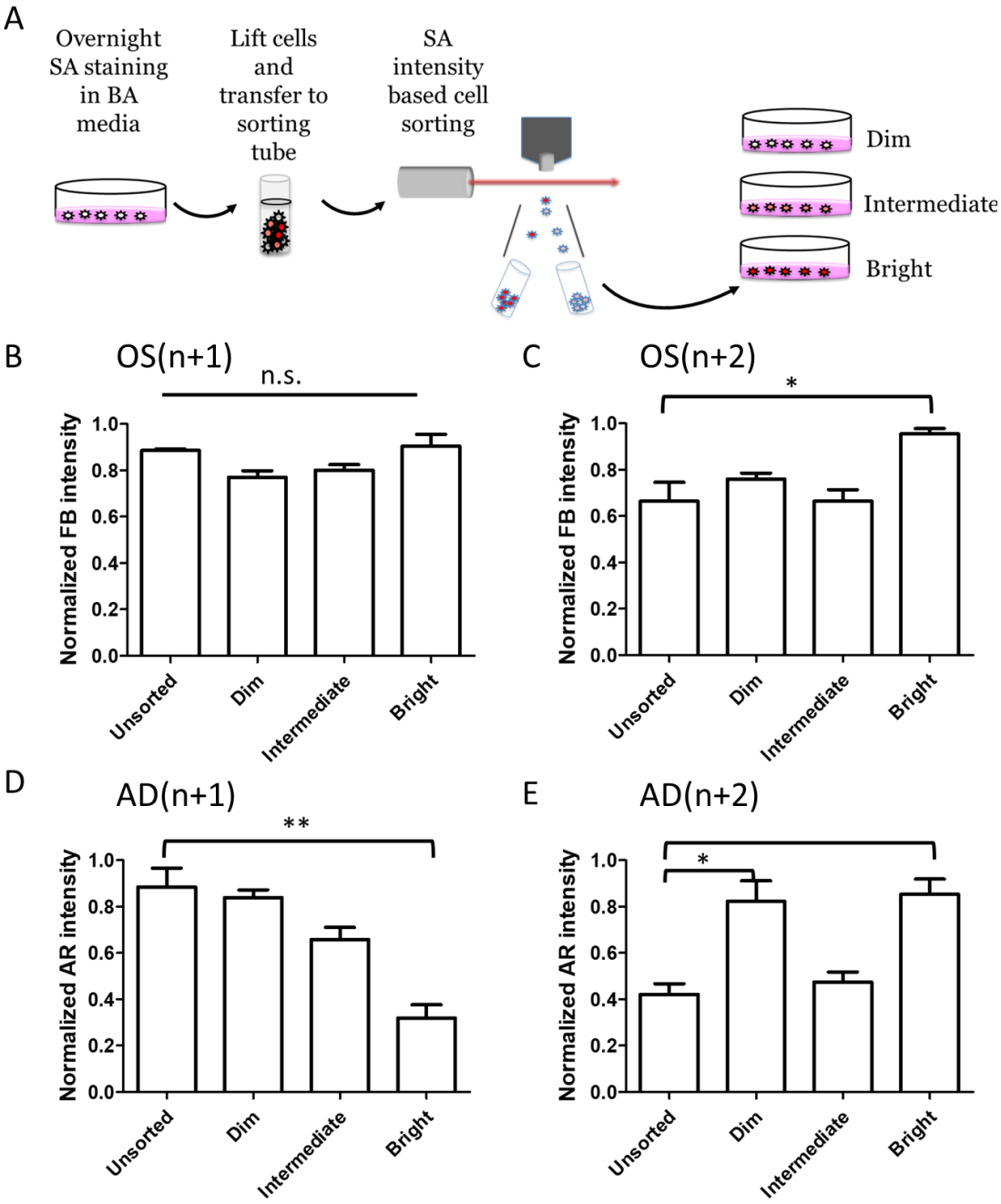

Fig. 4.5. SiR actin intensity-based cell sorting of MSCs into three potential sub-populations for enhanced MSC differentiation potential: A. Cell sorting strategy. SA intensity based sorted cells showed distinct proclivities after cell culture in OS **(B, C)** or AD **(D, E)** media for 2 weeks. For image analysis, fast blue- and adipored (AR) staining were normalized (*continued on next page)*

Continued from previous page: with hoescht (n+1: after one passage, n+2: after two passages following cell sorting). The mean values were compared using one-way analysis of variance (ANOVA) *p<0.05, **p<0.01 vs Unsorted cells.

simplicity as: Dim, Intermediate, and Bright cells (i.e. high, intermediate and low actin turnover of single cells, respectively) (Supplementary Fig. 1). Post-sorting, cells were cultured in basal media. Next day after sorting, MSCs were evaluated for their cytoskeletal features. “Dim” cells displayed a spindle shaped cell body with smaller area. While, the “Bright” cells had larger surface area, and more stress fibers. “Intermediate” cells were closer to “Dim” cells morphologically, but the SA intensity was much higher (Supplementary Fig. 2). Therefore, SA labeling could be used to resolve MSCs into distinct sub-populations based on their actin dynamics.

Next, we investigated whether SA sorted naïve MSC populations demonstrate a higher intrinsic proclivity for cell differentiation. The sorted cells were expanded, and differentiation studies were conducted for 2 consecutive passages. “Dim” cells with faster actin dynamics showed highest adipogenesis among all groups (Fig. 4.5D). A possible explanation for this observation could be that adipogenesis involves gradual degeneration of the actin cytoskeleton and the “Dim” cells with a less complex cytoskeleton and fewer stress fibers might have a higher proclivity to make adipocytes. On the contrary, “Bright” cells with slower actin dynamics showed highest osteogenesis among all groups (Fig. 4.5B). During osteogenesis, actin cytoskeleton leads to increase in actin stress fibers and actin cytoskeleton [185]. Since, the “Bright” cells have an inherently actin filament rich cytoskeleton, they might be inclined to become osteoblastic. Next, we allowed the cells to grow for another passage to test if the differentiation proclivity maintains in the sub-populations. Upon OS induction, “Bright” cells showed highest differentiation among all

groups (Fig. 4.5C). While, after AD induction, both “Dim” and “Bright” groups showed higher differentiation compared to unsorted groups (Fig. 4.5D). Therefore, actin turnover has the potential to be harnessed as a single marker for not just isolation of cells based on their inherent actin dynamics but also to isolate sub-populations with a higher proclivity for distinct lineages.

4.5 Discussion

The actin cytoskeleton plays a vital role in diverse cellular functions and has been extensively correlated with stem cell differentiation for regenerative medicine [84, 179, 232, 275]. In this paper, we highlight a live stem cell tracking methodology focused on harnessing the dynamics of the actin reorganization in the context of stem cell differentiation. We have described multiple ways in which SA labeling based actin turnover tracking can be used for long-term evaluation of actin dynamics during stem cell differentiation and as a dynamic marker for isolation of MSCs using flow-cytometry.

It is well recognized that cells undergo rapid change in cell shape during differentiation, regulated via the cytoskeleton, resulting in divergent phenotypic fates [84, 179, 193]. Most of the prior work focused on cytoskeleton-based cell profiling metrics was based on fixed cells; therefore, only considered the cytoskeleton as a static snap-shot of the cellular phenotype[84, 179, 185, 193, 206] Given the highly dynamic nature of actin cytoskeleton, the cytoskeletal dynamics itself can offer deeper insights about the temporal trajectory of cell populations that could be used to sensitively parse the cellular lineage potential. Previously, we reported a new approach involving SA, which has the unique feature of labeling actin structures based on their dynamic status to illustrate early changes in the actin turnover of differentiating MSCs [255]. Yet, the prior study was

conducted only for few hours after stimulation with differentiation media, which restricted its utility to early divergence of cellular phenotypes.

Using SA labeling, we are able to gain new insights about the status of actin turnover during the course of MSC differentiation for several days (Fig. 4.2). The onset of AD and CH differentiation involves a decline in RhoA/ROCK signaling resulting in reduced actin polymerization and loss of F-actin [275]. But we observed retention of SA after 7 days of culture in AD and CH media, instead of losing the probe due to loss of F-actin. This could be because of diminished actin polymerization, suggesting the actin filaments were preserved or remained static until transition to a functional specific lineage cell type. On the other hand, OS differentiation is supposed to increase actin polymerization and stress-fibers that should provide more binding sites for SA binding [193]. At Day 2, OS showed higher SA labeling compared to BA but we observed a small fraction of SA labeling compared to AD or CH. A possible explanation for lower SA labeling could be the OS induced actin reorganization that resulted in rapid loss of SA from the actin cytoskeleton. After 7 days of induction, SA labeling declined sharply in OS condition (Fig. 4.2). In order to more carefully evaluate the late stage dynamics of actin turnover, we re-labeled the differentiating cells described in Fig. 4.2 overnight with SA after 6 days of induction, removed the staining media the following morning and imaged further until the 10th day of initial differentiation stimulation i.e. 3rd day after relabeling (Supplementary Fig. 4.3). Both AD and CH showed higher SA labeling like Fig. 4.2, but cells in CH had more prominent labeling of stress fibers (Supplementary Fig. 4.3). Therefore, SA labeling offers a new way to probe actin turnover in live cells for several days. Live cell change in SA intensity conveys that upon actin cytoskeletal reorganization, a highly dynamic process leads to decline in observed probe intensity as SA comes off from

its binding site on F-actin[60]. The non-dynamic changes in SA labeling are not clearly described in the literature, but SA labeling is likely to be influenced by intracellular concentration, availability of binding sites and several other stochastic events that involve actin reorganization (e.g. cell cycle). There is a need for further in-vitro characterization of SA labeling, but regardless, the method can be extended iteratively as cells can be relabeled with SA to extend the duration of actin dynamics tracking.

Following SA labeling, immunostaining of differentiated cells showed intra-population heterogeneity of actin dynamics. A quantitative correlation plot of SA against differentiation specific marker helps to understand transition of actin dynamics from naïve to differentiated cells (Fig. 4.3). Especially during AD induction, it is possible to observe distinct sub-populations after 7 days of induction. Previously, we reported immediate slowdown in actin turnover after AD induction [255]. Therefore, it is possible that all cells start as SA^{high} $PPARG^{low}$ during AD induction. After 7 days, the observation of undifferentiated SA^{high} cells could be due to senescence or spontaneous differentiation towards a different lineage that enabled SA retention (Fig. 4.3.1). Subsequent transition to $PPARG^{high}$ happened after gradual decline in SA. On the other hand, OS differentiation induction showed that cells with intermediate SA labeling changed to OS phenotype without much change in SA labeling. Given the highly dynamic nature of cells in OS (Fig. 4.2), SA labeling after 7 days of induction suggests that that certain regions on F-actin are preserved during OS differentiation, where SA remains even when cells started expressing RUNX2. In future, we plan to perform this study with longer differentiation stimulation period (2-4 weeks) with the hope of obtaining improved dataset. However, it will be important to validate SA expression at measurable levels, especially in basal condition, where low SA expression was observed after a week of staining (Fig. 4.2). Therefore, SA

labeling in conjunction with immunolabeling highlights the heterogeneity of actin turnover in single cells during MSC differentiation.

Early dynamics of actin cytoskeleton during iPSC differentiation have not been explored in the literature to date[249-251, 276, 277]. Similar to MSCs, a differentiation induced immediate slowdown in actin turnover was observed during stimulation with both CDM and NDM as early as 3.5 hours of stimulation. Next, we explored if the higher retention of SA probe during short term live-imaging experiment could be due to lineage progression. Immunostaining pre-SA labeled cells after differentiation induction as early as day 2 showed that cells positive for differentiation markers showed a higher retention of SA. This phenomenon could be due to a slowdown in actin dynamics of the differentiating cells. After 2 days of induction, NDM demonstrated two distinct sub-populations where $SOX1^{high}$ cells correlated with brighter SA. On the other hand, SA^{low} cells showed low SA intensity. Perhaps, SA^{low} cells represent the naïve cells that remained undifferentiated and had a more dynamic cytoskeleton, similar to cells cultured in basal media as shown in Fig 4.4.1 A, B. CDM stimulation resulted in prolonged retention of the probe in all cells but did not resolve into distinct sub-populations (Fig. 4.4.2 B). This could be due to two factors, first SA retention in CDM was higher compared to NDM i.e. undifferentiated cells could be showing similar levels of SA labeling to the differentiated cells. Second, longer CDM induction might help to separate the differentiating cells from the naive cells. Still, $BRACHYURY^{high}$ cells showed a positive correlation with SA expression. Our findings suggest that actin dynamics could be used as an early marker to parse differentiating iPSCs from naïve cells. In future, the genetic and epigenetic profiling of the SA^{low} vs SA^{high} sub-populations would further reveal the role of key factors associated with cytoskeletal dynamics in the context of stem cell differentiation.

We have also introduced a new method where actin turnover can be used as a dynamic marker for selection of subsets of MSC populations (Fig. 4.5). This promises to be the first such methodological approach in the literature to segregate cells based on the native actin dynamics, which could correlate with lineage-related enrichment of differentiation. Next, we examined the effect of sub-culturing on the differentiation proclivity of the sorted cells. A decline in the purity of the sorted cells would indicate a reduction in AD and OS differentiation to the levels of unsorted cells. In contrast, however, we found a higher differentiation tendency in the sorted cells compared to the unsorted cells in terms of both AD and OS induction. This suggests that cells exhibiting equivalent levels of actin dynamics can be enriched during cell culture which resulted in increased differentiation proclivity. The observed propensity towards enhanced differentiation warrants further studies to investigate the interplay between actin dynamics and stem cell differentiation and elucidate via epigenetic or transcriptional profiling of the sorted MSC sub-populations the mechanistic and molecular basis for the variation among the groups that underlies enhanced differentiation. Another application of the method could be used to isolate and enrich young MSCs from senescent cells, given the correlation between slower actin dynamics and cellular aging [255, 278].

We have described four different methods to use SA based labeling in the context of following actin dynamics in MSCs and iPSCs. Namely, live cell tracking (Fig. 4.2), immunostaining (Fig. 4.3), flow cytometry (Fig. 4.4) and cell sorting (Fig 4.5). These methods might be helpful to other researchers who are interested in observing actin dynamics with other cells as well, but it is important to conduct preliminary experiments to determine the appropriate staining protocol. We used SA at 100nM concentration for

all experiments, as this dosage has minimal influence on the actin dynamics, cytotoxicity and differentiation[201, 255]. A more detailed description of the influence of SA labeling and dosage with multiple *in vitro* assays and cell types can be found in the first SA paper by Lukinavičius et al. [201].

Taken together, we have introduced a novel dynamic marker-based cell sorting method that has the potential to discern cell phenotypic populations based on actin turnover. Given our observation of a prolonged retention of SA probe during both iPSC and MSC differentiation, we propose that cells might have an inherent inclination towards a certain lineage based on the endogenous actin turnover of each cell. To explore the efficacy of our approach we conducted a proof of concept study of SA-labeling and imaging followed by sorting. We found increased osteogenesis and adipogenesis with low and fast actin turnover displaying cells respectively (Fig. 4.5). Interestingly, the cells retained this increased inclination towards a specific lineage even after cell passaging. Moreover, the differentiation was enhanced further which could be due to increase in proportion of the sorted cells during tissue culture maintenance. Therefore, our approach has the potential to be used for isolation of cells based on actin turnover for robust promotion of MSC differentiation even after cell passaging.

4.6 Conclusion

Actin turnover has the potential to be used as a dynamic marker of stem cell differentiation. Fluorescent labeling of live MSCs revealed cell fate-specific changes in the actin turnover. Additionally, SA labeling was found to correlate with differentiation markers in both MSCs and iPSCs. Therefore, we have introduced a new versatile platform that not only enables FACS-based high throughput probing of heterogeneity among

differentiating cells but also offers a more informative dataset in conjunction with immunolabeling based approach to illustrate changing cell states during cell differentiation. As demonstrated by our pilot study, SA can be used to isolate cells based on their actin turnover to study how cellular functions are influenced by the dynamic status of actin turnover of the cells.

4.7 Supplementary Figures

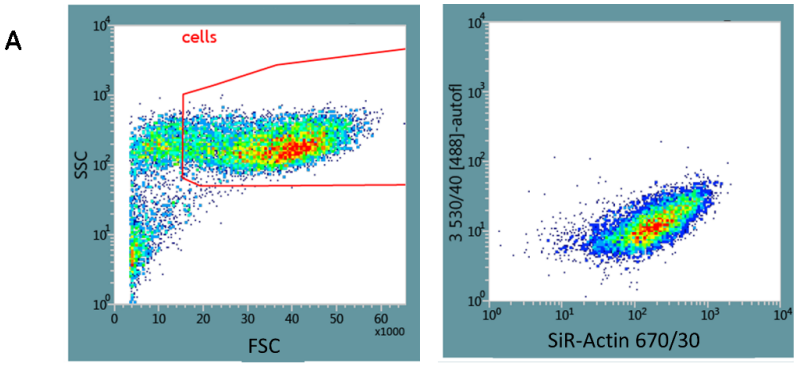

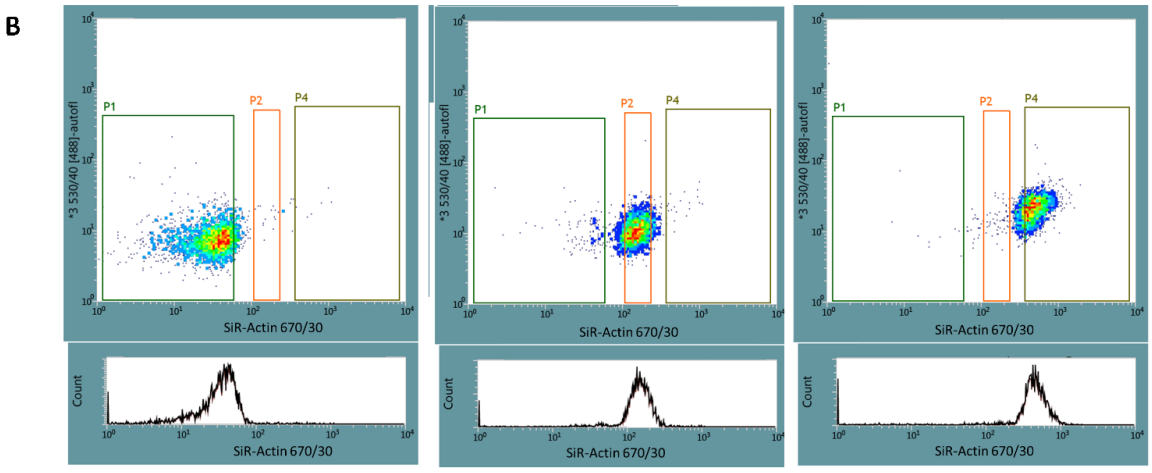

Post sort SA intensity	Dim (P1)	Interme diate (P2)	Bright (P4)	Mean P1 intensity
Dim (n=3435)	93.31%	0.44%	0.22%	37

Post sort SA intensity	Dim (P1)	Interme diate (P2)	Bright (P4)	Mean P1 intensity
Intermedi ate (n=3167)	3.71%	80%	0.73%	159

Post sort SA intensity	Dim (P1)	Interme diate (P2)	Bright (P4)	Mean P1 intensity
Bright (n=3251)	0.32%	1.83%	80.63%	539

Supplementary Fig. 4.1. SiR actin intensity based cell sorting of MSCs in to 3 sub-populations: dim (P1), intermediate (P2), bright (P4). **A.** Gating strategy, distribution of Sir-intensity **B.** Post-sort analysis to confirm cell sorting

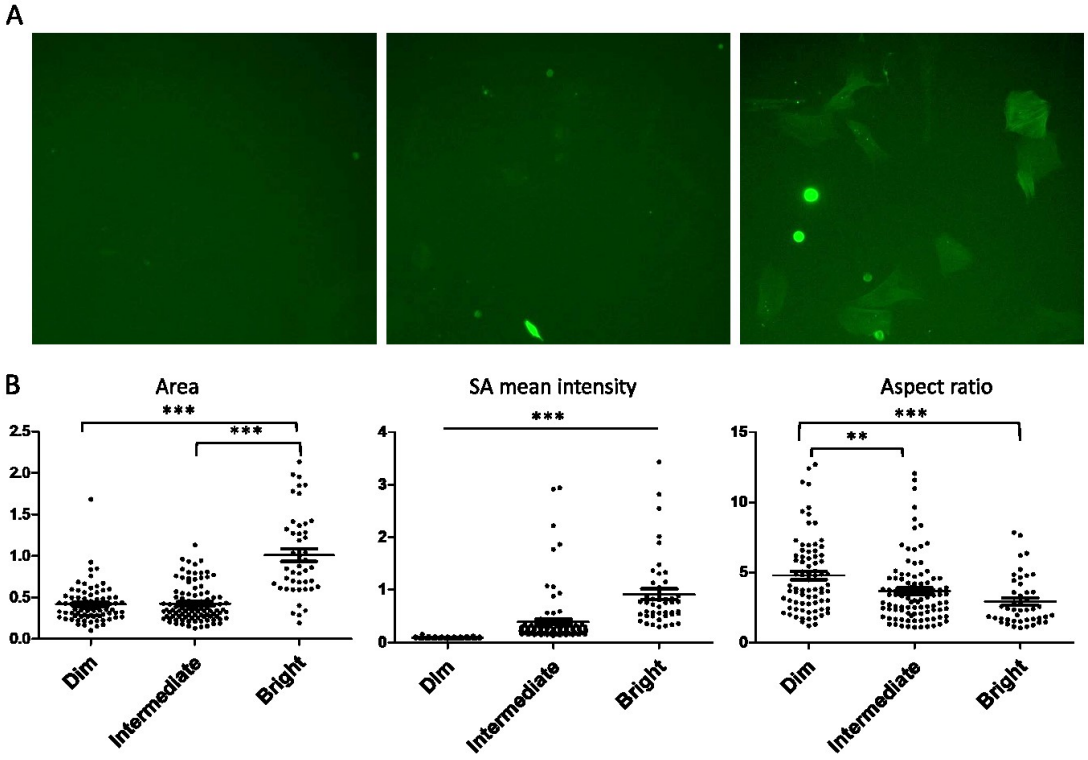

Supplementary Fig. 4.2. Morphological characterization of SA intensity based sorted cells after 24 hours of Flow cytometry. **A.** SA labeling of cells in "dim", "intermediate" and "bright" groups. **B.** Morphometric analysis of sub-populations: cell area, SA mean intensity and aspect ratio of single cells were calculated using imageJ. N= 77 (dim), 98 (intermediate), 45 (bright) cells. Means of all groups were compared using turkey's multiple comparison test ($p<0.001$ ***, $p<0.01$ **).

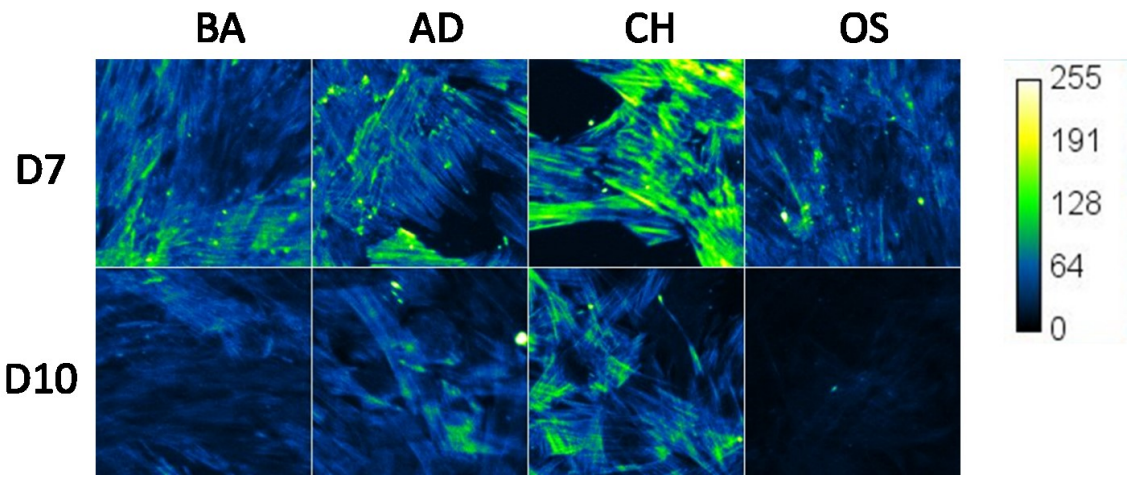

Supplementary Fig. 4.3. Second SA labeling after 6 days of maintenance in BA, AD, OS and CH media: SA labeling can be repeated to extend the duration of actin turnover probing.

Supplementary note 4.1. iPSC culture: Detailed protocol

IPS cells were derived from human foreskin fibroblasts electroporated with a single EBNA1/Ori based plasmid with a CAG promoter driven expression of a "2A" based polycistronic vector containing Oct4, Sox2, KLF4, and L-Myc and a fusion of mRFP and Blasticidin-S-Deaminase (pERCv2, courtesy of Dr. Rick Cohen).

Briefly, discarded human foreskin tissue (CHTN) was used to derive fibroblast cultures using standard techniques [279]. The tissue was placed into a glass 10 cm petri dish and minced into 1-2 mm cubes by crossing two 10 blade scalpels. The pieces were placed into a TC grade 24 well dish in Fibroblast medium (PeproTech Inc) containing 2% FBS, 10 ug/ml ciprofloxacin and amphotericin B. After two weeks in this media, the antibiotic was changed to 10 ug/ml gentamycin. Once cells began to emanate from the tissue, the pieces were removed using sterile foreceps and replated onto fresh wells. The remaining cells were passaged with TrypLE and expanded on to 10 cm dishes. This process was carried out over the course of 5 tissue replating and 5 cell passages which resulted in a fibroblast line called PM1Ep5 which was used for reprogramming protocols.

Reprogramming of Human Foreskin Fibroblasts: PM1Ep5 cultures (30-40% confluence) were treated with 1 uM Cyclic Pifithrin-alpha (BioGems) and Q-VD-O-PH (ApexBio) three days prior to electroporation (NEON, ThermoFisher) to inhibit p53 to enhance reprogramming [257] and caspase 3 to enhance post-electroporation viability. The cells were removed from the culture plate using 3 mls of TrypLE (ThermoFisher), neutralized with 7 mls of fibroblast medium with serum, and counted. The cells were collected by centrifugation at 300 x g for 5 min at RT and resuspended at a density of 1x10^7 cells in Electroporation Buffer R containing no more than 10% V/V of double

endotoxin free plasmid (Omega BioTek, with an extra Triton X-114 phase separation [280, 281]) at a ratio of 12ug plasmid/1.2x10^6 cells/120 ul total. The cells were electroporated using the 100 ul tip with following parameters; 10 ug of plasmid per 1x10^6 cells with 1600 volts, 10 ms pulse time, and 3 pulses [257]. The cells were placed into a 6 well dish coated with 5 ug/ml of vitronectin (PeproTech Inc) in Recovery Media overnight (Fibroblast Media with 10% FBS, and 1 uM Cyclic Pifithrin-alpha (BioGems). The following day the media was changed to Reprogramming/Selection Media (Low osmo DMEM/F12 (PeproTech) containing 20% v/v KOSR (ThermoFisher), 0.1 mM 2-mercaptoethanol, 20 ng/ml FGF-2 (146 a.a., PeproTech), 5 small molecules (BIOGEMS); 5 uM PS48, a PDK1 agonist; 250 uM sodium butyrate, an HDAC inhibitor; 0.5 uM A-83-01, a TGF-beta pathway inhibitor; 1 uM Cyclic Pifithrin-alpha, a p53 inhibitor; 50 nM SGC-0946, a DOT1L inhibitor; and 5-20 ug/ml of Blasticidin. The cultures were fed every other day for 7 days with Blasticidin to eliminate cells that were not electroporated. The Reprogramming media was used for up to 30 days, during which distinct IPSC colonies were formed. The first passage colonies were removed in bulk using Enzyme-free Passaging Media (PeproTech), settled by gravity for 10-15 min in 15 ml conical tubes with 10 mls of media, and subcultured onto 6 well dishes coated with vitronectin (PeproTech) using Reprogramming Media with 2 uM Y-27632. After 24 hrs, the media was changed to PeproGrow-hESC media containing additional 10 ug/ml of Insulin. This “settling” technique was carried out during the first three passages and resulted in only the retention of small cell clusters that formed mature round IPSC colonies. The cell line, “PM1eP5-ERCv2” was cryopreserved at passage 4-7, characterized by immunocytochemistry as Oct4+/SSEA4+/SSEA1- and Nanog+/Lin28+/Tra-1-60+ , and found to reliably form both neurons [258] and cardiomyocytes (TnT1+, beating clusters) using standard protocols ([15, 16]). Neural Differentiation Media (NDM) is based on Neural Stem Cell

Media (PeproTech) with 1x NSC supplement with additional 10 uM EC23 and 5 uM Y27632 [258]. Cardiac Differentiation Media and protocol for the time window used (2 days) was based on work of Burridge and coworkers ([15, 16]) and was composed of RPMI (ThermoFisher) with 200 mM L-Ascorbic Acid and 6 uM CHIR99021.

Chapter 5 Summary and Future Directions

Research Summary

In the era of emergent cell-based therapies, it is crucial to assess the necessary functionality of cells in an efficient and reliable manner as early as possible. This is particularly important in stem cell-based therapeutics where the issue of poor characterization and in-vitro heterogeneity can adversely impact the translational outcomes. The principal objective of this thesis dissertation was to investigate live cell imaging methods that could enable the temporal assessment of evolving stem cell states in distinct microenvironments. To this end, we primarily focused on fluorescence labeled actin cytoskeleton as the primary reporter for cell profiling. Prior research from several laboratories including our group, have shown that actin cytoskeleton can act as a predictor and influencer of stem cell features such as differentiation and aging. Existing actin based image informatics have typically excluded live cell dynamics which could offer more comprehensive data compared to fixed-timepoint assays. In this work, we have identified and explored a robust live-cell cytoskeletal imaging platform and presented a new paradigm to assess actin dynamics in live cells for two broad goals: 1) Early parsing of stem cell lineage divergence and senescence; 2) Profiling stem cell functional evolution, heterogeneity and phenotypic lineage parsing.

This thesis research was initiated with the goal of exploring a number of broad approaches with potential to support live-cell profiling of MSCs. With the goal of creating a multi-reporter cyto-nuclear library of mechanosensory fluororeporters, lentiviral vectors with inducible fluororeporter expression were created for YAP, TAZ, SC35, and HP1α. The lentiviral infections were successful in creating stable fluororeporter expressing cell lines for HEK293 and MSCs. However, during antibiotic selection, MSCs lost their ability to

proliferate and differentiate so we did not pursue stable cell lines any further. Next, we attempted transient lentiviral transductions for MSCs, but found that the lentiviral expression interfered with MSC differentiation. Before moving on to actin dynamics based studies later, we investigated another approach for live-cell labeling, via glass-bead antibody loading, but because of non-specific background fluorescence we looked for other alternatives for dynamic cell profiling.

In the following portion of this thesis (Chapter 3), we introduced a novel platform for real-time tracking of actin turnover dynamics in live cells harnessing a cell permeable probe, SiR-actin (SA). Following SA labeling, cells cultured in various differentiation media showed lineage specific loss of the fluorogenic probe demonstrating a trend of actin reorganization during early stages of lineage diversification. Analogous prior work with actin cytoskeleton for cell fate parsing took at least 24 hours, but our approach could discern various cell fates within few minutes (adipogenic) or hours (chondrogenic). Next, we introduced a new approach for composite analysis of actin cytoskeleton labeling that involves a competing stain to SA, phalloidin. This complementary staining allowed to highlight the dynamic and static regions in the cytoskeleton. A high-content image analysis of the complementary labels showed clear phenotypic parsing of cell fates as early as 1 hour of induction. Lastly, we showed that change in actin turnover due to cellular aging *in vitro* was able to parse the younger cells within one hour of simultaneous analysis.

Lastly, we demonstrated that SA labeling can be used for long-term studies as well to probe lineage specific change in actin dynamics during the course of differentiation in live MSCs. Subsequently, we performed a high throughput single cell analytics to highlight cellular heterogeneity of actin dynamics during adipogenic or osteogenic differentiation.

An analogous study was conducted in iPSCs, where differentiating cells showed a progressive slowdown in actin turnover upon stimulation with neural or cardiac media. Finally, we conducted a pilot study to test how inherent actin dynamics guide MSC differentiation. To this end, SA labeled MSCs were sorted based on the probe intensity in to three distinct sub-populations with low, intermediate or high actin dynamics. Sub-populations with faster actin dynamics demonstrated increased adipogenesis while the cells with slower actin dynamics demonstrated higher osteogenesis.

Future Directions

5.1 Live Cell Imaging Based Modeling of Stem Cell Dynamics

Our framework for fluorescence imaging-based quantification of actin turnover has a significant potential to be elaborated further for more complex datasets. Most of our live-cell experiments were conducted with limited kinetic analysis. We propose that the empirical quantitative modeling of SA decay profiles could be used to stratify or forecast cell lineage kinetics. For example, in chapter 3, we proposed a mathematical model to describe parameters that could describe the dynamics of SA labeling during association and dissociation by the following equation:

$$\frac{dC}{dt} = k_f R_T (C_0 - C) - k_r C$$

Where $C_0 - C$ denotes the concentration of free SA ligands while the available binding sites on actin filaments are denoted by R_T and are assumed to be in excess. Fitting the dissociation kinetics deconvolutes the values of the parameters: k_r and $k_f^d = k_f R_T$. We propose that quantification of actin turnover based on empirical k_r and k_f^d will provide a

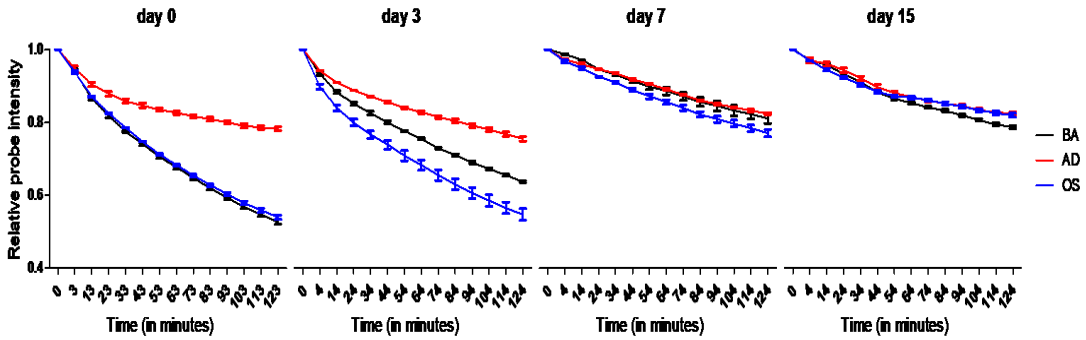

Fig. 5.1. Long term SMAT profiling for dynamic assessment of changing actin turnover during MSC differentiation

more accurate model for the changing cell states. As a proof of concept, we generated the values for these parameters during a long-term SMAT experiment during MSC differentiation. Briefly, cells were cultured in basal, adipogenic and osteogenic media and SMAT analysis was performed at different timepoints: Day 0, 3, 7 and 15. SA staining was done the evening before the imaging timepoint, for instance, for the day 7 timepoint, SiR-actin was added to the respective media on day 6, and imaging was done after removing the staining media i.e. cells remained in the same differentiation media before and after removal of SiR-actin containing media. All three media showed distinct actin turnover rates at different timepoints which could be indicative of the actin dynamics at that stage during differentiation [Fig. 5.1].

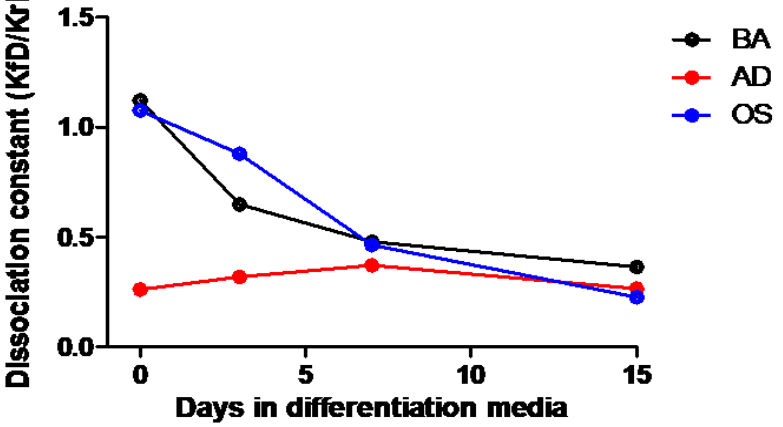

Fig. 5.2. K_f/k_r plots during MSC differentiation experiment described in Fig. 5.1

The variable k_f/k_r is the estimated dissociation constant kinetics based on in-silico modeling of SMAT data. Cells in OS showed similar k_f/k_r as BA at day 0 followed by faster decay on day 3 and 7, while at day 15 it showed similar k_f/k_r as AD. The decay constants for OS indicate that osteogenic differentiation showed higher actin dynamics in the first

seven days but by day 15 timepoint, there was a slow-down in actin turnover similar to the level of cells in AD. While AD condadsasitions showed slight increase in k_f/k_r till day 7, these levels declined by day 15 [Fig. 5.2.]. This implies that adipogenesis involves keeping the actin turnover lower than BA and OS consistently. This interpretation is also supported by literature, as it is well known that osteogenesis involves increasing actin polymerization and adipogenesis involves gradual deconstruction of actin cytoskeleton. Our k_f/k_r data is in agreement with a previous study by Sonowal et al. where they did a qualitative assessment of actin morphological reorganization (not actin turnover or dynamics) [185]. Therefore, our data indicates that changing cell states during MSC differentiation could be characterized by the actin dynamics. Further characterization and optimization of k_f/k_r values could be extended for immediate early changes in cell functions.

5.2 Forecasting stem cell behavior based on fluorescence labeling of actin cytoskeleton for high throughput screening of biomaterials

Biomaterials have been extensively used in regenerative medicine for guiding cell behavior as they offer optimal mechanical and physicochemical properties. Biomaterials influence stem cells by regulating their spreading [282], migration [283], self-renewal [284], differentiation [285], engraftment [286], gene expression [287], and immunomodulation [288]. The chemistry, stiffness, dimensionality and topography of the materials offer a mechanotransductive milieu that induce changes in downstream signaling pathways such as the integrin-rho-actin axis [289]. The traditional methods to assess the biological response of biomaterials on cells [such as qPCR, western blot, immunostaining, microarray etc. [290]], are invasive to the cells and time-consuming. With ever-increasing demand for better biomaterials, there is a need to develop a more efficient method to assess functional response of cells to diverse array of biomaterials.

Given that SA labeling of MSCs was able to highlight the early changes in cells during differentiation induction, and biomaterials can influence stem cell differentiation, it might be possible to use SMAT approach to cellular response to various biomaterials.

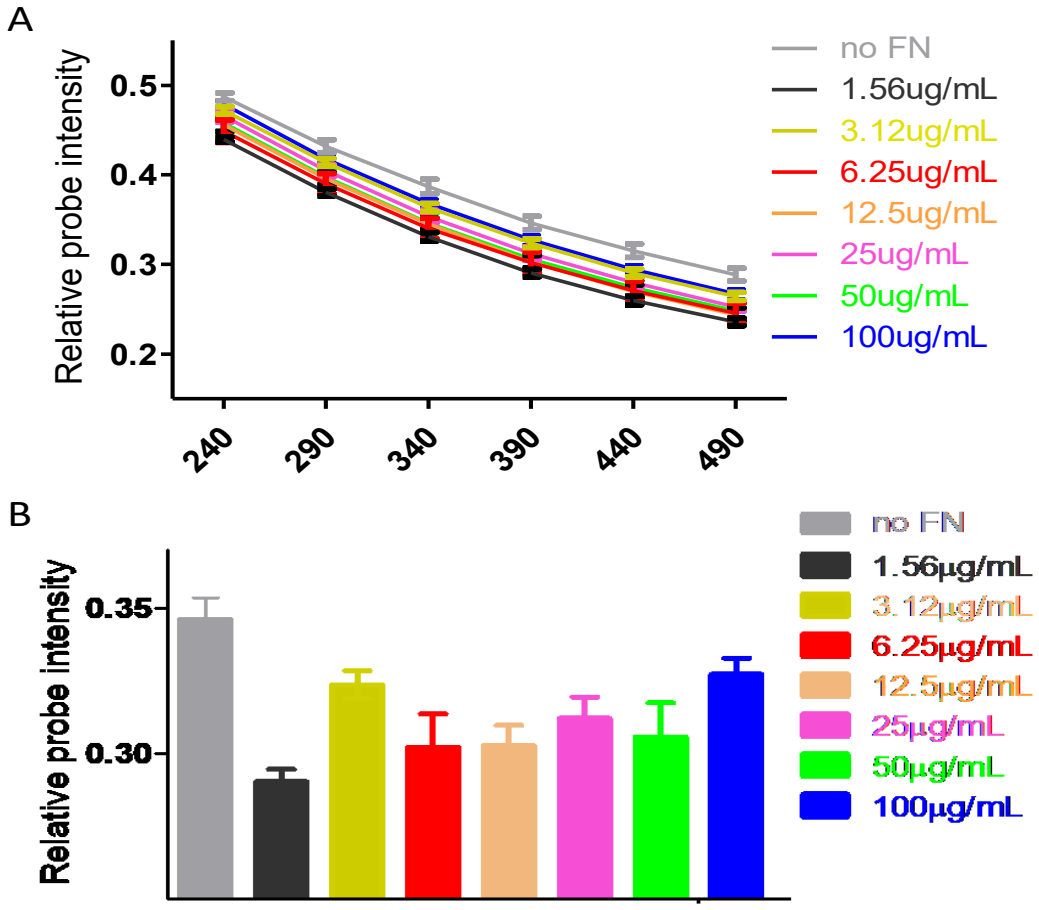

Fig. 5.3. Probing SA decay after fibronectin coating at different concentrations: MSCs were seeded on fibronectin coated surface, SA stained and after removing the staining media, the change in SA intensity was plotted with time (A). For lucid visualization, the data at 390 min from (A) is shown in B.

5.2.1 Characterizing the influence of fibronectin on actin dynamics via SMAT

Fibronectin is an ECM protein that influences cell adhesion, spreading and MSC differentiation [291]. MSCs utilize their own contractile force generated as a result of interaction with fibronectin to upregulate differentiation [292]. As a proof of concept, we tested if change in actin dynamics by fibronectin could be detected at different ligand concentrations. Briefly, a 96 well dish was coated with fibronectin for 2hrs with concentrations ranging from 0, 1.56, 3.12, 6.25, 12.5, 25, 50 and 100 μg/mL. Then MSCs were seeded, allowed to attach and stained with SA in BA media overnight. Next day, the staining media was removed and SMAT analysis was performed as described previously. We were able to discern the coated surfaces based on SA intensity, indicating distinct influence of fibronectin on actin turnover [Fig. 5.3A]. The plots for each concentration started to separate around 4 hrs (240 min) compared to the uncoated control surface, the resolution improved further around 390 minutes (6.5hrs) of imaging [Fig. 5.3B]. These results suggest that SMAT analysis has the potential to be used to distinguish cellular response to ligand concentration of extracellular matrix coated biomaterials.

5.2.2 Actin turnover based high-throughput biomaterial screening to forecast MSC differentiation

In chapter 3, change in actin turnover due to lineage divergence in MSCs was evident within few minutes. Based on the section above (5.2.1), we hypothesize that by determining a correlation between early SA decay profile and terminal MSC differentiation, it might be possible to forecast MSC differentiation with various biomaterials. Given that our SMAT protocol utilizes a low magnification imaging protocol,

imaging multiple substrates with a rapid imaging system in a high-throughput format is also possible.

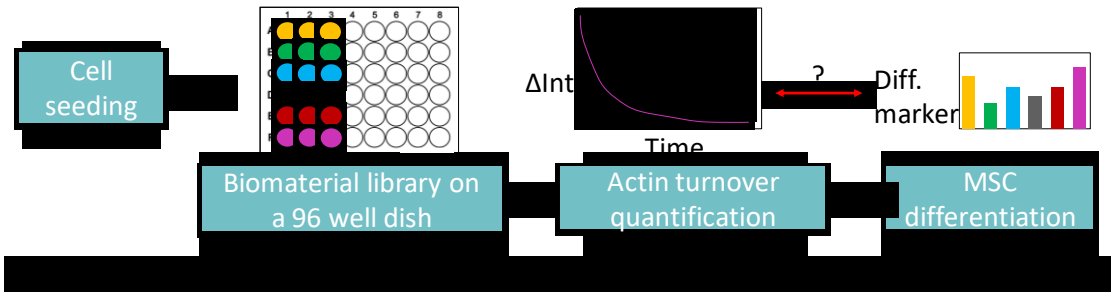

Fig. 5.4. Actin turnover based rapid biomaterial screening for long-term prediction of MSC differentiation: cells will be seeded on biomaterial library at day 0. After cell attachment, SA labeling will be conducted overnight. On day 1, SMAT profiles will be generated for the biomaterials, followed by cell culture in differentiation media for 14 days. On day 15 of the study, mathematical modeling will be harnessed to determine the relation between SA decay kinetics and MSC differentiation specific marker expression.

Following is the study design to assess if short-term monitoring (1-2 hours) of live cell actin turnover could be used as a dynamic marker to forecast MSC differentiation. In the pilot study, the effect of biomaterials could be inquired with a single cell fate such as osteogenesis. The array of diverse biomaterials (e.g. different polymer chemistry or topography) could be synthesized in a 96 well format in triplicates along with uncoated surface and a positive control (such as fibronectin coating that is known to promote osteogenesis [292]). After cell attachment, SMAT analytics will be applied to generate SA decay profiles. Subsequently, cells will be stimulated with osteogenic media for 2 weeks. The end point-assay will be conducted with functional staining such as fast blue staining or alkaline phosphatase quantification [Fig. 5.4]. Then SA decay profiles will be correlated with MSC differentiation on biomaterials by a mathematical modeling approach described

in section 5.1 to generate decay constants (K_f/K_r), keeping the time of analysis constant for all biomaterials, as a function of fast blue (FB) expression for individual biomaterial (n):

$$FB(n)= f(K_{fn}/K_{rn}), for\ n \in \{1, 2, 3,\ldots\ldots, n\}$$

After successful derivation of the variables empirically, the next step would be to apply this approach with novel biomaterials to validate if immediate SA decay profiles could determine long-term differentiation. If successful, this approach will create a robust platform for rapid evaluation of myriads of biomaterials.

The proposed biomaterial screening method has other advantages in addition to providing real-time insights about the cell behavior in response to biomaterials. After SA staining, MSCs still possess the ability to differentiate [255], leaving the scope for utilizing other biomolecular assays. This approach precludes the need for long-term cell cultures thereby saving resources and time. There are a few caveats that need to be considered with as well. Our screening platform requires transparent biomaterials that are compatible with fluorescent imaging. Alternatively, fluorescence plate readers could be tested, but their sensitivity might be limited compared to microscope imaging. Next, there is a need for a rapid imaging system such as IN Cell Analyzer 6000 (GE healthcare) equipped with high-throughput imaging and atmosphere control for optimal cell health during imaging. In SMAT protocol, after changing the staining media, the SA intensity declines rapidly, so it is important to identify an appropriate time-window to achieve distinct trends in SA plot, otherwise missing early timepoints might result in poor resolution. We reported in chapter 3 that SA decay profile is influenced by cell passage number, therefore, appropriate controls need to be included for each imaging experiment.

5.2.3 Measuring actin turnover in 3D encapsulated hydrogel matrix

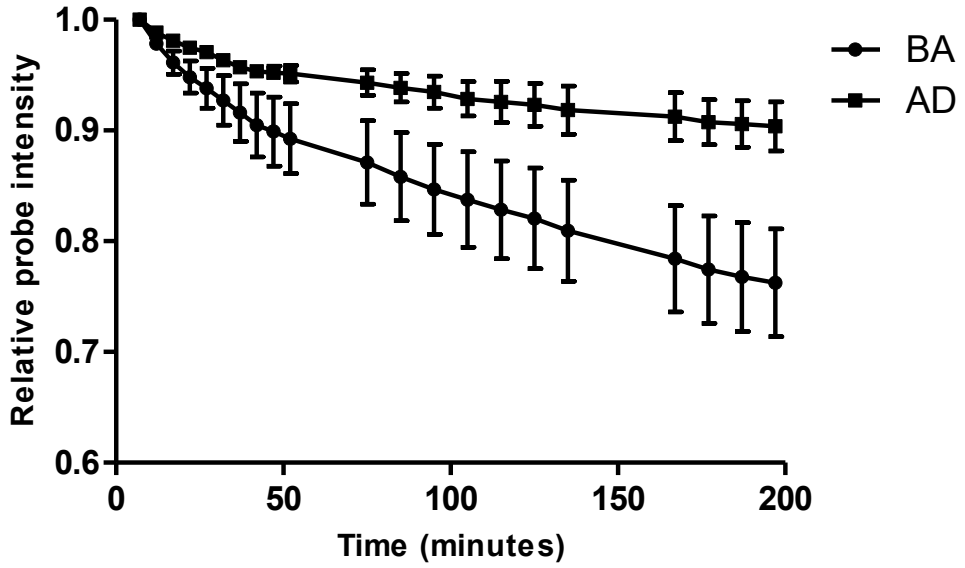

Fig. 5.5: Tracking changing actin dynamics within hydrogel encapsulated cells: MSCs seeded within Puramatrix hydrogels were induced with adiogenic media. SMAT analysis enabled quantification of change in actin turnover even in this complex milieu of soluble cues (induction media) and biophysical factors (hydrogel).

The conventional monolayer tissue culture techniques provide a controlled robust platform to understand the basic physiology and functions of MSCs, however they do not represent the complex 3D microenvironment experienced by the cells in vivo. A 3D scaffold promotes intercellular interactions and provide favorable environment for MSC survival, differentiation and regeneration making them suitable for tissue engineering applications [293]. To quantify actin-remodeling dynamics in 3D, we conducted a preliminary study where MSCs were encapsulated in synthetic peptide based self-assembling Puramatrix hydrogel system that mimics ECM with 3D nanoscale morphologic features [294]. After allowing the gelation of 1:1 1% puramatrix-cell mix for 1 hr, 100nM

SiR-actin staining was done in basal media overnight. Unlike the tissue culture plastic-ware or glass bottom dishes, where cells spread with distinct stress fibers, the soft hydrogel led to rounding up of cells. The staining media was removed, and washes were done with basal media to remove residual staining media. Subsequently, the encapsulated cells were incubated in either basal or adipogenic media and time-lapse imaging was done to capture z-stacks to image cells in different planes for 3 hrs. Subsequently, the maximum intensity projections of the z-stacks were made, and SiR-actin intensity was measured using imageJ. The SiR-actin intensity in each image was normalized to their first time-point and plotted with time. We could measure the reduced actin dynamics in response to the adipogenic media compared to the basal media ($p<0.05$ at 167 min) (Fig. 5.5). It is important to note that in 2D culture, spontaneous cell motility and change of cell shape can alter actin dynamics, but in the encapsulated cells, there was minimal cell movement or change in cell shape during the time-lapse imaging. So, the changing actin dynamics demonstrate cytoskeletal rearrangements mainly in response to the Adipogenic media. These results support the utility of SMAT for quantifying dynamics in a complex milieu of soluble cues in a 3D hydrogel system. To our knowledge, this is the first method that enables measurement of actin dynamics in 3D matrix encapsulated live cells, therefore needs further investigation.

5.3. Follow up studies for advanced characterization SA intensity sorted stem cell subpopulations (SSPs)

Actin cytoskeleton plays an important role in guiding MSC differentiation [185, 232]. In chapter 4, we reasoned that inherent actin turnover of MSCs could be used as a marker for differentiation potential. Subsequently, flow cytometry was used to isolate MSCs after SA labeling, in to 3 distinct sorted sub-populations (SSPs): “dim”, “intermediate” and “bright”, that represent cells with high, intermediate or low actin turnover. Interestingly,

we found distinct differentiation potential among these sub-populations. Future studies are warranted to better characterize the SSPs and decipher the underlying biological mechanisms. Following is the list of experiments that need to be conducted further for improved comprehension of the relationship between actin dynamics and stem cell functionality.

- ***Cytoskeletal characterization of SSPs:*** With a view to check the status of actin polymerization status of the cells, F/G actin ratio will be measured by western blots [295]. Focal adhesion kinases play an important role as one of the key molecular sensors in the focal adhesion complex in regulating MSC morphology, differentiation and cell proliferation. Therefore, the distribution and density of FAK will be assessed by fluorescence imaging or western blots [296, 297]. Successful engraftment of stem cells is dependent on migration to the tissue of interest. Therefore, it is important to evaluate the cell migration among the SSPs [298]. *In vitro* migration will be evaluated using a transwell migration system as described in [299].
- ***Cell proliferation among SSPs:*** Use of MSCs in regenerative medicine is favored by their inherent ability to proliferate. To assess which groups possess the ability for highest proliferation, colony forming unit-fibroblastic capacity (CFU-F assay) and proliferation assay and commercially available 5-ethynyl-2-deoxyuridine (EdU) kit [300, 301].
- ***Differentiation proclivity assessment among SSPs:*** Previously (chapter 4), we only conducted functional staining to assess differentiation (fast blue staining for osteogenesis, AdipoRed staining for adipogenesis). More insights could be obtained by including other assays and different time-points. For instance, qPCR could be conducted with early and late markers of MSC

differentiation to assess if one of the SSPs demonstrate accelerated lineage commitment. Upon implantation, in-situ dedifferentiation might diminish the therapeutic effect of the stem cells. We would then evaluate the robustness of differentiation among SSPs by inducing dedifferentiation as described in chapter 3 by replacing differentiation media with basal media. Lastly, we would test the SSPs for their chondrogenic potential which was not included previously.

- ***Investigating cytoskeletal memory after sub-passaging SSPs:*** Following the cell sorting step, it is important to test if cells retain their unique actin dynamics among the sub-populations without getting diluted due to sub-passaging. In chapter 4, SSPs were found to retain increased differentiation potential compared to unsorted cells up to 2 passages following cell sort. This data suggests that the MSC sub-populations possess cytoskeletal memory, allowing them to keep elevated differentiation potential after passaging. To test the notion of cytoskeletal memory, we will test 3 key features influenced by multiple passaging: proliferation, senescence and differentiation. The outcome could be significant if we manage to find the SSP with prolonged ability to proliferate and differentiate while expressing lower levels of senescence markers [302].
- ***Genetic and epigenetic analysis of SSPs:*** If the aforementioned studies led to identification of SSP with higher tendency for differentiation or proliferation, it will be interesting to investigate the underlying mechanisms. Gene expression can be evaluated for genes involved in cell cycle, cytoskeleton, immunomodulation, differentiation, metabolism and senescence using trascriptome analysis [303]. The epigenetic landscape of the SSPs will be studied primarily focusing on histone modifications such as trimethylations as these have been well characterized by our group in the context of lineage commitment [165, 304].

- ***Multi-color cell sort:*** In addition to the use of the primary fluorophore used in this thesis, SA, additional fluorescent reporters in cell sorting might help with generating SSPs with better functionality. For instance, one could repeat the cell sort of MSCs with a stemness surface marker (such as CD105 [305]) to ensure exclusion of non-naïve MSCs. Also, SA intensity-based cell sorting can be performed for iPSCs as well, along with pluripotency markers (such as OCT4, Nanog etc.[306]).

5.4 Deciphering biological relevance of SA labeling by combinatorial labeling with cell function specific reporters

We established SMAT pipeline for measurement of actin turnover in live cells (chapter 3), but it was limited to describing the correlation between an extracellular cue (such as differentiation media, cytoskeletal drugs etc.) and actin dynamics. Understanding the biological relevance of change in actin turnover requires additional cellular markers. In Chapter 4, co-expression of differentiation markers and SA intensity was demonstrated in iPSCs showing that slowdown in actin turnover is an early sign of lineage commitment, but this study was conducted with fixed cells. In future, a similar study but with live cell reporters might develop a better temporal model of early changes during lineage commitment in stem cells.

5.4.1 Dynamic profiling of stem cell populations using SA labeling in conjunction with other cellular reporters

Biological relevance of change in actin turnover could be enhanced by the addition of another live cell reporter to the SMAT protocol. For this study, one could consider a reporter with well-defined temporal roles in cell differentiation and actin cytoskeleton. RhoA, a member of family of GTPases, plays an important role in actin polymerization, proliferation and cell differentiation [307]. In MSCs, RhoA-ROCK signaling plays a

decisive role during lineage commitment, where its upregulation results in osteogenesis while downregulation results in adipogenesis [194, 218]. For RhoA visualization, a genetically encoded, single-chain biosensor with intramolecular fluorescence resonance energy transfer (FRET) can be used [308]. One approach could be to seed cells and allow attachment overnight. Next day, RhoA-biosensor would be transfected to the cells, along with SA staining overnight. The following day, cells would be imaged after stimulation with adipogenic and osteogenic media and fluorescence of both SA and RhoA-biosensor will be calculated based on change from the first timepoint. The 3D plots are likely to offer better temporal resolution among the test conditions. This approach could be extended to other studies as well where there is a need to evaluate RhoA-actin signaling axis.

5.4.2 Single cell 4D spatiotemporal profiling of actin turnover

One of the main strengths of our SMAT workflow lies in the low magnification imaging protocol that allows rapid imaging of cell populations across multiple conditions. But, this approach provides an average of the cellular response, instead of highlighting individual differences among the populations. We propose that by developing a high magnification imaging protocol, we will acquire z-stack images and perform volumetric evaluation of actin cytoskeletal dynamics in 3D. Further inclusion of a secondary reporter similar to section 5.4.1 would provide even richer dataset. By dual reporter imaging of single cells at high resolution, we will generate spatiotemporal heat maps highlighting the regions of high activity within a cell [Fig. 5.6.]. For instance, early signaling changes in MSCs during differentiation will be evaluated by co-expression of SA and RhoA-biosensor described in the previous section. Upon differentiation induction, we might notice elevated RhoA activity, leading to increase in level of actin polymerization i.e. higher actin turnover rates that will lead to more diffused expression of SA and vice versa. It will be interesting to highlight the regions within a cell that contribute to early change in cell state during

lineage induction. Furthermore, RhoA signaling belongs to the immediate-early gene category that can be activated and transcribed within minutes after stimulation. Therefore, this dual imaging of RhoA activity and actin turnover via SA labeling could provide novel insights to discern inside-out vs outside-in signaling in response to

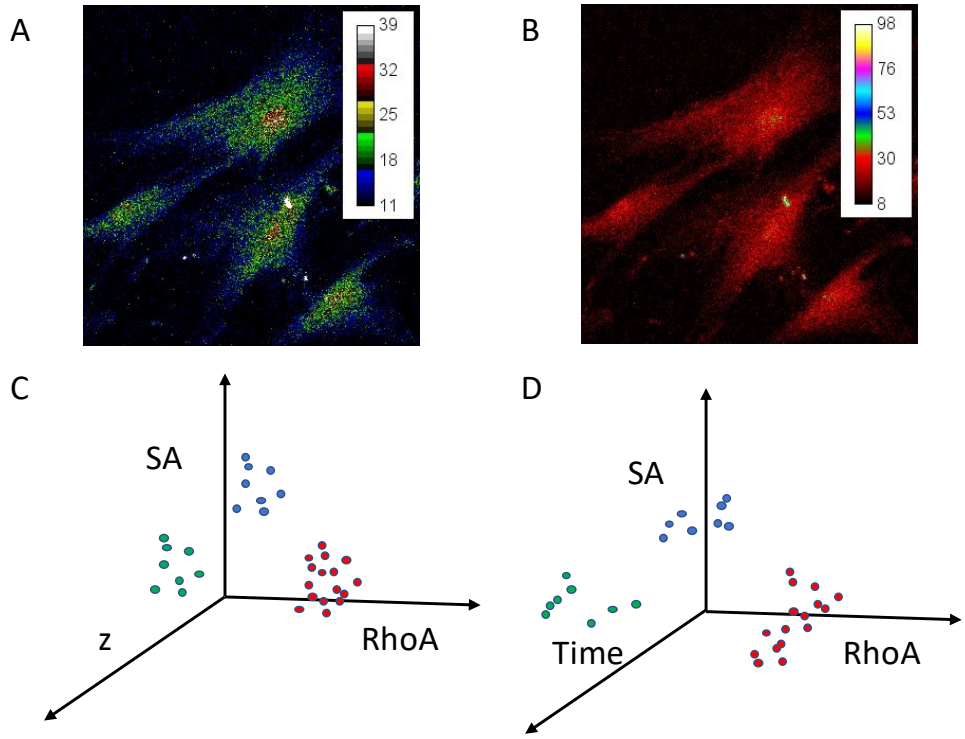

Fig. 5.6: Single cell SA kinetics coupled with another live reporter (e.g. RhoA-biosensor) for 4D data-acquisition: when stimulated with extracellular cues (such as growth factors), cells will respond differently and demonstrate spatiotemporal differences in RhoA-biosensor (A) or SA expression (B) **(**Note that these images are pseudocolored for illustrations only and not actually labeled with SA or RhoA). C, and D show representative data analytics after 4D profiling of actin turnover. By coupling two reporters, we will attain improved and earlier resolution among test conditions.

extracellular cues. Caveats with single cell imaging include higher risk of photobleaching,

low data throughput and challenging image acquisition due to pronounced cell-movement at higher magnification.

References

1. Blanchoin, L., R. Boujemaa-Paterski, C. Sykes, and J. Plastino, *Actin dynamics, architecture, and mechanics in cell motility*. Physiol Rev, 2014. **94**(1): p. 235-63.
2. Bianco, P., P.G. Robey, and P.J. Simmons, *Mesenchymal stem cells: revisiting history, concepts, and assays*. Cell Stem Cell, 2008. **2**(4): p. 313-9.
3. Pollard, T.D., *Actin and Actin-Binding Proteins*. Cold Spring Harb Perspect Biol, 2016. **8**(8).
4. Hanna, S. and M. El-Sibai, *Signaling networks of Rho GTPases in cell motility*. Cell Signal, 2013. **25**(10): p. 1955-61.
5. Bryan, K.E. and P.A. Rubenstein, *An intermediate form of ADP-F-actin*. J Biol Chem, 2005. **280**(2): p. 1696-703.
6. Milroy, L.G., S. Rizzo, A. Calderon, B. Ellinger, S. Erdmann, J. Mondry, P. Verveer, P. Bastiaens, H. Waldmann, L. Dehmelt, and H.D. Arndt, *Selective chemical imaging of static actin in live cells*. J Am Chem Soc, 2012. **134**(20): p. 8480-6.
7. Wang, S., X. Qu, and R.C. Zhao, *Clinical applications of mesenchymal stem cells*. J Hematol Oncol, 2012. **5**: p. 19.
8. Thomson, J.A., J. Itskovitz-Eldor, S.S. Shapiro, M.A. Waknitz, J.J. Swiergiel, V.S. Marshall, and J.M. Jones, *Embryonic stem cell lines derived from human blastocysts*. Science, 1998. **282**(5391): p. 1145-7.
9. Carlier, M.F. and S. Shekhar, *Global treadmilling coordinates actin turnover and controls the size of actin networks*. Nat Rev Mol Cell Biol, 2017. **18**(6): p. 389-401.
10. Kudryashov, D.S. and E. Reisler, *ATP and ADP actin states*. Biopolymers, 2013. **99**(4): p. 245-56.
11. Xu, C., M.S. Inokuma, J. Denham, K. Golds, P. Kundu, J.D. Gold, and M.K. Carpenter, *Feeder-free growth of undifferentiated human embryonic stem cells*. Nat Biotechnol, 2001. **19**(10): p. 971-4.
12. Levenberg, S., J.S. Golub, M. Amit, J. Itskovitz-Eldor, and R. Langer, *Endothelial cells derived from human embryonic stem cells*. Proc Natl Acad Sci U S A, 2002. **99**(7): p. 4391-6.
13. Semrau, S., J.E. Goldmann, M. Soumillon, T.S. Mikkelsen, R. Jaenisch, and A. van Oudenaarden, *Dynamics of lineage commitment revealed by single-cell transcriptomics of differentiating embryonic stem cells*. Nat Commun, 2017. **8**(1): p. 1096.
14. Takahashi, K. and S. Yamanaka, *Induction of pluripotent stem cells from mouse embryonic and adult fibroblast cultures by defined factors*. Cell, 2006. **126**(4): p. 663-76.
15. Manzini, S., L.E. Viiri, S. Marttila, and K. Aalto-Setala, *A Comparative View on Easy to Deploy non-Integrating Methods for Patient-Specific iPSC Production*. Stem Cell Rev Rep, 2015. **11**(6): p. 900-8.
16. Lu, X. and T. Zhao, *Clinical therapy using iPSCs: hopes and challenges*. Genomics Proteomics Bioinformatics, 2013. **11**(5): p. 294-8.
17. Ye, Z., B.K. Chou, and L. Cheng, *Promise and challenges of human iPSC-based hematologic disease modeling and treatment*. Int J Hematol, 2012. **95**(6): p. 601-9.
18. Volarevic, V., B.S. Markovic, M. Gazdic, A. Volarevic, N. Jovicic, N. Arsenijevic, L. Armstrong, V. Djonov, M. Lako, and M. Stojkovic, *Ethical and Safety Issues of Stem Cell-Based Therapy*. International journal of medical sciences, 2018. **15**(1): p. 36-45.
19. Poggi, A. and M.R. Zocchi, *Immunomodulatory Properties of Mesenchymal Stromal Cells: Still Unresolved "Yin and Yang"*. Curr Stem Cell Res Ther, 2019. **14**(4): p. 344-350.

20. Liu, Y., A.J. Goldberg, J.E. Dennis, G.A. Gronowicz, and L.T. Kuhn, *One-step derivation of mesenchymal stem cell (MSC)-like cells from human pluripotent stem cells on a fibrillar collagen coating*. PLoS One, 2012. **7**(3): p. e33225.
21. Lin, L., L. Bolund, and Y. Luo, *Towards Personalized Regenerative Cell Therapy: Mesenchymal Stem Cells Derived from Human Induced Pluripotent Stem Cells*. Curr Stem Cell Res Ther, 2016. **11**(2): p. 122-30.
22. Caplan, A.I., *Mesenchymal stem cells*. J Orthop Res, 1991. **9**(5): p. 641-50.
23. Pittenger, M.F., A.M. Mackay, S.C. Beck, R.K. Jaiswal, R. Douglas, J.D. Mosca, M.A. Moorman, D.W. Simonetti, S. Craig, and D.R. Marshak, *Multilineage potential of adult human mesenchymal stem cells*. Science, 1999. **284**(5411): p. 143-7.
24. Dominici, M., K. Le Blanc, I. Mueller, I. Slaper-Cortenbach, F. Marini, D. Krause, R. Deans, A. Keating, D. Prockop, and E. Horwitz, *Minimal criteria for defining multipotent mesenchymal stromal cells. The International Society for Cellular Therapy position statement*. Cytotherapy, 2006. **8**(4): p. 315-7.
25. Riekstina, U., I. Cakstina, V. Parfejevs, M. Hoogduijn, G. Jankovskis, I. Muiznieks, R. Muceniece, and J. Ancans, *Embryonic stem cell marker expression pattern in human mesenchymal stem cells derived from bone marrow, adipose tissue, heart and dermis*. Stem Cell Rev Rep, 2009. **5**(4): p. 378-86.
26. Russell, K.C., D.G. Phinney, M.R. Lacey, B.L. Barrilleaux, K.E. Meyertholen, and K.C. O'Connor, *In vitro high-capacity assay to quantify the clonal heterogeneity in trilineage potential of mesenchymal stem cells reveals a complex hierarchy of lineage commitment*. Stem Cells, 2010. **28**(4): p. 788-98.
27. Whitfield, M.J., W.C. Lee, and K.J. Van Vliet, *Onset of heterogeneity in culture-expanded bone marrow stromal cells*. Stem Cell Res, 2013. **11**(3): p. 1365-77.
28. Mets, T. and G. Verdonk, *In vitro aging of human bone marrow derived stromal cells*. Mech Ageing Dev, 1981. **16**(1): p. 81-9.
29. Deans, R.J. and A.B. Moseley, *Mesenchymal stem cells: biology and potential clinical uses*. Exp Hematol, 2000. **28**(8): p. 875-84.
30. Haynesworth, S.E., J. Goshima, V.M. Goldberg, and A.I. Caplan, *Characterization of cells with osteogenic potential from human marrow*. Bone, 1992. **13**(1): p. 81-8.
31. McLeod, C.M. and R.L. Mauck, *On the origin and impact of mesenchymal stem cell heterogeneity: new insights and emerging tools for single cell analysis*. Eur Cell Mater, 2017. **34**: p. 217-231.
32. Wagner, W. and A.D. Ho, *Mesenchymal stem cell preparations--comparing apples and oranges*. Stem Cell Rev, 2007. **3**(4): p. 239-48.
33. Maleki, M., F. Ghanbarvand, M. Reza Behvarz, M. Ejtemaei, and E. Ghadirkhomi, *Comparison of mesenchymal stem cell markers in multiple human adult stem cells*. Int J Stem Cells, 2014. **7**(2): p. 118-26.
34. Wagner, W., R.E. Feldmann, Jr., A. Seckinger, M.H. Maurer, F. Wein, J. Blake, U. Krause, A. Kalenka, H.F. Burgers, R. Saffrich, P. Wuchter, W. Kuschinsky, and A.D. Ho, *The heterogeneity of human mesenchymal stem cell preparations--evidence from simultaneous analysis of proteomes and transcriptomes*. Exp Hematol, 2006. **34**(4): p. 536-48.
35. Zhuang, H., X. Zhang, C. Zhu, X. Tang, F. Yu, G.W. Shang, and X. Cai, *Molecular Mechanisms of PPAR-gamma Governing MSC Osteogenic and Adipogenic Differentiation*. Curr Stem Cell Res Ther, 2016. **11**(3): p. 255-64.
36. James, A.W., *Review of Signaling Pathways Governing MSC Osteogenic and Adipogenic Differentiation*. Scientifica (Cairo), 2013. **2013**: p. 684736.
37. Vega, S.L., A. Dhaliwal, V. Arvind, P.J. Patel, N.R. Beijer, J. de Boer, N.S. Murthy, J. Kohn, and P.V. Moghe, *Organizational metrics of interchromatin speckle factor*

domains: integrative classifier for stem cell adhesion & lineage signaling. Integr Biol (Camb), 2015. 7(4): p. 435-46.
38. Hao, J., Y. Zhang, D. Jing, Y. Shen, G. Tang, S. Huang, and Z. Zhao, *Mechanobiology of mesenchymal stem cells: Perspective into mechanical induction of MSC fate*. Acta Biomater, 2015. **20**: p. 1-9.
39. Pelttari, K., E. Steck, and W. Richter, *The use of mesenchymal stem cells for chondrogenesis*. Injury, 2008. **39 Suppl 1**: p. S58-65.
40. Le Blanc, K., *Mesenchymal stromal cells: tissue repair and immune modulation.* Cytotherapy, 2006. **8**(6): p. 559-561.
41. Rasmusson, I., *Immune modulation by mesenchymal stem cells.* Experimental Cell Research, 2006. **312**(12): p. 2169-2179.
42. Kean, T.J., P. Lin, A.I. Caplan, and J.E. Dennis, *MSCs: Delivery Routes and Engraftment, Cell-Targeting Strategies, and Immune Modulation.* Stem Cells Int, 2013. **2013**: p. 732742.
43. Ren, G., L. Zhang, X. Zhao, G. Xu, Y. Zhang, A.I. Roberts, R.C. Zhao, and Y. Shi, *Mesenchymal stem cell-mediated immunosuppression occurs via concerted action of chemokines and nitric oxide.* Cell Stem Cell, 2008. **2**(2): p. 141-50.
44. Weiss, A.R.R. and M.H. Dahlke, *Immunomodulation by Mesenchymal Stem Cells (MSCs): Mechanisms of Action of Living, Apoptotic, and Dead MSCs.* Front Immunol, 2019. **10**: p. 1191.
45. Brandt, L., S. Schubert, P. Scheibe, W. Brehm, J. Franzen, C. Gross, and J. Burk, *Tenogenic Properties of Mesenchymal Progenitor Cells Are Compromised in an Inflammatory Environment*. Int J Mol Sci, 2018. **19**(9).
46. Yao, Y., J. Huang, Y. Geng, H. Qian, F. Wang, X. Liu, M. Shang, S. Nie, N. Liu, X. Du, J. Dong, and C. Ma, *Paracrine action of mesenchymal stem cells revealed by single cell gene profiling in infarcted murine hearts.* PLoS One, 2015. **10**(6): p. e0129164.
47. McMurray, R.J., N. Gadegaard, P.M. Tsimbouri, K.V. Burgess, L.E. McNamara, R. Tare, K. Murawski, E. Kingham, R.O. Oreffo, and M.J. Dalby, *Nanoscale surfaces for the long-term maintenance of mesenchymal stem cell phenotype and multipotency*. Nat Mater, 2011. **10**(8): p. 637-44.
48. Zaim, M., S. Karaman, G. Cetin, and S. Isik, *Donor age and long-term culture affect differentiation and proliferation of human bone marrow mesenchymal stem cells*. Ann Hematol, 2012. **91**(8): p. 1175-86.
49. Rombouts, W.J. and R.E. Ploemacher, *Primary murine MSC show highly efficient homing to the bone marrow but lose homing ability following culture.* Leukemia, 2003. **17**(1): p. 160-70.
50. Moravcikova, E., E.M. Meyer, M. Corselli, V.S. Donnenberg, and A.D. Donnenberg, *Proteomic Profiling of Native Unpassaged and Culture-Expanded Mesenchymal Stromal Cells (MSC).* Cytometry A, 2018. **93**(9): p. 894-904.
51. Lo Surdo, J. and S.R. Bauer, *Quantitative approaches to detect donor and passage differences in adipogenic potential and clonogenicity in human bone marrow-derived mesenchymal stem cells.* Tissue Eng Part C Methods, 2012. **18**(11): p. 877-89.
52. Lin, H., J. Sohn, H. Shen, M.T. Langhans, and R.S. Tuan, *Bone marrow mesenchymal stem cells: Aging and tissue engineering applications to enhance bone healing*. Biomaterials, 2019. **203**: p. 96-110.
53. Squillaro, T., G. Peluso, and U. Galderisi, *Clinical Trials With Mesenchymal Stem Cells: An Update*. Cell Transplant, 2016. **25**(5): p. 829-48.
54. Rosova, I., M. Dao, B. Capoccia, D. Link, and J.A. Nolta, *Hypoxic preconditioning results in increased motility and improved therapeutic potential of human mesenchymal stem cells*. Stem Cells, 2008. **26**(8): p. 2173-82.

55. Noronha, N.C., A. Mizukami, C. Caliari-Oliveira, J.G. Cominal, J.L.M. Rocha, D.T. Covas, K. Swiech, and K.C.R. Malmegrim, *Priming approaches to improve the efficacy of mesenchymal stromal cell-based therapies*. Stem Cell Res Ther, 2019. **10**(1): p. 131.
56. Galipeau, J. and L. Sensebe, *Mesenchymal Stromal Cells: Clinical Challenges and Therapeutic Opportunities*. Cell Stem Cell, 2018. **22**(6): p. 824-833.
57. Pittenger, M.F., G. Mbalaviele, M. Black, J.D. Mosca, and D.R. Marshak, *Mesenchymal stem cells*, in *Human cell culture*. 2001, Springer. p. 189-207.
58. Pittenger, M.F., D.E. Discher, B.M. Péault, D.G. Phinney, J.M. Hare, and A.I. Caplan, *Mesenchymal stem cell perspective: cell biology to clinical progress*. NPJ Regenerative medicine, 2019. **4**: p. 22-22.
59. Chen, Y., Z. Shu, K. Qian, J. Wang, and H. Zhu, *Harnessing the Properties of Biomaterial to Enhance the Immunomodulation of Mesenchymal Stem Cells*. Tissue Eng Part B Rev, 2019. **25**(6): p. 492-499.
60. Kabat, M., I. Bobkov, S. Kumar, and M. Grumet, *Trends in mesenchymal stem cell clinical trials 2004-2018: Is efficacy optimal in a narrow dose range?* Stem Cells Transl Med, 2020. **9**(1): p. 17-27.
61. Rani, S., A.E. Ryan, M.D. Griffin, and T. Ritter, *Mesenchymal Stem Cell-derived Extracellular Vesicles: Toward Cell-free Therapeutic Applications*. Mol Ther, 2015. **23**(5): p. 812-823.
62. Xiang, M.X., A.N. He, J.A. Wang, and C. Gui, *Protective paracrine effect of mesenchymal stem cells on cardiomyocytes*. J Zhejiang Univ Sci B, 2009. **10**(8): p. 619-24.
63. Yin, K., S. Wang, and R.C. Zhao, *Exosomes from mesenchymal stem/stromal cells: a new therapeutic paradigm*. Biomark Res, 2019. **7**: p. 8.
64. Phinney, D.G. and M.F. Pittenger, *Concise Review: MSC-Derived Exosomes for Cell-Free Therapy*. Stem Cells, 2017. **35**(4): p. 851-858.
65. Boregowda, S.V., V. Krishnappa, C.L. Haga, L.A. Ortiz, and D.G. Phinney, *A Clinical Indications Prediction Scale Based on TWIST1 for Human Mesenchymal Stem Cells*. EBioMedicine, 2016. **4**: p. 62-73.
66. Vemuri, M.C., L.G. Chase, and M.S. Rao, *Mesenchymal stem cell assays and applications*. Methods Mol Biol, 2011. **698**: p. 3-8.
67. Khatiwala, C.B., P.D. Kim, S.R. Peyton, and A.J. Putnam, *ECM compliance regulates osteogenesis by influencing MAPK signaling downstream of RhoA and ROCK*. J Bone Miner Res, 2009. **24**(5): p. 886-98.
68. Kostura, L., D.L. Kraitchman, A.M. Mackay, M.F. Pittenger, and J.W. Bulte, *Feridex labeling of mesenchymal stem cells inhibits chondrogenesis but not adipogenesis or osteogenesis*. NMR Biomed, 2004. **17**(7): p. 513-7.
69. Billing, A.M., H. Ben Hamidane, S.S. Dib, R.J. Cotton, A.M. Bhagwat, P. Kumar, S. Hayat, N.A. Yousri, N. Goswami, K. Suhre, A. Rafii, and J. Graumann, *Comprehensive transcriptomic and proteomic characterization of human mesenchymal stem cells reveals source specific cellular markers*. Sci Rep, 2016. **6**: p. 21507.
70. Strupp, B.J., *Improvement of memory by a vasopressin fragment: importance of individual differences in mnemonic function*. Behav Neurosci, 1989. **103**(4): p. 743-54.
71. Marklein, R.A., M.W. Klinker, K.A. Drake, H.G. Polikowsky, E.C. Lessey-Morillon, and S.R. Bauer, *Morphological profiling using machine learning reveals emergent subpopulations of interferon-gamma-stimulated mesenchymal stromal cells that predict immunosuppression*. Cytotherapy, 2019. **21**(1): p. 17-31.
72. Marklein, R.A., J.L. Lo Surdo, I.H. Bellayr, S.A. Godil, R.K. Puri, and S.R. Bauer, *High Content Imaging of Early Morphological Signatures Predicts Long Term*

Mineralization Capacity of Human Mesenchymal Stem Cells upon Osteogenic Induction. Stem Cells, 2016. **34**(4): p. 935-47.
73. Shi, C., X. Wang, S. Wu, Y. Zhu, L.W. Chung, and H. Mao, *HRMAS 1H-NMR measured changes of the metabolite profile as mesenchymal stem cells differentiate to targeted fat cells in vitro: implications for non-invasive monitoring of stem cell differentiation in vivo*. J Tissue Eng Regen Med, 2008. **2**(8): p. 482-90.
74. Matsuoka, F., I. Takeuchi, H. Agata, H. Kagami, H. Shiono, Y. Kiyota, H. Honda, and R. Kato, *Characterization of time-course morphological features for efficient prediction of osteogenic potential in human mesenchymal stem cells*. Biotechnol Bioeng, 2014. **111**(7): p. 1430-9.
75. Gordonov, S., M.K. Hwang, A. Wells, F.B. Gertler, D.A. Lauffenburger, and M. Bathe, *Time series modeling of live-cell shape dynamics for image-based phenotypic profiling*. Integr Biol (Camb), 2016. **8**(1): p. 73-90.
76. Diggins, K.E., P.B. Ferrell, Jr., and J.M. Irish, *Methods for discovery and characterization of cell subsets in high dimensional mass cytometry data*. Methods, 2015. **82**: p. 55-63.
77. Jonczyk, R., T. Kurth, A. Lavrentieva, J.G. Walter, T. Scheper, and F. Stahl, *Living Cell Microarrays: An Overview of Concepts*. Microarrays (Basel), 2016. **5**(2).
78. Lv, F.J., R.S. Tuan, K.M. Cheung, and V.Y. Leung, *Concise review: the surface markers and identity of human mesenchymal stem cells*. Stem Cells, 2014. **32**(6): p. 1408-19.
79. De Ugarte, D.A., Z. Alfonso, P.A. Zuk, A. Elbarbary, M. Zhu, P. Ashjian, P. Benhaim, M.H. Hedrick, and J.K. Fraser, *Differential expression of stem cell mobilization-associated molecules on multi-lineage cells from adipose tissue and bone marrow*. Immunol Lett, 2003. **89**(2-3): p. 267-70.
80. Al-Nbaheen, M., R. Vishnubalaji, D. Ali, A. Bouslimi, F. Al-Jassir, M. Megges, A. Prigione, J. Adjaye, M. Kassem, and A. Aldahmash, *Human stromal (mesenchymal) stem cells from bone marrow, adipose tissue and skin exhibit differences in molecular phenotype and differentiation potential*. Stem Cell Rev Rep, 2013. **9**(1): p. 32-43.
81. Li, B., U. Menzel, C. Loebel, H. Schmal, M. Alini, and M.J. Stoddart, *Monitoring live human mesenchymal stromal cell differentiation and subsequent selection using fluorescent RNA-based probes*. Sci Rep, 2016. **6**: p. 26014.
82. Yang, H.N., J.S. Park, K. Na, D.G. Woo, Y.D. Kwon, and K.H. Park, *The use of green fluorescence gene (GFP)-modified rabbit mesenchymal stem cells (rMSCs) co-cultured with chondrocytes in hydrogel constructs to reveal the chondrogenesis of MSCs*. Biomaterials, 2009. **30**(31): p. 6374-85.
83. Quinn, K.P., G.V. Sridharan, R.S. Hayden, D.L. Kaplan, K. Lee, and I. Georgakoudi, *Quantitative metabolic imaging using endogenous fluorescence to detect stem cell differentiation*. Sci Rep, 2013. **3**: p. 3432.
84. Treiser, M.D., E.H. Yang, S. Gordonov, D.M. Cohen, I.P. Androulakis, J. Kohn, C.S. Chen, and P.V. Moghe, *Cytoskeleton-based forecasting of stem cell lineage fates*. Proc Natl Acad Sci U S A, 2010. **107**(2): p. 610-5.
85. Lee, S.H. and R. Dominguez, *Regulation of actin cytoskeleton dynamics in cells*. Mol Cells, 2010. **29**(4): p. 311-25.
86. Krause, M. and A. Gautreau, *Steering cell migration: lamellipodium dynamics and the regulation of directional persistence*. Nat Rev Mol Cell Biol, 2014. **15**(9): p. 577-90.
87. Gupton, S.L. and F.B. Gertler, *Filopodia: the fingers that do the walking*. Sci STKE, 2007. **2007**(400): p. re5.
88. Chugh, P. and E.K. Paluch, *The actin cortex at a glance*. J Cell Sci, 2018. **131**(14).

89. Zaidel-Bar, R., G. Zhenhuan, and C. Luxenburg, *The contractome--a systems view of actomyosin contractility in non-muscle cells*. J Cell Sci, 2015. **128**(12): p. 2209-17.
90. Pellegrin, S. and H. Mellor, *Actin stress fibres*. J Cell Sci, 2007. **120**(Pt 20): p. 3491-9.
91. Merino, F., S. Pospich, J. Funk, T. Wagner, F. Kullmer, H.D. Arndt, P. Bieling, and S. Raunser, *Structural transitions of F-actin upon ATP hydrolysis at near-atomic resolution revealed by cryo-EM*. Nat Struct Mol Biol, 2018. **25**(6): p. 528-537.
92. Dominguez, R. and K.C. Holmes, *Actin structure and function*. Annu Rev Biophys, 2011. **40**: p. 169-86.
93. Dominguez, R., *Actin filament nucleation and elongation factors--structure-function relationships*. Crit Rev Biochem Mol Biol, 2009. **44**(6): p. 351-66.
94. Xue, B., C. Leyrat, J.M. Grimes, and R.C. Robinson, *Structural basis of thymosin-beta4/profilin exchange leading to actin filament polymerization*. Proc Natl Acad Sci U S A, 2014. **111**(43): p. E4596-605.
95. Suarez, C., R.T. Carroll, T.A. Burke, J.R. Christensen, A.J. Bestul, J.A. Sees, M.L. James, V. Sirotkin, and D.R. Kovar, *Profilin regulates F-actin network homeostasis by favoring formin over Arp2/3 complex*. Dev Cell, 2015. **32**(1): p. 43-53.
96. Winder, S.J. and K.R. Ayscough, *Actin-binding proteins*. J Cell Sci, 2005. **118**(Pt 4): p. 651-4.
97. Firat-Karalar, E.N. and M.D. Welch, *New mechanisms and functions of actin nucleation*. Curr Opin Cell Biol, 2011. **23**(1): p. 4-13.
98. Kovar, D.R. and T.D. Pollard, *Progressing actin: Formin as a processive elongation machine*. Nat Cell Biol, 2004. **6**(12): p. 1158-9.
99. Paul, A.S. and T.D. Pollard, *The role of the FH1 domain and profilin in formin-mediated actin-filament elongation and nucleation*. Curr Biol, 2008. **18**(1): p. 9-19.
100. Chesarone, M.A. and B.L. Goode, *Actin nucleation and elongation factors: mechanisms and interplay*. Curr Opin Cell Biol, 2009. **21**(1): p. 28-37.
101. Chen, X.J., A.J. Squarr, R. Stephan, B. Chen, T.E. Higgins, D.J. Barry, M.C. Martin, M.K. Rosen, S. Bogdan, and M. Way, *Ena/VASP proteins cooperate with the WAVE complex to regulate the actin cytoskeleton*. Dev Cell, 2014. **30**(5): p. 569-84.
102. Rotty, Jeremy D., C. Wu, Elizabeth M. Haynes, C. Suarez, Jonathan D. Winkelman, Heath E. Johnson, Jason M. Haugh, David R. Kovar, and James E. Bear, *Profilin-1 Serves as a Gatekeeper for Actin Assembly by Arp2/3-Dependent and -Independent Pathways*. Developmental Cell, 2015. **32**(1): p. 54-67.
103. Falzone, T.T., M. Lenz, D.R. Kovar, and M.L. Gardel, *Assembly kinetics determine the architecture of alpha-actinin crosslinked F-actin networks*. Nat Commun, 2012. **3**: p. 861.
104. Shekhar, S., M. Kerleau, S. Kuhn, J. Pernier, G. Romet-Lemonne, A. Jegou, and M.F. Carlier, *Formin and capping protein together embrace the actin filament in a menage a trois*. Nat Commun, 2015. **6**: p. 8730.
105. Edwards, M., A. Zwolak, D.A. Schafer, D. Sept, R. Dominguez, and J.A. Cooper, *Capping protein regulators fine-tune actin assembly dynamics*. Nat Rev Mol Cell Biol, 2014. **15**(10): p. 677-89.
106. Kotila, T., H. Wioland, G. Enkavi, K. Kogan, I. Vattulainen, A. Jegou, G. Romet-Lemonne, and P. Lappalainen, *Mechanism of synergistic actin filament pointed end depolymerization by cyclase-associated protein and cofilin*. Nat Commun, 2019. **10**(1): p. 5320.
107. Akin, O. and R.D. Mullins, *Capping protein increases the rate of actin-based motility by promoting filament nucleation by the Arp2/3 complex*. Cell, 2008. **133**(5): p. 841-51.

108. Miki, H. and T. Takenawa, *Regulation of actin dynamics by WASP family proteins*. J Biochem, 2003. **134**(3): p. 309-13.
109. Schwartz, M., *Rho signalling at a glance*. J Cell Sci, 2004. **117**(Pt 23): p. 5457-8.
110. Etienne-Manneville, S. and A. Hall, *Rho GTPases in cell biology*. Nature, 2002. **420**(6916): p. 629-35.
111. Heasman, S.J. and A.J. Ridley, *Mammalian Rho GTPases: new insights into their functions from in vivo studies*. Nat Rev Mol Cell Biol, 2008. **9**(9): p. 690-701.
112. Tojkander, S., G. Gateva, and P. Lappalainen, *Actin stress fibers--assembly, dynamics and biological roles*. J Cell Sci, 2012. **125**(Pt 8): p. 1855-64.
113. Kimura, K., M. Ito, M. Amano, K. Chihara, Y. Fukata, M. Nakafuku, B. Yamamori, J. Feng, T. Nakano, K. Okawa, A. Iwamatsu, and K. Kaibuchi, *Regulation of myosin phosphatase by Rho and Rho-associated kinase (Rho-kinase)*. Science, 1996. **273**(5272): p. 245-8.
114. Havrylenko, S., P. Noguera, M. Abou-Ghali, J. Manzi, F. Faqir, A. Lamora, C. Guerin, L. Blanchoin, and J. Plastino, *WAVE binds Ena/VASP for enhanced Arp2/3 complex-based actin assembly*. Mol Biol Cell, 2015. **26**(1): p. 55-65.
115. Hall, A., *Rho family gtpases*. 2012, Portland Press Ltd.
116. Guilluy, C., R. Garcia-Mata, and K. Burridge, *Rho protein crosstalk: another social network?* Trends Cell Biol, 2011. **21**(12): p. 718-26.
117. Dupont, S., L. Morsut, M. Aragona, E. Enzo, S. Giulitti, M. Cordenonsi, F. Zanconato, J. Le Digabel, M. Forcato, S. Bicciato, N. Elvassore, and S. Piccolo, *Role of YAP/TAZ in mechanotransduction*. Nature, 2011. **474**(7350): p. 179-83.
118. Halder, G., S. Dupont, and S. Piccolo, *Transduction of mechanical and cytoskeletal cues by YAP and TAZ*. Nat Rev Mol Cell Biol, 2012. **13**(9): p. 591-600.
119. Kilian, K.A., B. Bugarija, B.T. Lahn, and M. Mrksich, *Geometric cues for directing the differentiation of mesenchymal stem cells*. Proc Natl Acad Sci U S A, 2010. **107**(11): p. 4872-7.
120. Zhang, Y., D. Khan, J. Delling, and E. Tobiasch, *Mechanisms underlying the osteo- and adipo-differentiation of human mesenchymal stem cells*. ScientificWorldJournal, 2012. **2012**: p. 793823.
121. Park, J.S., J.S. Chu, A.D. Tsou, R. Diop, Z. Tang, A. Wang, and S. Li, *The effect of matrix stiffness on the differentiation of mesenchymal stem cells in response to TGF-β*. Biomaterials, 2011. **32**(16): p. 3921-3930.
122. Connelly, J.T., J.E. Gautrot, B. Trappmann, D.W. Tan, G. Donati, W.T. Huck, and F.M. Watt, *Actin and serum response factor transduce physical cues from the microenvironment to regulate epidermal stem cell fate decisions*. Nat Cell Biol, 2010. **12**(7): p. 711-8.
123. Sen, B., G. Uzer, R.M. Samsonraj, Z. Xie, C. McGrath, M. Styner, A. Dudakovic, A.J. van Wijnen, and J. Rubin, *Intranuclear Actin Structure Modulates Mesenchymal Stem Cell Differentiation*. Stem Cells, 2017. **35**(6): p. 1624-1635.
124. Chen, L., K. Shi, C.E. Frary, N. Ditzel, H. Hu, W. Qiu, and M. Kassem, *Inhibiting actin depolymerization enhances osteoblast differentiation and bone formation in human stromal stem cells*. Stem Cell Res, 2015. **15**(2): p. 281-9.
125. Zhang, Z., J. Messana, N.S. Hwang, and J.H. Elisseeff, *Reorganization of actin filaments enhances chondrogenic differentiation of cells derived from murine embryonic stem cells*. Biochem Biophys Res Commun, 2006. **348**(2): p. 421-7.
126. Kamishibahara, Y., H. Kawaguchi, and N. Shimizu, *Rho kinase inhibitor Y-27632 promotes neuronal differentiation in mouse embryonic stem cells via phosphatidylinositol 3-kinase*. Neurosci Lett, 2016. **615**: p. 44-9.

127. Watanabe, K., M. Ueno, D. Kamiya, A. Nishiyama, M. Matsumura, T. Wataya, J.B. Takahashi, S. Nishikawa, S. Nishikawa, K. Muguruma, and Y. Sasai, *A ROCK inhibitor permits survival of dissociated human embryonic stem cells*. Nat Biotechnol, 2007. **25**(6): p. 681-6.
128. Carlson, A.L., C.A. Florek, J.J. Kim, T. Neubauer, J.C. Moore, R.I. Cohen, J. Kohn, M. Grumet, and P.V. Moghe, *Microfibrous substrate geometry as a critical trigger for organization, self-renewal, and differentiation of human embryonic stem cells within synthetic 3-dimensional microenvironments*. Faseb j, 2012. **26**(8): p. 3240-51.
129. Sakurai, K., I. Talukdar, V.S. Patil, J. Dang, Z. Li, K.Y. Chang, C.C. Lu, V. Delorme-Walker, C. Dermardirossian, K. Anderson, D. Hanein, C.S. Yang, D. Wu, Y. Liu, and T.M. Rana, *Kinome-wide functional analysis highlights the role of cytoskeletal remodeling in somatic cell reprogramming*. Cell Stem Cell, 2014. **14**(4): p. 523-34.
130. Chen, G., Z. Hou, D.R. Gulbranson, and J.A. Thomson, *Actin-myosin contractility is responsible for the reduced viability of dissociated human embryonic stem cells*. Cell Stem Cell, 2010. **7**(2): p. 240-8.
131. Liu, X., V. Ory, S. Chapman, H. Yuan, C. Albanese, B. Kallakury, O.A. Timofeeva, C. Nealon, A. Dakic, V. Simic, B.R. Haddad, J.S. Rhim, A. Dritschilo, A. Riegel, A. McBride, and R. Schlegel, *ROCK inhibitor and feeder cells induce the conditional reprogramming of epithelial cells*. Am J Pathol, 2012. **180**(2): p. 599-607.
132. Pakzad, M., M. Totonchi, A. Taei, A. Seifinejad, S.N. Hassani, and H. Baharvand, *Presence of a ROCK inhibitor in extracellular matrix supports more undifferentiated growth of feeder-free human embryonic and induced pluripotent stem cells upon passaging*. Stem Cell Rev Rep, 2010. **6**(1): p. 96-107.
133. Compagnucci, C., F. Piemonte, A. Sferra, E. Piermarini, and E. Bertini, *The cytoskeletal arrangements necessary to neurogenesis*. Oncotarget, 2016. **7**(15): p. 19414-29.
134. Toyoda, T., A. Kimura, H. Tanaka, T. Ameku, A. Mima, Y. Hirose, M. Nakamura, A. Watanabe, and K. Osafune, *Rho-Associated Kinases and Non-muscle Myosin IIs Inhibit the Differentiation of Human iPSCs to Pancreatic Endoderm*. Stem Cell Reports, 2017. **9**(2): p. 419-428.
135. Zhao, M., Y. Tang, P.J. Ernst, A. Kahn-Krell, C. Fan, D. Pretorius, H. Zhu, X. Lou, L. Zhou, J. Zhang, and W. Zhu, *Enhancing the Engraftment of Human Induced Pluripotent Stem Cell-derived Cardiomyocytes via a Transient Inhibition of Rho Kinase Activity*. J Vis Exp, 2019(149).
136. Boraas, L.C., J.B. Guidry, E.T. Pineda, and T. Ahsan, *Cytoskeletal Expression and Remodeling in Pluripotent Stem Cells*. PLoS One, 2016. **11**(1): p. e0145084.
137. Ross, R., H. Jonuleit, M. Bros, X.L. Ross, S. Yamashiro, F. Matsumura, A.H. Enk, J. Knop, and A.B. Reske-Kunz, *Expression of the actin-bundling protein fascin in cultured human dendritic cells correlates with dendritic morphology and cell differentiation*. J Invest Dermatol, 2000. **115**(4): p. 658-63.
138. Peng, K.Y., Y.W. Lee, P.J. Hsu, H.H. Wang, Y. Wang, J.Y. Liou, S.H. Hsu, K.K. Wu, and B.L. Yen, *Human pluripotent stem cell (PSC)-derived mesenchymal stem cells (MSCs) show potent neurogenic capacity which is enhanced with cytoskeletal rearrangement*. Oncotarget, 2016. **7**(28): p. 43949-43959.
139. Compagnucci, C., E. Piermarini, A. Sferra, R. Borghi, A. Niceforo, S. Petrini, F. Piemonte, and E. Bertini, *Cytoskeletal dynamics during in vitro neurogenesis of induced pluripotent stem cells (iPSCs)*. Mol Cell Neurosci, 2016. **77**: p. 113-124.
140. Jansen, K.A., P. Atherton, and C. Ballestrem, *Mechanotransduction at the cell-matrix interface*. Semin Cell Dev Biol, 2017. **71**: p. 75-83.

141. Mack, C.P., A.V. Somlyo, M. Hautmann, A.P. Somlyo, and G.K. Owens, *Smooth muscle differentiation marker gene expression is regulated by RhoA-mediated actin polymerization*. J Biol Chem, 2001. **276**(1): p. 341-7.
142. Swift, J., I.L. Ivanovska, A. Buxboim, T. Harada, P.C. Dingal, J. Pinter, J.D. Pajerowski, K.R. Spinler, J.W. Shin, M. Tewari, F. Rehfeldt, D.W. Speicher, and D.E. Discher, *Nuclear lamin-A scales with tissue stiffness and enhances matrix-directed differentiation*. Science, 2013. **341**(6149): p. 1240104.
143. Talele, N.P., J. Fradette, J.E. Davies, A. Kapus, and B. Hinz, *Expression of alpha-Smooth Muscle Actin Determines the Fate of Mesenchymal Stromal Cells*. Stem Cell Reports, 2015. **4**(6): p. 1016-30.
144. Liu, L., Q. Luo, J. Sun, and G. Song, *Cytoskeletal control of nuclear morphology and stiffness are required for OPN-induced bone-marrow-derived mesenchymal stem cell migration.* Biochem Cell Biol, 2019. **97**(4): p. 463-470.
145. Oh, S., K.S. Brammer, Y.S. Li, D. Teng, A.J. Engler, S. Chien, and S. Jin, *Stem cell fate dictated solely by altered nanotube dimension.* Proc Natl Acad Sci U S A, 2009. **106**(7): p. 2130-5.
146. Seo, H.R., H.J. Joo, D.H. Kim, L.H. Cui, S.C. Choi, J.H. Kim, S.W. Cho, K.B. Lee, and D.S. Lim, *Nanopillar Surface Topology Promotes Cardiomyocyte Differentiation through Cofilin-Mediated Cytoskeleton Rearrangement.* ACS Appl Mater Interfaces, 2017. **9**(20): p. 16803-16812.
147. Abagnale, G., A. Sechi, M. Steger, Q. Zhou, C.C. Kuo, G. Aydin, C. Schalla, G. Muller-Newen, M. Zenke, I.G. Costa, P. van Rijn, A. Gillner, and W. Wagner, *Surface Topography Guides Morphology and Spatial Patterning of Induced Pluripotent Stem Cell Colonies*. Stem Cell Reports, 2017. **9**(2): p. 654-666.
148. Narva, E., A. Stubb, C. Guzman, M. Blomqvist, D. Balboa, M. Lerche, M. Saari, T. Otonkoski, and J. Ivaska, *A Strong Contractile Actin Fence and Large Adhesions Direct Human Pluripotent Colony Morphology and Adhesion*. Stem Cell Reports, 2017. **9**(1): p. 67-76.
149. Guo, J., Y. Wang, F. Sachs, and F. Meng, *Actin stress in cell reprogramming*. Proc Natl Acad Sci U S A, 2014. **111**(49): p. E5252-61.
150. Abdeen, A.A., J. Lee, Y. Li, and K.A. Kilian, *Cytoskeletal Priming of Mesenchymal Stem Cells to a Medicinal Phenotype.* Regenerative Engineering and Translational Medicine, 2017. **3**(1): p. 5-14.
151. Ferlin, K.M., M.E. Prendergast, M.L. Miller, B.N. Nguyen, D.S. Kaplan, and J.P. Fisher, *Development of a dynamic stem cell culture platform for mesenchymal stem cell adhesion and evaluation*. Mol Pharm, 2014. **11**(7): p. 2172-81.
152. Sart, S., A. Errachid, Y.J. Schneider, and S.N. Agathos, *Modulation of mesenchymal stem cell actin organization on conventional microcarriers for proliferation and differentiation in stirred bioreactors*. J Tissue Eng Regen Med, 2013. **7**(7): p. 537-51.
153. Liu, H., L.A. MacQueen, J.F. Usprech, H. Maleki, K.L. Sider, M.G. Doyle, Y. Sun, and C.A. Simmons, *Microdevice arrays with strain sensors for 3D mechanical stimulation and monitoring of engineered tissues*. Biomaterials, 2018. **172**: p. 30-40.
154. Vega, S.L., E. Liu, P.J. Patel, A.B. Kulesa, A.L. Carlson, Y. Ma, M.L. Becker, and P.V. Moghe, *High-content imaging-based screening of microenvironment-induced changes to stem cells*. J Biomol Screen, 2012. **17**(9): p. 1151-62.
155. Vega, S.L., V. Arvind, P. Mishra, J. Kohn, N. Sanjeeva Murthy, and P.V. Moghe, *Substrate micropatterns produced by polymer demixing regulate focal adhesions, actin anisotropy, and lineage differentiation of stem cells*. Acta Biomater, 2018. **76**: p. 21-28.

156. Gourlay, C.W., L.N. Carpp, P. Timpson, S.J. Winder, and K.R. Ayscough, *A role for the actin cytoskeleton in cell death and aging in yeast*. J Cell Biol, 2004. **164**(6): p. 803-9.
157. Vigelsø, A., R. Dybboe, C.N. Hansen, F. Dela, J.W. Helge, and A. Guadalupe Grau, *GAPDH and β-actin protein decreases with aging, making Stain-Free technology a superior loading control in Western blotting of human skeletal muscle*. Journal of applied physiology, 2015. **118**(3): p. 386-394.
158. Tormos, A.M., S. Rius-Perez, M. Jorques, P. Rada, L. Ramirez, A.M. Valverde, A.R. Nebreda, J. Sastre, and R. Talens-Visconti, *p38alpha regulates actin cytoskeleton and cytokinesis in hepatocytes during development and aging*. PLoS One, 2017. **12**(2): p. e0171738.
159. Higuchi, R., J.D. Vevea, T.C. Swayne, R. Chojnowski, V. Hill, I.R. Boldogh, and L.A. Pon, *Actin dynamics affect mitochondrial quality control and aging in budding yeast*. Curr Biol, 2013. **23**(23): p. 2417-22.
160. Cichon, J., C. Sun, B. Chen, M. Jiang, X.A. Chen, Y. Sun, Y. Wang, and G. Chen, *Cofilin aggregation blocks intracellular trafficking and induces synaptic loss in hippocampal neurons*. J Biol Chem, 2012. **287**(6): p. 3919-29.
161. Liu, J., Y. Ding, Z. Liu, and X. Liang, *Senescence in Mesenchymal Stem Cells: Functional Alterations, Molecular Mechanisms, and Rejuvenation Strategies*. Front Cell Dev Biol, 2020. **8**: p. 258.
162. Dhaliwal, A., M. Brenner, P. Wolujewicz, Z. Zhang, Y. Mao, M. Batish, J. Kohn, and P.V. Moghe, *Profiling stem cell states in three-dimensional biomaterial niches using high content image informatics*. Acta Biomater, 2016. **45**: p. 98-109.
163. Vega, S.L., E. Liu, V. Arvind, J. Bushman, H.J. Sung, M.L. Becker, S. Lelievre, J. Kohn, P.A. Vidi, and P.V. Moghe, *High-content image informatics of the structural nuclear protein NuMA parses trajectories for stem/progenitor cell lineages and oncogenic transformation*. Exp Cell Res, 2017. **351**(1): p. 11-23.
164. Liu, E., S. Gordonov, M.D. Treiser, and P.V. Moghe, *Parsing the early cytoskeletal and nuclear organizational cues that demarcate stem cell lineages*. Cell Cycle, 2010. **9**(11): p. 2108-17.
165. Kim, J.J., N.K. Bennett, M.S. Devita, S. Chahar, S. Viswanath, E.A. Lee, G. Jung, P.P. Shao, E.P. Childers, S. Liu, A. Kulesa, B.A. Garcia, M.L. Becker, N.S. Hwang, A. Madabhushi, M.P. Verzi, and P.V. Moghe, *Optical High Content Nanoscopy of Epigenetic Marks Decodes Phenotypic Divergence in Stem Cells*. Sci Rep, 2017. **7**: p. 39406.
166. Minguell, J.J., A. Erices, and P. Conget, *Mesenchymal stem cells*. Exp Biol Med (Maywood), 2001. **226**(6): p. 507-20.
167. Ding, D.C., W.C. Shyu, and S.Z. Lin, *Mesenchymal stem cells*. Cell Transplant, 2011. **20**(1): p. 5-14.
168. Otero-Vinas, M. and V. Falanga, *Mesenchymal Stem Cells in Chronic Wounds: The Spectrum from Basic to Advanced Therapy*. Adv Wound Care (New Rochelle), 2016. **5**(4): p. 149-163.
169. Robey, P., *"Mesenchymal stem cells": fact or fiction, and implications in their therapeutic use*. F1000Res, 2017. **6**.
170. Vaananen, H.K., *Mesenchymal stem cells*. Ann Med, 2005. **37**(7): p. 469-79.
171. Samsonraj, R.M., B. Rai, P. Sathiyanathan, K.J. Puan, O. Rotzschke, J.H. Hui, M. Raghunath, L.W. Stanton, V. Nurcombe, and S.M. Cool, *Establishing criteria for human mesenchymal stem cell potency*. Stem Cells, 2015. **33**(6): p. 1878-91.
172. Hoemann, C.D., H. El-Gabalawy, and M.D. McKee, *In vitro osteogenesis assays: influence of the primary cell source on alkaline phosphatase activity and mineralization*. Pathol Biol (Paris), 2009. **57**(4): p. 318-23.

173. Diekman, B.O., C.R. Rowland, D.P. Lennon, A.I. Caplan, and F. Guilak, *Chondrogenesis of adult stem cells from adipose tissue and bone marrow: induction by growth factors and cartilage-derived matrix*. Tissue Eng Part A, 2010. **16**(2): p. 523-33.
174. Joseph, R., J. Poschmann, R. Sukarieh, P.G. Too, S.G. Julien, F. Xu, A.L. Teh, J.D. Holbrook, K.L. Ng, Y.S. Chong, P.D. Gluckman, S. Prabhakar, and W. Stunkel, *ACSL1 Is Associated With Fetal Programming of Insulin Sensitivity and Cellular Lipid Content*. Mol Endocrinol, 2015. **29**(6): p. 909-20.
175. Aldridge, A., D. Kouroupis, S. Churchman, A. English, E. Ingham, and E. Jones, *Assay validation for the assessment of adipogenesis of multipotential stromal cells--a direct comparison of four different methods*. Cytotherapy, 2013. **15**(1): p. 89-101.
176. Solchaga, L.A., K.J. Penick, and J.F. Welter, *Chondrogenic differentiation of bone marrow-derived mesenchymal stem cells: tips and tricks*. Methods Mol Biol, 2011. **698**: p. 253-78.
177. Kim, J.J. and P.V. Moghe, *Parsing Stem Cell Lineage Development Using High Content Image Analysis of Epigenetic Spatial Markers*. Curr Protoc Stem Cell Biol, 2018. **46**(1): p. e54.
178. Cockrell, A.S. and T. Kafri, *Gene delivery by lentivirus vectors*. Mol Biotechnol, 2007. **36**(3): p. 184-204.
179. Rodriguez, J.P., M. Gonzalez, S. Rios, and V. Cambiazo, *Cytoskeletal organization of human mesenchymal stem cells (MSC) changes during their osteogenic differentiation*. J Cell Biochem, 2004. **93**(4): p. 721-31.
180. Mattout, A., Y. Aaronson, B.S. Sailaja, E.V. Raghu Ram, A. Harikumar, J.P. Mallm, K.H. Sim, M. Nissim-Rafinia, E. Supper, P.B. Singh, S.K. Sze, S.M. Gasser, K. Rippe, and E. Meshorer, *Heterochromatin Protein 1beta (HP1beta) has distinct functions and distinct nuclear distribution in pluripotent versus differentiated cells*. Genome Biol, 2015. **16**: p. 213.
181. Ichim, C.V. and R.A. Wells, *Generation of high-titer viral preparations by concentration using successive rounds of ultracentrifugation*. J Transl Med, 2011. **9**: p. 137.
182. Das, A.T., L. Tenenbaum, and B. Berkhout, *Tet-On Systems For Doxycycline-inducible Gene Expression*. Curr Gene Ther, 2016. **16**(3): p. 156-67.
183. Yang, Y.K., C.R. Ogando, C. Wang See, T.Y. Chang, and G.A. Barabino, *Changes in phenotype and differentiation potential of human mesenchymal stem cells aging in vitro*. Stem Cell Res Ther, 2018. **9**(1): p. 131.
184. Guo, W., K.M. Zhang, K. Tu, Y.X. Li, L. Zhu, H.S. Xiao, Y. Yang, and J.R. Wu, *Adipogenesis licensing and execution are disparately linked to cell proliferation*. Cell Res, 2009. **19**(2): p. 216-23.
185. Sonowal, H., A. Kumar, J. Bhattacharyya, P.K. Gogoi, and B.G. Jaganathan, *Inhibition of actin polymerization decreases osteogeneic differentiation of mesenchymal stem cells through p38 MAPK pathway*. J Biomed Sci, 2013. **20**: p. 71.
186. Hamm, A., N. Krott, I. Breibach, R. Blindt, and A.K. Bosserhoff, *Efficient transfection method for primary cells*. Tissue Eng, 2002. **8**(2): p. 235-45.
187. Nanba, D., N. Matsushita, F. Toki, and S. Higashiyama, *Efficient expansion of human keratinocyte stem/progenitor cells carrying a transgene with lentiviral vector*. Stem Cell Res Ther, 2013. **4**(5): p. 127.
188. Lin, P., Y. Lin, D.P. Lennon, D. Correa, M. Schluchter, and A.I. Caplan, *Efficient lentiviral transduction of human mesenchymal stem cells that preserves proliferation and differentiation capabilities*. Stem Cells Transl Med, 2012. **1**(12): p. 886-97.
189. Muthukuru, M. and J. Sun, *Doxycycline counteracts bone morphogenic protein 2-induced osteogenic mediators*. J Periodontol, 2013. **84**(5): p. 656-65.

190. Wang, F., J.E. Dennis, A. Awadallah, L.A. Solchaga, J. Molter, Y. Kuang, N. Salem, Y. Lin, H. Tian, J.A. Kolthammer, Y. Kim, Z.B. Love, S.L. Gerson, and Z. Lee, *Transcriptional profiling of human mesenchymal stem cells transduced with reporter genes for imaging*. Physiol Genomics, 2009. **37**(1): p. 23-34.
191. Hayashi-Takanaka, Y., K. Yamagata, T. Wakayama, T.J. Stasevich, T. Kainuma, T. Tsurimoto, M. Tachibana, Y. Shinkai, H. Kurumizaka, N. Nozaki, and H. Kimura, *Tracking epigenetic histone modifications in single cells using Fab-based live endogenous modification labeling*. Nucleic Acids Res, 2011. **39**(15): p. 6475-88.
192. Rui, Y., L. Xu, R. Chen, T. Zhang, S. Lin, Y. Hou, Y. Liu, F. Meng, Z. Liu, M. Ni, K.S. Tsang, F. Yang, C. Wang, H.C. Chan, X. Jiang, and G. Li, *Epigenetic memory gained by priming with osteogenic induction medium improves osteogenesis and other properties of mesenchymal stem cells*. Sci Rep, 2015. **5**: p. 11056.
193. Yourek, G., M.A. Hussain, and J.J. Mao, *Cytoskeletal changes of mesenchymal stem cells during differentiation*. ASAIO J, 2007. **53**(2): p. 219-28.
194. McBeath, R., D.M. Pirone, C.M. Nelson, K. Bhadriraju, and C.S. Chen, *Cell shape, cytoskeletal tension, and RhoA regulate stem cell lineage commitment*. Dev Cell, 2004. **6**(4): p. 483-95.
195. Lim, Y.B., S.S. Kang, T.K. Park, Y.S. Lee, J.S. Chun, and J.K. Sonn, *Disruption of actin cytoskeleton induces chondrogenesis of mesenchymal cells by activating protein kinase C-alpha signaling*. Biochem Biophys Res Commun, 2000. **273**(2): p. 609-13.
196. Mathieu, P.S. and E.G. Loboa, *Cytoskeletal and focal adhesion influences on mesenchymal stem cell shape, mechanical properties, and differentiation down osteogenic, adipogenic, and chondrogenic pathways*. Tissue Eng Part B Rev, 2012. **18**(6): p. 436-44.
197. Sliogeryte, K., S.D. Thorpe, D.A. Lee, L. Botto, and M.M. Knight, *Stem cell differentiation increases membrane-actin adhesion regulating cell blebability, migration and mechanics*. Sci Rep, 2014. **4**: p. 7307.
198. Bonab, M.M., K. Alimoghaddam, F. Talebian, S.H. Ghaffari, A. Ghavamzadeh, and B. Nikbin, *Aging of mesenchymal stem cell in vitro*. BMC Cell Biol, 2006. **7**: p. 14.
199. Webb, D.J., J.T. Parsons, and A.F. Horwitz, *Adhesion assembly, disassembly and turnover in migrating cells -- over and over and over again*. Nat Cell Biol, 2002. **4**(4): p. E97-100.
200. Lodish H, B.A., Zipursky SL, et al., *Molecular Cell Biology, 4th edition*. 4th edition ed. The Dynamics of Actin assembly. 2000, New York: W. H. Freeman.
201. Lukinavicius, G., L. Reymond, E. D'Este, A. Masharina, F. Gottfert, H. Ta, A. Guther, M. Fournier, S. Rizzo, H. Waldmann, C. Blaukopf, C. Sommer, D.W. Gerlich, H.D. Arndt, S.W. Hell, and K. Johnsson, *Fluorogenic probes for live-cell imaging of the cytoskeleton*. Nat Methods, 2014. **11**(7): p. 731-3.
202. Machesky, L.M. and A. Hall, *Role of actin polymerization and adhesion to extracellular matrix in Rac- and Rho-induced cytoskeletal reorganization*. J Cell Biol, 1997. **138**(4): p. 913-26.
203. Ullah, M., S. Stich, M. Notter, J. Eucker, M. Sittinger, and J. Ringe, *Transdifferentiation of mesenchymal stem cells-derived adipogenic-differentiated cells into osteogenic- or chondrogenic-differentiated cells proceeds via dedifferentiation and have a correlation with cell cycle arresting and driving genes*. Differentiation, 2013. **85**(3): p. 78-90.
204. Ganguly, P., J.J. El-Jawhari, P.V. Giannoudis, A.N. Burska, F. Ponchel, and E.A. Jones, *Age-related Changes in Bone Marrow Mesenchymal Stromal Cells: A Potential Impact on Osteoporosis and Osteoarthritis Development*. Cell Transplant, 2017. **26**(9): p. 1520-1529.

205. Neuhuber, B., G. Gallo, L. Howard, L. Kostura, A. Mackay, and I. Fischer, *Reevaluation of in vitro differentiation protocols for bone marrow stromal cells: disruption of actin cytoskeleton induces rapid morphological changes and mimics neuronal phenotype*. J Neurosci Res, 2004. **77**(2): p. 192-204.
206. Arnsdorf, E.J., P. Tummala, R.Y. Kwon, and C.R. Jacobs, *Mechanically induced osteogenic differentiation--the role of RhoA, ROCKII and cytoskeletal dynamics*. J Cell Sci, 2009. **122**(Pt 4): p. 546-53.
207. Dalby, M.J., N. Gadegaard, R. Tare, A. Andar, M.O. Riehle, P. Herzyk, C.D. Wilkinson, and R.O. Oreffo, *The control of human mesenchymal cell differentiation using nanoscale symmetry and disorder*. Nat Mater, 2007. **6**(12): p. 997-1003.
208. Pollard, T.D. and G.G. Borisy, *Cellular motility driven by assembly and disassembly of actin filaments*. Cell, 2003. **112**(4): p. 453-65.
209. Ayscough, K.R., J. Stryker, N. Pokala, M. Sanders, P. Crews, and D.G. Drubin, *High rates of actin filament turnover in budding yeast and roles for actin in establishment and maintenance of cell polarity revealed using the actin inhibitor latrunculin-A*. J Cell Biol, 1997. **137**(2): p. 399-416.
210. Danowski, B.A., *Fibroblast contractility and actin organization are stimulated by microtubule inhibitors*. J Cell Sci, 1989. **93 (Pt 2)**: p. 255-66.
211. Tee, Y.H., T. Shemesh, V. Thiagarajan, R.F. Hariadi, K.L. Anderson, C. Page, N. Volkmann, D. Hanein, S. Sivaramakrishnan, M.M. Kozlov, and A.D. Bershadsky, *Cellular chirality arising from the self-organization of the actin cytoskeleton*. Nat Cell Biol, 2015. **17**(4): p. 445-57.
212. Vasquez, R.J., B. Howell, A.M. Yvon, P. Wadsworth, and L. Cassimeris, *Nanomolar concentrations of nocodazole alter microtubule dynamic instability in vivo and in vitro*. Mol Biol Cell, 1997. **8**(6): p. 973-85.
213. Brenner, S.L. and E.D. Korn, *Substoichiometric concentrations of cytochalasin D inhibit actin polymerization. Additional evidence for an F-actin treadmill*. J Biol Chem, 1979. **254**(20): p. 9982-5.
214. Peng, G.E., S.R. Wilson, and O.D. Weiner, *A pharmacological cocktail for arresting actin dynamics in living cells*. Mol Biol Cell, 2011. **22**(21): p. 3986-94.
215. Cooper, J.A., *Effects of cytochalasin and phalloidin on actin*. J Cell Biol, 1987. **105**(4): p. 1473-8.
216. Bubb, M.R., I. Spector, B.B. Beyer, and K.M. Fosen, *Effects of jasplakinolide on the kinetics of actin polymerization. An explanation for certain in vivo observations*. J Biol Chem, 2000. **275**(7): p. 5163-70.
217. Titushkin, I.A. and M.R. Cho, *Controlling cellular biomechanics of human mesenchymal stem cells*. Conf Proc IEEE Eng Med Biol Soc, 2009. **2009**: p. 2090-3.
218. Meyers, V.E., M. Zayzafoon, J.T. Douglas, and J.M. McDonald, *RhoA and cytoskeletal disruption mediate reduced osteoblastogenesis and enhanced adipogenesis of human mesenchymal stem cells in modeled microgravity*. J Bone Miner Res, 2005. **20**(10): p. 1858-66.
219. Wagner, W., S. Bork, G. Lepperdinger, S. Joussen, N. Ma, D. Strunk, and C. Koch, *How to track cellular aging of mesenchymal stromal cells?* Aging (Albany NY), 2010. **2**(4): p. 224-30.
220. Engler, A.J., S. Sen, H.L. Sweeney, and D.E. Discher, *Matrix elasticity directs stem cell lineage specification*. Cell, 2006. **126**(4): p. 677-89.
221. De Ugarte, D.A., K. Morizono, A. Elbarbary, Z. Alfonso, P.A. Zuk, M. Zhu, J.L. Dragoo, P. Ashjian, B. Thomas, P. Benhaim, I. Chen, J. Fraser, and M.H. Hedrick, *Comparison of multi-lineage cells from human adipose tissue and bone marrow*. Cells Tissues Organs, 2003. **174**(3): p. 101-9.

222. Fritzsche, M., R.A. Fernandes, V.T. Chang, H. Colin-York, M.P. Clausen, J.H. Felce, S. Galiani, C. Erlenkamper, A.M. Santos, J.M. Heddleston, I. Pedroza-Pacheco, D. Waithe, J.B. de la Serna, B.C. Lagerholm, T.L. Liu, T.L. Chew, E. Betzig, S.J. Davis, and C. Eggeling, *Cytoskeletal actin dynamics shape a ramifying actin network underpinning immunological synapse formation*. Sci Adv, 2017. **3**(6): p. e1603032.
223. van de Peppel, J., T. Strini, J. Tilburg, H. Westerhoff, A.J. van Wijnen, and J.P. van Leeuwen, *Identification of Three Early Phases of Cell-Fate Determination during Osteogenic and Adipogenic Differentiation by Transcription Factor Dynamics*. Stem Cell Reports, 2017. **8**(4): p. 947-960.
224. Hishida, T., M. Nishizuka, S. Osada, and M. Imagawa, *The role of C/EBPdelta in the early stages of adipogenesis*. Biochimie, 2009. **91**(5): p. 654-7.
225. Deisenroth, C., M.B. Black, S. Pendse, L. Pluta, S.M. Witherspoon, P.D. McMullen, and R.S. Thomas, *MYC is an early response regulator of human adipogenesis in adipose stem cells*. PLoS One, 2014. **9**(12): p. e114133.
226. Ohgushi, M., M. Minaguchi, and Y. Sasai, *Rho-Signaling-Directed YAP/TAZ Activity Underlies the Long-Term Survival and Expansion of Human Embryonic Stem Cells*. Cell Stem Cell, 2015. **17**(4): p. 448-61.
227. Zheng, B., M. Han, M. Bernier, and J.K. Wen, *Nuclear actin and actin-binding proteins in the regulation of transcription and gene expression*. FEBS J, 2009. **276**(10): p. 2669-85.
228. Nobusue, H., N. Onishi, T. Shimizu, E. Sugihara, Y. Oki, Y. Sumikawa, T. Chiyoda, K. Akashi, H. Saya, and K. Kano, *Regulation of MKL1 via actin cytoskeleton dynamics drives adipocyte differentiation*. Nat Commun, 2014. **5**: p. 3368.
229. Wu, C.C., F.L. Liu, H.K. Sytwu, C.Y. Tsai, and D.M. Chang, *CD146+ mesenchymal stem cells display greater therapeutic potential than CD146- cells for treating collagen-induced arthritis in mice*. Stem Cell Res Ther, 2016. **7**: p. 23.
230. Kuci, S., Z. Kuci, R. Schafer, G. Spohn, S. Winter, M. Schwab, E. Salzmann-Manrique, T. Klingebiel, and P. Bader, *Molecular signature of human bone marrow-derived mesenchymal stromal cell subsets*. Sci Rep, 2019. **9**(1): p. 1774.
231. Kawaguchi, N., C. Sundberg, M. Kveiborg, B. Moghadaszadeh, M. Asmar, N. Dietrich, C.K. Thodeti, F.C. Nielsen, P. Moller, A.M. Mercurio, R. Albrechtsen, and U.M. Wewer, *ADAM12 induces actin cytoskeleton and extracellular matrix reorganization during early adipocyte differentiation by regulating beta1 integrin function*. J Cell Sci, 2003. **116**(Pt 19): p. 3893-904.
232. Muller, P., A. Langenbach, A. Kaminski, and J. Rychly, *Modulating the actin cytoskeleton affects mechanically induced signal transduction and differentiation in mesenchymal stem cells*. PLoS One, 2013. **8**(7): p. e71283.
233. Abraham, E., B.B. Ahmadian, K. Holderness, Y. Levinson, and E. McAfee, *Platforms for Manufacturing Allogeneic, Autologous and iPSC Cell Therapy Products: An Industry Perspective*. Adv Biochem Eng Biotechnol, 2018. **165**: p. 323-350.
234. Kim, C., *Disease modeling and cell based therapy with iPSC: future therapeutic option with fast and safe application*. Blood Res, 2014. **49**(1): p. 7-14.
235. Kimura, Y., T. Shofuda, Y. Higuchi, I. Nagamori, M. Oda, M. Nakamori, M. Onodera, D. Kanematsu, A. Yamamoto, A. Katsuma, H. Suemizu, T. Nakano, Y. Kanemura, and H. Mochizuki, *Human Genomic Safe Harbors and the Suicide Gene-Based Safeguard System for iPSC-Based Cell Therapy*. Stem Cells Transl Med, 2019. **8**(7): p. 627-638.
236. Li, Y., L. Chan, H.V. Nguyen, and S.H. Tsang, *Personalized Medicine: Cell and Gene Therapy Based on Patient-Specific iPSC-Derived Retinal Pigment Epithelium Cells*. Adv Exp Med Biol, 2016. **854**: p. 549-55.

237. Rao, M., *iPSC-Based cell therapy: an important step forward*. Stem Cell Reports, 2013. **1**(4): p. 281-2.
238. Rhee, J.W. and J.C. Wu, *Cardiac Cell Cycle Activation as a Strategy to Improve iPSC-Derived Cardiomyocyte Therapy*. Circ Res, 2018. **122**(1): p. 14-16.
239. Oh, Y. and J. Jang, *Directed Differentiation of Pluripotent Stem Cells by Transcription Factors*. Mol Cells, 2019. **42**(3): p. 200-209.
240. Fujita, J., S. Tohyama, Y. Kishino, M. Okada, and Y. Morita, *Concise Review: Genetic and Epigenetic Regulation of Cardiac Differentiation from Human Pluripotent Stem Cells*. Stem Cells, 2019. **37**(8): p. 992-1002.
241. Kempf, H. and R. Zweigerdt, *Scalable Cardiac Differentiation of Pluripotent Stem Cells Using Specific Growth Factors and Small Molecules*. Adv Biochem Eng Biotechnol, 2018. **163**: p. 39-69.
242. Devalla, H.D. and R. Passier, *Cardiac differentiation of pluripotent stem cells and implications for modeling the heart in health and disease*. Sci Transl Med, 2018. **10**(435).
243. Bordoni, M., F. Rey, V. Fantini, O. Pansarasa, A.M. Di Giulio, S. Carelli, and C. Cereda, *From Neuronal Differentiation of iPSCs to 3D Neuro-Organoids: Modelling and Therapy of Neurodegenerative Diseases*. Int J Mol Sci, 2018. **19**(12).
244. Bianchi, F., M. Malboubi, Y. Li, J.H. George, A. Jerusalem, F. Szele, M.S. Thompson, and H. Ye, *Rapid and efficient differentiation of functional motor neurons from human iPSC for neural injury modelling*. Stem Cell Res, 2018. **32**: p. 126-134.
245. Natalwala, A. and T. Kunath, *Preparation, characterization, and banking of clinical-grade cells for neural transplantation: Scale up, fingerprinting, and genomic stability of stem cell lines*. Prog Brain Res, 2017. **230**: p. 133-150.
246. Lewandowski, J., T.J. Kolanowski, and M. Kurpisz, *Techniques for the induction of human pluripotent stem cell differentiation towards cardiomyocytes*. J Tissue Eng Regen Med, 2017. **11**(5): p. 1658-1674.
247. Iyer, N.R., T.S. Wilems, and S.E. Sakiyama-Elbert, *Stem cells for spinal cord injury: Strategies to inform differentiation and transplantation*. Biotechnol Bioeng, 2017. **114**(2): p. 245-259.
248. Schwach, V. and R. Passier, *Generation and purification of human stem cell-derived cardiomyocytes*. Differentiation, 2016. **91**(4-5): p. 126-38.
249. Zuppinger, C., G. Gibbons, P. Dutta-Passecker, A. Segiser, H. Most, and T.M. Suter, *Characterization of cytoskeleton features and maturation status of cultured human iPSC-derived cardiomyocytes*. Eur J Histochem, 2017. **61**(2): p. 2763.
250. Boraas, L.C., E.T. Pineda, and T. Ahsan, *Actin and myosin II modulate differentiation of pluripotent stem cells*. PLoS One, 2018. **13**(4): p. e0195588.
251. Magliocca, V., S. Petrini, T. Franchin, R. Borghi, A. Niceforo, Z. Abbaszadeh, E. Bertini, and C. Compagnucci, *Identifying the dynamics of actin and tubulin polymerization in iPSCs and in iPSC-derived neurons*. Oncotarget, 2017. **8**(67): p. 111096-111109.
252. Ohara, Y., N. Koganezawa, H. Yamazaki, R.T. Roppongi, K. Sato, Y. Sekino, and T. Shirao, *Early-stage development of human induced pluripotent stem cell-derived neurons*. J Neurosci Res, 2015. **93**(12): p. 1804-13.
253. Xia, S., Y.B. Lim, Z. Zhang, Y. Wang, S. Zhang, C.T. Lim, E.K.F. Yim, and P. Kanchanawong, *Nanoscale Architecture of the Cortical Actin Cytoskeleton in Embryonic Stem Cells*. Cell Rep, 2019. **28**(5): p. 1251-1267 e7.
254. Melak, M., M. Plessner, and R. Grosse, *Actin visualization at a glance*. J Cell Sci, 2017. **130**(3): p. 525-530.

255. Mishra, P., D.C. Martin, I.P. Androulakis, and P.V. Moghe, *Fluorescence Imaging of Actin Turnover Parses Early Stem Cell Lineage Divergence and Senescence.* Sci Rep, 2019. **9**(1): p. 10377.
256. Toma, J.G., I.A. McKenzie, D. Bagli, and F.D. Miller, *Isolation and characterization of multipotent skin-derived precursors from human skin.* Stem Cells, 2005. **23**(6): p. 727-37.
257. Okita, K., Y. Matsumura, Y. Sato, A. Okada, A. Morizane, S. Okamoto, H. Hong, M. Nakagawa, K. Tanabe, K. Tezuka, T. Shibata, T. Kunisada, M. Takahashi, J. Takahashi, H. Saji, and S. Yamanaka, *A more efficient method to generate integration-free human iPS cells.* Nat Methods, 2011. **8**(5): p. 409-12.
258. Francis, N.L., N. Zhao, H.R. Calvelli, A. Saini, J.J. Gifford, G.C. Wagner, R.I. Cohen, Z.P. Pang, and P.V. Moghe, *Peptide-Based Scaffolds for the Culture and Transplantation of Human Dopaminergic Neurons.* Tissue Eng Part A, 2019.
259. Burridge, P.W., A. Holmstrom, and J.C. Wu, *Chemically Defined Culture and Cardiomyocyte Differentiation of Human Pluripotent Stem Cells.* Curr Protoc Hum Genet, 2015. **87**: p. 21 3 1-21 3 15.
260. Burridge, P.W., E. Matsa, P. Shukla, Z.C. Lin, J.M. Churko, A.D. Ebert, F. Lan, S. Diecke, B. Huber, N.M. Mordwinkin, J.R. Plews, O.J. Abilez, B. Cui, J.D. Gold, and J.C. Wu, *Chemically defined generation of human cardiomyocytes.* Nat Methods, 2014. **11**(8): p. 855-60.
261. Muruganandan, S., A.A. Roman, and C.J. Sinal, *Adipocyte differentiation of bone marrow-derived mesenchymal stem cells: cross talk with the osteoblastogenic program.* Cell Mol Life Sci, 2009. **66**(2): p. 236-53.
262. Moreno-Navarrete, J.M. and J.M. Fernández-Real, *Adipocyte differentiation*, in *Adipose tissue biology*. 2017, Springer. p. 69-90.
263. Pankratz, M.T., X.J. Li, T.M. Lavaute, E.A. Lyons, X. Chen, and S.C. Zhang, *Directed neural differentiation of human embryonic stem cells via an obligated primitive anterior stage.* Stem Cells, 2007. **25**(6): p. 1511-20.
264. Parekkadan, B., Y. Berdichevsky, D. Irimia, A. Leeder, G. Yarmush, M. Toner, J.B. Levine, and M.L. Yarmush, *Cell-cell interaction modulates neuroectodermal specification of embryonic stem cells.* Neurosci Lett, 2008. **438**(2): p. 190-5.
265. Pevny, L.H., S. Sockanathan, M. Placzek, and R. Lovell-Badge, *A role for SOX1 in neural determination.* Development, 1998. **125**(10): p. 1967-78.
266. Andrews, P.W., I. Damjanov, J. Berends, S. Kumpf, V. Zappavigna, F. Mavilio, and K. Sampath, *Inhibition of proliferation and induction of differentiation of pluripotent human embryonal carcinoma cells by osteogenic protein-1 (or bone morphogenetic protein-7).* Lab Invest, 1994. **71**(2): p. 243-51.
267. Rathjen, J., J.A. Lake, M.D. Bettess, J.M. Washington, G. Chapman, and P.D. Rathjen, *Formation of a primitive ectoderm like cell population, EPL cells, from ES cells in response to biologically derived factors.* J Cell Sci, 1999. **112 (Pt 5)**: p. 601-12.
268. Forristal, C.E., K.L. Wright, N.A. Hanley, R.O. Oreffo, and F.D. Houghton, *Hypoxia inducible factors regulate pluripotency and proliferation in human embryonic stem cells cultured at reduced oxygen tensions.* Reproduction, 2010. **139**(1): p. 85-97.
269. Sivasubramaniyan, K., R. Pal, S. Totey, V.S. Bhat, and S. Totey, *Rho kinase inhibitor y27632 alters the balance between pluripotency and early differentiation events in human embryonic stem cells.* Curr Stem Cell Res Ther, 2010. **5**(1): p. 2-12.
270. Pan, G.J., Z.Y. Chang, H.R. Scholer, and D. Pei, *Stem cell pluripotency and transcription factor Oct4.* Cell Res, 2002. **12**(5-6): p. 321-9.
271. Pekkanen-Mattila, M., M. Pelto-Huikko, V. Kujala, R. Suuronen, H. Skottman, K. Aalto-Setala, and E. Kerkela, *Spatial and temporal expression pattern of germ layer*

markers during human embryonic stem cell differentiation in embryoid bodies. Histochem Cell Biol, 2010. **133**(5): p. 595-606.
272. Zhang, P., J. Li, Z. Tan, C. Wang, T. Liu, L. Chen, J. Yong, W. Jiang, X. Sun, L. Du, M. Ding, and H. Deng, *Short-term BMP-4 treatment initiates mesoderm induction in human embryonic stem cells*. Blood, 2008. **111**(4): p. 1933-41.
273. Adler, S., C. Pellizzer, L. Hareng, T. Hartung, and S. Bremer, *First steps in establishing a developmental toxicity test method based on human embryonic stem cells*. Toxicol In Vitro, 2008. **22**(1): p. 200-11.
274. Bamburg, J.R., *Proteins of the ADF/cofilin family: essential regulators of actin dynamics*. Annu Rev Cell Dev Biol, 1999. **15**: p. 185-230.
275. Kim, M., K. Song, E.J. Jin, and J. Sonn, *Staurosporine and cytochalasin D induce chondrogenesis by regulation of actin dynamics in different way*. Exp Mol Med, 2012. **44**(9): p. 521-8.
276. Hogrebe, N.J., P. Augsornworawat, K.G. Maxwell, L. Velazco-Cruz, and J.R. Millman, *Targeting the cytoskeleton to direct pancreatic differentiation of human pluripotent stem cells*. Nat Biotechnol, 2020.
277. Pires, R.H., N. Shree, E. Manu, E. Guzniczak, and O. Otto, *Cardiomyocyte mechanodynamics under conditions of actin remodelling*. Philos Trans R Soc Lond B Biol Sci, 2019. **374**(1786): p. 20190081.
278. Kasper, G., L. Mao, S. Geissler, A. Draycheva, J. Trippens, J. Kuhnisch, M. Tschirschmann, K. Kaspar, C. Perka, G.N. Duda, and J. Klose, *Insights into mesenchymal stem cell aging: involvement of antioxidant defense and actin cytoskeleton*. Stem Cells, 2009. **27**(6): p. 1288-97.
279. Byrne, J.A., H.N. Nguyen, and R.A. Reijo Pera, *Enhanced generation of induced pluripotent stem cells from a subpopulation of human fibroblasts*. PLoS One, 2009. **4**(9): p. e7118.
280. Cotten, M., A. Baker, M. Saltik, E. Wagner, and M. Buschle, *Lipopolysaccharide is a frequent contaminant of plasmid DNA preparations and can be toxic to primary human cells in the presence of adenovirus*. Gene Ther, 1994. **1**(4): p. 239-46.
281. Ma, R., J. Zhao, H.C. Du, S. Tian, and L.W. Li, *Removing endotoxin from plasmid samples by Triton X-114 isothermal extraction*. Anal Biochem, 2012. **424**(2): p. 124-6.
282. Wen, J.H., L.G. Vincent, A. Fuhrmann, Y.S. Choi, K.C. Hribar, H. Taylor-Weiner, S. Chen, and A.J. Engler, *Interplay of matrix stiffness and protein tethering in stem cell differentiation*. Nat Mater, 2014. **13**(10): p. 979-87.
283. Hilderbrand, A.M., E.M. Ovadia, M.S. Rehmann, P.M. Kharkar, C. Guo, and A.M. Kloxin, *Biomaterials for 4D stem cell culture*. Curr Opin Solid State Mater Sci, 2016. **20**(4): p. 212-224.
284. Gilbert, P.M., K.L. Havenstrite, K.E. Magnusson, A. Sacco, N.A. Leonardi, P. Kraft, N.K. Nguyen, S. Thrun, M.P. Lutolf, and H.M. Blau, *Substrate elasticity regulates skeletal muscle stem cell self-renewal in culture*. Science, 2010. **329**(5995): p. 1078-81.
285. Guvendiren, M. and J.A. Burdick, *Stiffening hydrogels to probe short- and long-term cellular responses to dynamic mechanics*. Nat Commun, 2012. **3**: p. 792.
286. Cosgrove, B.D., P.M. Gilbert, E. Porpiglia, F. Mourkioti, S.P. Lee, S.Y. Corbel, M.E. Llewellyn, S.L. Delp, and H.M. Blau, *Rejuvenation of the muscle stem cell population restores strength to injured aged muscles*. Nat Med, 2014. **20**(3): p. 255-64.
287. Neuss, S., B. Denecke, L. Gan, Q. Lin, M. Bovi, C. Apel, M. Woltje, A. Dhanasingh, J. Salber, R. Knuchel, and M. Zenke, *Transcriptome analysis of MSC and MSC-derived osteoblasts on Resomer(R) LT706 and PCL: impact of biomaterial substrate on osteogenic differentiation*. PLoS One, 2011. **6**(9): p. e23195.

288. Mao, A.S., B. Ozkale, N.J. Shah, K.H. Vining, T. Descombes, L. Zhang, C.M. Tringides, S.W. Wong, J.W. Shin, D.T. Scadden, D.A. Weitz, and D.J. Mooney, *Programmable microencapsulation for enhanced mesenchymal stem cell persistence and immunomodulation.* Proc Natl Acad Sci U S A, 2019. **116**(31): p. 15392-15397.
289. Khalili, A.A. and M.R. Ahmad, *A Review of Cell Adhesion Studies for Biomedical and Biological Applications.* Int J Mol Sci, 2015. **16**(8): p. 18149-84.
290. Chiellini, C., O. Cochet, L. Negroni, M. Samson, M. Poggi, G. Ailhaud, M.C. Alessi, C. Dani, and E.Z. Amri, *Characterization of human mesenchymal stem cell secretome at early steps of adipocyte and osteoblast differentiation.* BMC Mol Biol, 2008. **9**: p. 26.
291. Singh, P. and J.E. Schwarzbauer, *Fibronectin and stem cell differentiation - lessons from chondrogenesis.* J Cell Sci, 2012. **125**(Pt 16): p. 3703-12.
292. Li, B., C. Moshfegh, Z. Lin, J. Albuschies, and V. Vogel, *Mesenchymal stem cells exploit extracellular matrix as mechanotransducer.* Sci Rep, 2013. **3**: p. 2425.
293. Holmes, T.C., *Novel peptide-based biomaterial scaffolds for tissue engineering*. Trends Biotechnol, 2002. **20**(1): p. 16-21.
294. Dickhut, A., E. Gottwald, E. Steck, C. Heisel, and W. Richter, *Chondrogenesis of mesenchymal stem cells in gel-like biomaterials in vitro and in vivo.* Front Biosci, 2008. **13**: p. 4517-28.
295. Rasmussen, I., L.H. Pedersen, L. Byg, K. Suzuki, H. Sumimoto, and F. Vilhardt, *Effects of F/G-actin ratio and actin turn-over rate on NADPH oxidase activity in microglia.* BMC Immunol, 2010. **11**: p. 44.
296. Andalib, M.N., J.S. Lee, L. Ha, Y. Dzenis, and J.Y. Lim, *Focal adhesion kinase regulation in stem cell alignment and spreading on nanofibers.* Biochem Biophys Res Commun, 2016. **473**(4): p. 920-925.
297. Lee, F.Y., Y.Y. Zhen, C.M. Yuen, R. Fan, Y.T. Chen, J.J. Sheu, Y.L. Chen, C.J. Wang, C.K. Sun, and H.K. Yip, *The mTOR-FAK mechanotransduction signaling axis for focal adhesion maturation and cell proliferation.* Am J Transl Res, 2017. **9**(4): p. 1603-1617.
298. Zhao, W., D.G. Phinney, D. Bonnet, M. Dominici, and M. Krampera, *Mesenchymal stem cell biodistribution, migration, and homing in vivo.* Stem Cells Int, 2014. **2014**: p. 292109.
299. Lee, S.H., K.S. Jin, O.Y. Bang, B.J. Kim, S.J. Park, N.H. Lee, K.H. Yoo, H.H. Koo, and K.W. Sung, *Differential Migration of Mesenchymal Stem Cells to Ischemic Regions after Middle Cerebral Artery Occlusion in Rats.* PLoS One, 2015. **10**(8): p. e0134920.
300. Gothard, D., J.I. Dawson, and R.O. Oreffo, *Assessing the potential of colony morphology for dissecting the CFU-F population from human bone marrow stromal cells.* Cell Tissue Res, 2013. **352**(2): p. 237-47.
301. Ning, H., M. Albersen, G. Lin, T.F. Lue, and C.S. Lin, *Effects of EdU labeling on mesenchymal stem cells.* Cytotherapy, 2013. **15**(1): p. 57-63.
302. Li, Y., Q. Wu, Y. Wang, L. Li, H. Bu, and J. Bao, *Senescence of mesenchymal stem cells (Review).* Int J Mol Med, 2017. **39**(4): p. 775-782.
303. Fernando, R.C., D.R. Mazzotti, H. Azevedo, A.F. Sandes, E.G. Rizzatti, M.B. de Oliveira, V.L.F. Alves, A.I.P. Eugenio, F. de Carvalho, M.A. Dalboni, D.C. Martins, and G.W.B. Colleoni, *Transcriptome Analysis of Mesenchymal Stem Cells from Multiple Myeloma Patients Reveals Downregulation of Genes Involved in Cell Cycle Progression, Immune Response, and Bone Metabolism.* Sci Rep, 2019. **9**(1): p. 1056.
304. Perez-Campo, F.M. and J.A. Riancho, *Epigenetic Mechanisms Regulating Mesenchymal Stem Cell Differentiation.* Curr Genomics, 2015. **16**(6): p. 368-83.
305. Anderson, P., A.B. Carrillo-Galvez, A. Garcia-Perez, M. Cobo, and F. Martin, *CD105 (endoglin)-negative murine mesenchymal stromal cells define a new multipotent*

subpopulation with distinct differentiation and immunomodulatory capacities. PLoS One, 2013. **8**(10): p. e76979.
306. Bharathan, S.P., K.V. Manian, S.M. Aalam, D. Palani, P.A. Deshpande, M.D. Pratheesh, A. Srivastava, and S.R. Velayudhan, *Systematic evaluation of markers used for the identification of human induced pluripotent stem cells.* Biol Open, 2017. **6**(1): p. 100-108.
307. Yu, O.M. and J.H. Brown, *G Protein-Coupled Receptor and RhoA-Stimulated Transcriptional Responses: Links to Inflammation, Differentiation, and Cell Proliferation*. Mol Pharmacol, 2015. **88**(1): p. 171-80.
308. Pertz, O., L. Hodgson, R.L. Klemke, and K.M. Hahn, *Spatiotemporal dynamics of RhoA activity in migrating cells*. Nature, 2006. **440**(7087): p. 1069-72.